Title
Interactions of chromatin with the nuclear envelope

Author
Marshall, Wallace F.

Publication Date
1997

Peer reviewed|Thesis/dissertation

Interactions of Chromatin with the Nuclear Envelope

by

Wallace F. Marshall

DISSERTATION

Submitted in partial satisfaction of the requirements for the degree of

DOCTOR OF PHILOSOPHY

in

Biochemistry

in the

GRADUATE DIVISION

of the

UNIVERSITY OF CALIFORNIA

San Francisco

Date **University Librarian**

Degree Conferred: . . . . . .

Preface

Much of the data presented in the second chapter of this dissertation has been published as Marshall, W.F., Dernburg, A.F., Harmon, B., Agard, D.A., and Sedat, J.W. (1996). Specific interactions of chromatin with the nuclear envelope: positional determination within the nucleus in Drosophila melanogaster. *Molecular Biology of the Cell* 7,825-42 and is reprinted here by permission. Much of the data presented in chapter four has been published as Marshall, W.F., Agard, D.A., and Sedat, J.W. 1996. Chromosome mechanics in vivo: quantitative analysis of nonrigid 3D chromosome motion in living Drosophila embryos. *SPIE Proceedings* 2678,142-150, and is reprinted here by permission.

Dedicated to my parents

To be young and love learning
is to glow like the dawn.
To be at the prime of life and love learning
is to burn like the sun.
To be old and still love learning
is to shine like a candle in the dark.

- classical Chinese verse

Acknowledgments

I would like to extend my thanks to the many people who have directly and indirectly facilitated this work and made life during graduate school not only tolerable but also enjoyable. In addition to a blanket acknowledgment of the entire UCSF community for creating and maintaining an intense but friendly intellectual atmosphere, I would like to thank some specific individuals.

John Sedat, my advisor and truly a mentor in the broadest sense, for running a lab in which creativity is encouraged and individuality is mandatory. I particularly acknowledge John's courage to persevere in following his vision in spite of a vicious campaign by a certain funding agency, and even some simpleminded folks within our own department, to snuff out our lab. The successful careers of his students have more than vindicated John's approach to science, and I am both proud and fortunate to have been a part of this struggle in which we ultimately proved victorious.

Dave Agard, for providing the other half of the dialectic, for constant encouragement and support, and for useful advice all along the way.

Tim Mitchison and Cynthia Kenyon, my thesis committee, for providing both scientific advice and moral support.

Sue Parmelee, who helped set the tone of the Sedat lab and make it a zany place, and who helped break the monotony of work with rafting trips.

Abby Dernburg, for being a great baymate and colleague and scientific role model, for helping me to overcome my phobia of broken glass without actually ever embedding any pieces of it in me, and for basically handing to me, on a silver platter, all of the tools and methodologies I needed for my work.

Hans Chen and Diana Diggs (Hughes) for building the software that provides the basis for all our work. No other lab has the software resources we do, and this is due to Hans and Diana. I must also thank them for their patience with my impatience. If the past 5 years have represented a battle for survival for our lab, Hans and Diana were the secret weapons. I also thank Angus McDonald for the neverending, exhausting, and utterly painful task of maintaining all the computer systems that form the backbone of this operation.

Jason Swedlow, for teaching me lots of useful things in the early days, and for helpful suggestions all along the way.

Hank Bass for raising my capsaicin tolerance to a level I would have thought impossible, and for being a scholarly colleague.

Brian Harmon and Ryan Case, whose youthful enthusiasm and frightening computer literacy re-taught me something I had forgotten: either you are on the cutting edge of technology or you are a loser. Also I would like to thank the entire chronic Doom contingent, including not only Brian and Ryan, but also Jim Wilhelm, Orion Weiner, and Queelim Ch'ng, for helping to blast away stress and tension with chainsaws and gatling guns.

Hiro Itoi, for lessons on how to kill the opponent in tennis, and how not to kill the embryo when injecting.

Zvi Kam for many inspirational visits to the lab, and for helping me to not injure my knees by taking up running, by pointing out "you could run 100 miles and it would not help".

My collaborators, Karen Oegema and Jodi Nunnari, for exposing me to whole new realms of biology and for tolerating my slowness and/or grumpiness when I got overwhelmed. This is how science should be done always.

Aaron Straight for not only developing a diabolically clever system for tracking moving chromosomes, but also for saint-like goodwill in sharing it.

My parents, grampa, and aunts and uncles, for constant support, and whose guidance got me here in the first place. Perhaps the one thing that will ameliorate the pain of having to leave UCSF will be the pleasure of being closer to my family. I also want to acknowledge my brother James for being an inspirational character and a most excellent One-Time Commissioner of the State of California.

My in-laws, Wallace and May Fung, and all my aunts-and-uncles in law, especially Susan Kung, for being my family while I was here. I particularly thank Aunt Rita and Uncle James for providing a place to live during the last phase of grad school, and also Denis and Betsy for letting me live with them while I wrote this thesis, and also for treating us to many fine meals that we otherwise could not have afforded!

All of my classmates who have really made grad school fun, and from whom I have learned a great deal, especially Cara, Arshad (The Great One), Andy, Hernan, Lorrie, Susayn (or however the heck she insists on spelling it), Kayvan, Kent, Kevin (Patchogue boy), Ramon, and Mike.

I must give special thanks and recognition to Paul Peluso, my buddy and excellent colleague. No matter what the intellectual arena, be it advice on running columns, recognizing blue-fin toro by the marbled texture of the meat, or details of the members of the Chicago Symphony brass section, Paul has expanded my awareness and enriched my life. He has also taught me, not only that "gourmet" and "gourmand" are two different words, but that the two need not be mutually exclusive. The coffee breaks, gripe sessions, and late night visits of respect, will truly be missed.

Most of all, I thank Jennifer Fung, my labmate and mate. She is my sunshine.

Interactions of Chromatin with the Nuclear Envelope

Wallace F. Marshall

Abstract

Cytological studies have suggested that chromosomes may be nonrandomly arranged in the nucleus, which raises two questions. First, to what extent is the position of a given chromosomal locus determined within the nucleus, and second, to what extent can a given chromosomal locus move around within the nucleus. This work addresses these two questions. Fluorescence in situ hybridization (FISH) and three-dimensional microscopy were used to determine the position of 41 different DNA probes within the nucleus in *Drosophila melanogaster* embryos. Every locus was found to reproducibly occupy a distinct subregion of the nucleus. In particular, by using a Monte Carlo statistical test, a set of loci was identified that associate reproducibly with the nuclear envelope (NE). These NE association sites are distributed throughout the genome, spaced at intervals of roughly 1 Mb. NE association sites do not correspond to binding sites of known *Drosophila* chromatin proteins, to known boundary elements, or to scaffold attachment regions (SARs). NE association sites include both euchromatic and heterochromatic regions, and not all heterochromatin is NE associated. The NE associations defined by this work are not seen in telophase and are established later in interphase, demonstrating that this interaction does not play a role in post-mitotic NE reassembly.

The highly specific positioning observed by FISH raises the second question, is chromatin mobile within the interphase nucleus. To answer this, strategies were developed for measuring the diffusion of interphase chromatin in *Drosophila* and *Saccharomyces cerevisiae*. In both cases it was found that chromatin can indeed diffuse within the nucleus, with a diffusion constant of approximately 10^{-12} cm^2/s. In yeast, but

not Drosophila, the diffusion was constrained, implying that the chromatin is tethered to an internal nuclear structure. This diffusive motion is likely to be Brownian as it is unaffected by treatment of cells with azide, a metabolic inhibitor. The diffusion constant was found to be surprisingly size independent, such that a small plasmid diffused slower, rather than faster, than an entire yeast chromosome. This behavior is also consistent with a tethering model. This work together with the FISH experiments in Drosophila embryos, suggest a picture of nuclear architecture in which chromosomes are held in precisely defined positions by being tethered to an immobile internal structure. These results have important functional consequences for processes such as meiosis that involve large-scale chromosome motion.

Table of Contents

List of Tables

List of Figures

Chapter 1. Chromosome Positioning and Nuclear Architecture

Summary:

Recent advances in fluorescence in situ hybridization and 3D microscopy have revealed a high degree of large-scale order in the nucleus, in which the position of each gene within the nucleus is no longer random. Like any other biological phenomenon, this large-scale organization must ultimately be specified by molecular interactions. Biochemical and molecular investigations have revealed a small set of local molecular-scale interactions that can be used together in a combinatorial fashion to establish a global large-scale nuclear architecture and stabilize it against Brownian motion.

Introduction:

Since the early days of cytology, evidence that interphase chromatin is organized in a well-defined architecture has been slowly, but steadily, accumulating (Comings, 1980). More recently, the introduction of fluorescence in situ hybridization (FISH) techniques that minimally perturb the structure of the nucleus has allowed the position of specific loci to be visualized within the nucleus. By using FISH in combination with three-dimensional microscopy, the precise position of a specific locus within a nucleus can be measured, and by comparing many nuclei, it can be seen that particular loci reproducibly occupy different sub-regions in the nucleus (Chug et al., 1990; Ellison and Howard, 1981; Hochstrasser et al., 1986; Hoefers et al., 1993; Manuelidis and Borden, 1988; Nagele et al., 1995; van Dekken et al., 1990; Vourc'h et al., 1993; Zalensky et al., 1995). Recent evidence indicates, in fact, that all loci likely occupy defined positions (Marshall et al., 1996). But how could such large-scale organization be set up? In addition to revealing overall positioning within the nucleus, FISH studies have suggested a set of defined interactions (e.g. associations of chromatin with the nuclear envelope) which provide the basis for the overall order that is observed. Understanding these interactions will be the key to

manipulating nuclear architecture and thereby testing its biological role. Furthermore, these individual interactions may in and of themselves perform a variety of functional roles. The purpose of this review is to show how large-scale *global* nuclear order is built up from a small set of *local* molecular interactions which thus constitute the organizing principles of the nucleus.

We will consider separately a series of local molecular interactions and processes which can, in combination, give rise to the observed global arrangements of interphase chromatin. Each of these organizing principles has been directly demonstrated using FISH and 3D microscopy. For each proposed mechanism, we will define it in molecular and physical terms, discuss the evidence supporting its existence, and briefly discuss its possible role in overall nuclear architecture. We broadly group the local organizing principles into three classes: active positioning, interactions between chromosomes, and interactions of chromosomes with other structures. For each broad class, we list the known types of interactions and then discuss in detail one particular example.

Organizing Principle I: Active Positioning

The first organizing principle we will consider is active force applied locally to a chromosome. In several cases, it is known that chromosomes are actively moved into specific arrangements, the necessary force being provided by the cytoskeleton. For example, during anaphase, chromosomes are drawn out into parallel straight rods, and this conformation has profound consequences for nuclear organization in the subsequent interphase. Another example is the clustering of telomeres during meiosis (Chikashe et al., 1994; Dernburg et al., 1995), which appears to involve the cytoskeleton (Salonen et al., 1982). Finally, persistent directed motion of a subset of centromeres has recently been demonstrated during interphase in living HeLa cells (Shelby et al., 1996). This motion was too regular and directional to be explained by Brownian motion, and thus it may reflect the action of nuclear motor proteins on chromatin. One such motor protein, the kinesin-like nod gene product, has already been shown to be associated with chromosome arms during meiosis in Drosophila (Afshar et al., 1995). Other candidates for

motor proteins inside the nucleus include actin/myosin (both actin and actin-like proteins are found in nuclei) (Milankov and DeBoni, 1993; Weber et al., 1995) and also the SMC family of ATPases (Hirano et al., 1995) which have been proposed to act as motors in chromatin condensation. The ability of RNA polymerases to act as motors to move DNA has recently been demonstrated (Yin et al., 1996). Active positioning of chromatin by locally applied forces may thus turn out to be a widespread phenomenon. Of these examples given here, the consequences of anaphase forces remain the best understood.

At the end of anaphase, the chromosomes have been arranged as a set of parallel rods all oriented similarly with centromeres at one end and telomeres at the other. This configuration is maintained during interphase and causes the nucleus to be polarized, with centromeres clustering at one end of the nucleus, and telomeres at the opposite end (Figure 1A). This anaphase remnant is known as the "Rabl Configuration" (Comings, 1984). It has been observed in many cell types including Drosophila [3,4,11,21,22](Ellison and Howard, 1981; Hochstrasser et al., 1986; Marshall et al., 1996, Dernburg et al., 1996; Foe and Alberts, 1985), fission yeast (Funabiki et al., 1993), plants (Fussell, 1987), and mammalian cells (Haaf and Ward, 1995). The Rabl configuration defines an axis in the nucleus, running from one end of the nucleus to the other. In Drosophila embryos, not just centromeres and telomeres, but all loci are arranged along this axis, with the position along the axis corresponding to genomic position. Thus, forces applied *locally* at the kinetochore (by the spindle) lead to a *global* organization of the entire nucleus (i.e. the Rabl configuration).

What are the functional consequences of the Rabl configuration? This is currently the simplest aspect of nuclear architecture to address experimentally, since simple translocations can be used to shift the position of a relevant locus on the chromosome, moving towards or away from the centromere, and hence up or down relative to the Rabl axis. Indication that such manipulations can have functional consequences is provided by the phenomenon of position effect variegation (PEV) in Drosophila, where genomic distance away from the centromere has a profound effect on gene expression (Eissenberg, 1989). PEV occurs when a block of

heterochromatin (which in Drosophila is usually restricted to the region surrounding the centromere) is placed adjacent to a euchromatic gene in cis, causing that gene to be repressed. Rearrangements that move this gene together with the flanking heterochromatic block farther away on the chromosome from the centromere (where most of the heterochromatin is) lead to a suppression of PEV and a restoration of gene expression. One hypothesis is that heterochromatin near a gene can cause that gene to relocate in the nucleus to special heterochromatic compartment, thereby leading to its repression (Henikoff et al., 1995). Because in Drosophila essentially all the heterochromatin is found flanking the centromeres, this model implies that the farther the gene is genomically from the centromere, the farther it will be away from the centromeric heterochromatin spatially along the Rabl axis, and thus the gene will be less repressed. Recent evidence suggests that physical proximity of a variegating gene with the centric heterochromatin may indeed correspond to repression of that gene, because not only can the heterochromatin responsible for PEV cause the variegating gene to become associated with the centromeric heterochromatin (Dernburg et al., 1996; Csink and Henikoff, 1996), but the frequency of this association is reduced by rearrangements or mutations that suppress PEV (Henikoff et al., 1995; Csink and Henikoff, 1996). In cases such as Drosophila where the majority of heterochromatin is clustered around the centromeres, the Rabl configuration effectively partitions the nucleus into heterochromatic and euchromatic territories. Thus, highly *local* forces exerted at a single point on a chromosome (the centromere) end up influencing gene expression all throughout the genome as a result of their effects on *global* architecture.

Organizing Principle II: Interactions Between Chromosomes

The second organizing principle we will discuss is associations between chromosomes. Such interactions include somatic homolog pairing (see below), large-scale looping of chromatin (Dernburg et al., 1996; Rippe et al., 1995), and clustering of both centromeres and telomeres (Funabiki et al., 1993). Here we will focus on the pairing of homologous chromosomes.

Diploid organisms contain two copies of each chromosome which can be arranged so that the homologues are intimately associated with each other. This homologous chromosome pairing is of great importance for meiosis where homologues must synapse for proper chromosome segregation in the first division. Pairing also occurs in non-meiotic tissues. This somatic pairing has been directly observed using FISH in Drosophila (Hiraoka et al., 1993) and human cells (Arnoldus et al., 1989; LaSalle and Lalande, 1996), where instead of two distinct hybridization signals arising from the two homologs, only a single FISH signal is seen, implying that the two homologs have become paired. Somatic pairing has also been implicated in several epigenetic phenomena such as transvection (Wu, 1993), genetic imprinting (LaSalle and Lalande, 1996) and paramutation (Patterson et al., 1993), which seem to depend on the pairing state of the homologous chromosomes. In these cases, gene expression is modulated by proximity of the two homologues as evidenced by the fact that chromosome rearrangements, which disrupt homologue pairing, have a corresponding effect on gene expression. These phenomena taken together suggest that homologous pairing has a role in gene regulation.

This aspect of nuclear organization seems highly regulated. The extent of homologous pairing varies greatly between different organisms and even among different tissues within one organism (Arnoldus et al., 1989). Moreover, even in a given cell, pairing is nonuniform along the length of a chromosome, with a specific subset of the genes paired and others unpaired (Arnoldus et al., 1989). Loci closely linked to a pairing site will tend to be closer together than loci not near a pairing site. Moreover, even a few sites of homolog pairing will cause homologous chromosomes to be generally closer together than non-homologs. This results in a second level of nuclear architecture superimposed on the Rabl configuration, in which homologous pairing at a few discrete sites determines the distances between homologous and nonhomologous loci (Figure 1B). Once again we see that *local* interactions (homologous pairing at discrete sites on a chromosome) contribute to *global* architecture (distance between chromosomes).

Organizing Principle III: Chromatin Interactions with Other Structures

The third organizing principle we consider is binding of chromatin to large nuclear structures. We would expect Brownian motion, given enough time, to reduce even the most orderly chromosome configuration to a tangled mess. That a well defined architecture is still observed implies that chromatin must somehow be anchored, so as to prevent its randomization. Such anchoring requires a large, relatively immobile superstructure, and several nuclear structures may serve such a function. Candidate structures would include both the nuclear envelope and the nuclear matrix/nucleoskeleton. We will focus on interactions with the nuclear envelope since these are among the most obvious interactions visible by FISH experiments.

Associations of specific chromosome loci with the nuclear envelope have been clearly demonstrated in interphase (Chung et al., 1990; Hochstrasser et al., 1986; Vourc'h et al., 1993; Marshall et al., 1996). This association is likely due to local binding interactions between some component of the chromatin and some component of the nuclear envelope. A number of such potential interactions have been identified by in vitro binding studies. Lamins (Glass et al., 1993; Luderus et al., 1994; Taniura et al., 1995) and also lamin-associated proteins (Foisner and Gerace, 1993; Ye and Worman, 1996) have been shown to bind mitotic chromosomes and in some cases naked DNA (Glass et al., 1993; Luderus et al., 1994), histones (Taniura and Gerace, 1995), or heterochromatin proteins (Ye and Worman, 1996). At least one nuclear pore complex subunit contains zinc finger motifs which may indicate an ability to bind DNA (Sukegawa and Blobel, 1993). These binding interactions result in some loci being recruited to the NE while others remain in the nuclear interior. As a result, a radial position coordinate is defined, just as in a spherical coordinate system, with the radial position of each locus relative to the NE dictated by how near that locus on the chromosome to an NE binding site (Figure 1C). This represents a third level of nuclear organization superimposed on the Rabl configuration and homolog pairing. The main point is that once again, highly *local* interactions (e.g. lamins binding to histones or DNA) give rise to a large-scale *global* order (radial position) in the nucleus.

What role might chromatin-NE interactions play in interphase? There is some evidence to suggest that transcribed sequences are preferentially located near the nuclear periphery (Hutchinson and Weintraub, 1985). The gene-gating hypothesis (Blobel, 1985) proposes that genes are recruited to the NE to facilitate export of their transcripts. This concept is particularly compelling in the case of the apically localized pair-rule transcripts in Drosophila, because the strong Rabl configuration seen in these nuclei provides a natural nuclear asymmetry that could lead to the asymmetric localization of the transcripts. However, the nuclear localization of these genes does not appear to reflect the localization of the transcript (Davis et al., 1993), arguing against a role for nuclear positioning in directing transcript export or localization It is also possible that targeting specific genes to the NE could facilitate their interaction with other NE components besides the nuclear pores. Chromatin-NE interactions may also play a role in chromosome condensation, as condensation has been observed to initiate near the nuclear envelope in Drosophila embryos (Hiraoka et al., 1989). This may be an adaptation to facilitate the rapid segregation of chromosomes that must take place in these embryos: by causing separate chromosomes to condense onto different regions of the nuclear envelope, chromosomes can be disentangled and separated prior to the onset of anaphase itself.

Combinatorial Specification of Nuclear Position

Direct measurement of the nuclear position of a large number of sites indicates that all loci are likely confined to specific positions in the nucleus, the position of a given locus varying from the average position by only ±0.5 μm from cell to cell (Marshall et al., 1996). While none of the individual local interactions delineated above would be sufficient to give such precisely defined positioning, several of these interactions, working in combination, can give the localization that is observed. As a result of the anaphase forces, the position of a given site is specified along the Rabl axis, thus placing that site in a plane through the nucleus. However, it could be anywhere in this plane since the Rabl configuration only determines position along a single axis. However, interactions with the nuclear envelope, other chromosomes, and other nuclear structures, will

determine where within this plane the site resides. Together these constraints lead to a highly specified position. For example, a gene located near a centromere and close to an NE binding site will have a much different location in the nucleus from a gene located in the middle of a chromosome arm and far from any NE binding sites (the former will be on the nuclear periphery at one end of the nucleus, while the other will lie in the central region of the nucleus).

From this point of view, each type of interaction or organizing principle discussed above becomes, in effect, a separate degree of freedom. Because localization is a combinatorial function of these degrees of freedom, it should be possible to change one independently of the others, with predictable effects on nuclear organization. This is indeed true. If we use a rearrangement to shift a site to a different position on the chromosome, the Rabl axis position should shift without affecting the distance to the NE. This is indeed the case (Marshall et al., 1996). Likewise, if an NE association site is inserted near a given locus, the distance of that locus to the NE should decrease without affecting its position along the Rabl axis. This too has been experimentally demonstrated (Dernburg et al., 1996). Such manipulations finally provide means of testing the functional relevance of nuclear organization.

The fact that different loci have different localizations in the nucleus may to some extent explain the observation that when the positions of entire chromosomes in the nucleus are determined, it is found that different chromosomes occupy different territories within the nucleus (Hochstrasser et al., 1986; Cremer et al., 1993; Eils et al., 1996). Because the different loci composing each chromosome will be targeted to different regions of the nucleus by the local interactions described in this review, it follows that the chromosomes themselves must likewise occupy different nuclear regions.

Conclusions and Future Developments

As our understanding of the molecular basis of nuclear organization improves, so too will our ability to test the various hypothetical functions of nuclear architecture. Do nuclear envelope interactions facilitate export and localization of specific transcripts (Blobel, 1985) or

condensation of chromosomes (Hiraoka et al., 1989)? Do genes need to be sequestered in special compartments of the cell to be repressed (Henikoff et al., 1995) or transcribed (Hutchinson and Weintraub, 1985)? If we can, either by mutation or chromosome rearrangement, experimentally perturb nuclear architecture, we can observe the consequences of the perturbation and thereby probe which functions are or are not affected. The key to relating nuclear structure to function, then, is to identify the molecules involved in the interactions that establish nuclear organization. Because there are several well characterized genetic phenomena in Drosophila that appear to involve nuclear architecture, including transvection and position effect variegation, and because a large number of chromosome rearrangements and mutations exist which modify these phenomena, we anticipate that Drosophila will continue to play a pivotal role in elucidating the functional roles of nuclear architecture. The increasingly widespread use of three dimensional microscopy will further contribute to rapid progress in this area.

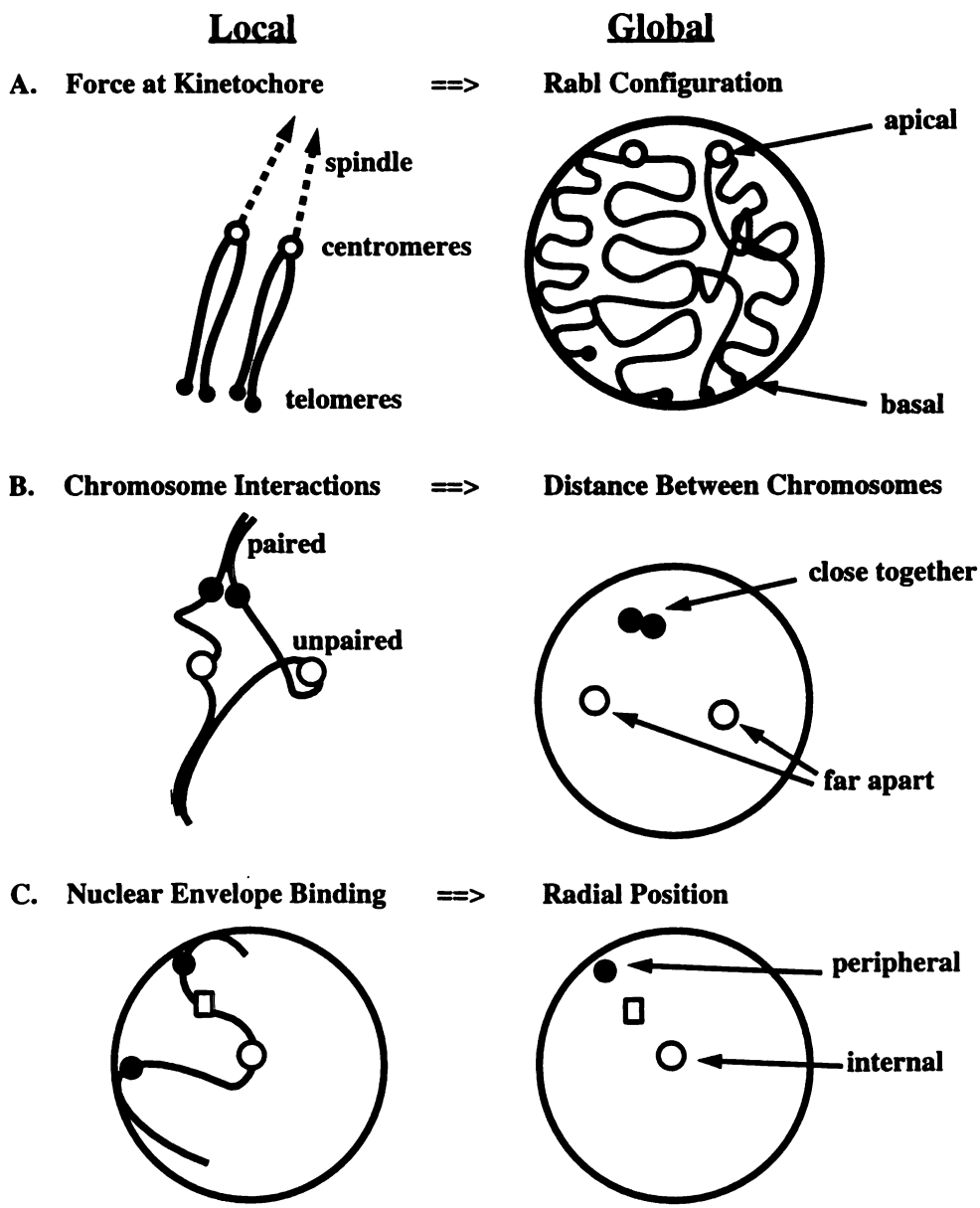

Figure 1.1. Nuclear architecture: global order from local interactions

Figure 1.1. Global nuclear architecture established by local interactions. (A) Forces applied locally at the kinetochore in mitosis lead to global polarization of the nucleus during interphase. (B) Local interactions between chromosomes lead to differences in relative positions. (C) Binding of specific sites to the nuclear envelope leads to global radial positioning.

References

Afshar K, Barton NR, Hawley RS, Goldstein LS. (1995). DNA binding and meiotic chromosomal localization of the Drosophila nod kinesin-like protein. Cell *81*,129-138.

Arnoldus EP, Peters AC, Bots GT, Raap AK, van der Ploeg M. (1989). Somatic pairing of chromosome I centromeres in interphase nuclei of human cerebellum. Human genetics *83*,231-234.

Blobel G. (1985). Gene gating: a hypothesis. Proc. Natl. Acad. Sci. U.S.A. *82*,8527-8529.

Chikashige Y, Ding DQ, Funabiki H, Haraguchi T, Mashiko S, Yanagida M, Hiraoka Y. (1994). Telomere-led premeiotic chromosome movement in fission yeast. Science *264*,270-273.

Chung HM, Shea C, Fields S, Taub RN, van der Ploeg LHT, Tse DB. (1990). Architectural organization in the interphase nucleus of the protozoan Trypanosoma Brucei: location of telomeres and mini-chromosomes. EMBO J *9*,2611-2619.

Comings DE. (1980). Arrangement of chromatin in the nucleus. Hum. Genet *53*,131-143.

Cremer T, Kurz A, Zirbel R, Dietzel S, Rinke B, Schroeck E, Speicher MR, Mathieu U, Jauch A, Emmerich P, Scherthan H, Ried T, Cremer C, Lichter P. (1993). Role of chromosome territories in the functional compartmentalization of the cell nucleus. Cold Spring Harbor Symp. Quant. Biol. *58*,777-792.

Csink A, Henikoff S. (1996). Genetic modification of heterochromatic association and nuclear organization in Drosophila. Nature *381*,529-31.

Davis I, Francis-Lang H, Ish-Horowicz D. (1993). Mechanisms of intracellular transcript localization and export in early Drosophila embryos. Cold Spring Harbor Symp. Quant. Biol. *58*,793-798.

Dernburg AF, Broman KW, Fung JC, Marshall WF, Philips J, Agard DA, Sedat JW. (1996). Perturbation of nuclear architecture by long-distance chromosome interactions. Cell 85,745-759.

Dernburg AF, Sedat JW, Cande WZ, Bass HW. (1995). Cytology of telomeres. In *Telomeres*, by E. H. Blackburn and C. W. Greider. Cold Spring Harbor, NY: Cold Spring Harbor Laboratory Press; 1995: 295--338

Eils R, Dietzel S, Bertin E, Schroeck E, Speicher MR, Ried T, Robert-Nicoud M, Cremer C, Cremer T. (1996). Three-dimensional reconstruction of painted human interphase chromosomes: active and inactive X chromosome territories have similar volumes but differ in shape and surface structure. J. Cell Biol. *135*,1427-1440.

Eissenberg JC. (1989). Position effect in Drosophila: towards a genetics of chromatin assembly. Bioessays *11*,14-17.

Ellison JR, Howard GC. (1981). Non-random position of the A-T rich DNA sequences in early embryos of Drosophila virilis. Chromosoma *83*,555-561.

Foe VE, Alberts BM. (1985). Reversible chromosome condensation induced in Drosophila embryos by anoxia: visualization of interphase nuclear organization. J. Cell Biol. *100*,1623-1636.

Foisner R, Gerace L. (1993). Integral membrane proteins of the nuclear envelope interact with lamins and chromosomes, and binding is modulated by mitotic phosphorylation. Cell *46*,521-530.

Funabiki H, Hagan I, Uzawa S, Yanagida M. (1993). Cell cycle-dependent specific positioning and clustering of centromeres and telomeres in fission yeast. J. Cell Biol. *121*,961-976.

Fussell CP. (1987). The Rabl orientation: A prelude to synapsis. In *Meiosis*, by P. B. Moens. Orlando, Florida: Academic Press; 275-79

Glass CA, Glass JR, Taniura H, Hasel KW, Blevitt JM, Gerace L. (1993). The a-helical rod domain of human lamins A and C contains a chromatin binding site. EMBO J. *12*,4413-4424.

Haaf T, Ward DC. (1995). Rabl orientation of CENP-B box sequences in Tupaia belangeri fibroblasts. Cyt. Cell Genet. *70*,258-262.

Henikoff S, Jackson JM, Talbert PB. (1995). Distance and pairing effects on the brownDominant heterochromatic element in Drosophila. Genetics *140*,1007-17.

Hirano T, Mitchison TJ, Swedlow JR. (1995). The SMC family: from chromosome condensation to dosage compensation. Curr. Opin. Cell Biol. *7*,329-336.

Hiraoka Y, Dernburg AF, Parmelee SJ, Rykowski MC, Agard DA, Sedat JW. (1993). The onset of homologous chromosome pairing during Drosophila melanogaster embryogenesis. J. Cell Biol. *120*,591-600.

Hiraoka Y, Minden JS, Swedlow JR, Sedat JW, Agard DA. (1989). Focal points for chromosome condensation and decondensation revealed by three-dimensional in vivo time-lapse microscopy. Nature *342*,293-296.

Hoefers C, Baumann P, Hummer G, Jovin TM, Arndt-Jovin DJ. (1993). The localization of chromosome domains in human interphase nuclei. Three-dimensional distance determinations of fluorescence in situ hybridization signals from confocal laser scanning microscopy. Bioimaging *1*,96-106.

Hochstrasser M, Mathog D, Gruenbaum Y, Saumweber H, Sedat JW. (1986). Spatial organization of chromosomes in the salivary gland nuclei of Drosophila melanogaster. J. Cell Biol. *102*,112-123.

Hutchison N, Weintraub H. (1985). Localization of DNAase I-sensitive sequences to specific regions of interphase nuclei. Cell *43*,471-482.

LaSalle JM, Lalande M. (1996). Homologous association of oppositely imprinted chromosomal domains. Science *272*,725-728.

Luderus ME, J.L. dB, de Smit OJ, Compton DA, van Driel R. (1994). Binding of matrix attachment regions to lamin polymers involves single-stranded regions and the minor groove. Mol. Cell. Biol. *14*,6297-6305.

Manuelidis L, Borden J. (1988). Reproducible compartmentalization of individual chromosome domains in human CNS cells revealed by in situ hybridization and three-dimensional reconstruction. Chromosoma *96*,396-410.

Marshall WF, Dernburg AF, Harmon B, Agard DA, Sedat JW. (1996). Interactions of chromatin with the nuclear envelope: positional determination within the nucleus in Drosophila melanogaster. Mol. Biol. of the Cell *7*,825-842.

Milankov K, DeBoni U. (1993). Cytochemical localization of actin and myosin aggregates in interphase nuclei. Exp. Cell Res. *209*,189-199.

Nagele R, Freeman T, McMorrow L, Lee HY. (1995). Precise spatial positioning of chromosomes during prometaphase: evidence for chromosomal order. Science *270*,1831-1835.

Patterson GI, Thorpe CJ, Chandler VL. (1993). Paramutation, an allelic interaction, is associated with a stable and heritable reduction of transcription of the Maize b regulatory gene. Genetics *135*,881-894.

Rippe K, von Hippel RH, Langowski J. (1995). Action at a distance: DNA-looping and initiation of transcription. Tr. Biochem. Sci *20*,500-6.

Salonen K, Paranko J, Parvinen M. (1982). A colcemid-sensitive mechanism involved in regulation of chromosome movements during meiotic pairing. Chromosoma *85*,611-8.

Shelby RD, Hahn KM, Sullivan KF. (1996). Dynamic elastic behavior of a-satellite DNA domains visualized in situ in living human cells. J. Cell Biol. *135*,545-558.

Sukegawa J, Blobel G. (1993). A nuclear pore complex protein that contains zinc finger motifs, binds DNA, and faces the nucleoplasm. Cell *72*,29-38.

Taniura H, Glass C, Gerace L. (1995). A chromatin binding site in the tail domain of nuclear lamins that interacts with core histones. J. Cell Biol. *131*,33-44.

van Dekken H, van Rotterdam A, Jonker R, van der Voort HTM, Brakenhoff GJ, Baumann JGJ. (1990). Confocal microscopy as a tool for the study of the intranuclear topography of chromosomes. J. Microscopy *158*,207-214.

Vourc'h C, Taruscio D, Boyle AL, Ward DC. (1993). Cell cycle-dependent distribution of telomeres, centromeres, and chromosome-specific subsatellite domains in the interphase nucleus of mouse lymphocytes. Exp. Cell Res. *205*,142-151.

Weber V, Harata M, Hauser H, Wintersberger U. (1995). The actin-related protein Act3p of Saccharomyces cerevisiae is located in the nucleus. Mol. Biol. of the Cell *6*,1263-1270.

Wu CT. (1993). Transvection, nuclear structure, and chromatin proteins. J. Cell Biol. *120*,587-590.

Ye Q, Worman HJ. (1996). Interaction between an integral protein of the nuclear envelope inner membrane and human chromodomain proteins homologous to Drosophila HP1. J. Biol. Chem. *271*,14653-14656.

Yin H, Wang MD, Svoboda K, Landick R, Block SM, Gelles J. (1996). Transcription against an applied force. Science *270*,1653-1657.

Zalensky AO, Allen MJ, Kobayashi A, Zalenskaya IA, Balhron R, Bradbury EM. (1995). Well-defined genome architecture in the human sperm nucleus. Chromosoma *103*,577-590.

Chapter 2. Specific Interactions of Chromatin with the Nuclear Envelope: Positional Determination within the Nucleus in *D. melanogaster*

SUMMARY

Specific interactions of chromatin with the nuclear envelope (NE) in early embryos of *Drosophila melanogaster* have been mapped and analyzed. A statistical method to detect sites nonrandomly associated with the NE was developed based on use of a surface harmonic expansion to model the nuclear surface. Using fluorescence in situ hybridization, the three-dimensional positions of 42 DNA probes, primarily to chromosome 2L, have been mapped in nuclei of intact Drosophila embryos, revealing 5 euchromatic and 2 heterochromatic regions associated with the NE. These results predict that there are approximately 15 NE contacts per chromosome arm, which delimit large chromatin loops of approximately 1-2 Mb. These NE association sites do not strictly correlate with scaffold-attachment regions (SARs), heterochromatin, or binding sites of known chromatin proteins. Pairs of neighboring probes surrounding one NE association site were used to delimit the NE association site more precisely, suggesting that peripheral localization of a large stretch of chromatin is likely to result from NE association at a single discrete site. These NE interactions are not established until after telophase, by which time the nuclear envelope has reassembled around the chromosomes, and they are thus unlikely to be involved in binding of NE vesicles to chromosomes following mitosis. Analysis of positions of these probes also reveals that the interphase nucleus is strongly polarized in a Rabl configuration which, together with specific targeting to the NE or to the nuclear interior, results in each locus occupying a highly determined position within the nucleus.

INTRODUCTION

Studies of nuclear organization suggest that the eukaryotic nucleus is not simply a bag of DNA but rather a highly structured organelle. For example, individual chromosomes and chromosome domains occupy well-defined territories within the nucleus, and in many cases the chromosomes assume characteristic configurations or positions (Comings, 1980, Mathog et al. 1984, Hilliker and Appels 1989, Cremer et al. 1993, Spector 1993). If chromatin was unconstrained and free to diffuse at random, such nuclear organization could not be maintained. Indeed, direct measurement of chromosome diffusion has revealed that this diffusion is indeed constrained (see Chapter 3). This constraint, and the corresponding persistence of a defined arrangement of chromosomes within the nucleus is thus likely to require interactions between chromosome domains and some other nuclear component which would serve as a scaffold or anchor. The most visibly obvious structure to which chromosomes can be anchored is the nuclear envelope, and chromatin-NE interactions are thus likely to play a major role in nuclear organization.

Associations between chromatin and the nuclear envelope (NE) have been observed cytologically for many years (DuPraw, 1965, Murray and Davies, 1979, Quick, 1980, Hochstrasser et al., 1986, Loidl, 1990, Paddy et al., 1990, Belmont et al., 1993). It has been proposed that these chromatin-NE interactions may play a role in a variety of processes, including organization of the interphase nucleus (Comings, 1980), gene regulation (Hutchison and Weintraub, 1985, Blobel, 1985, Palladino et al. 1993), chromatin condensation (Hiraoka, 1989), nuclear reassembly (reviewed in Wiese and Wilson, 1993), and meiotic homolog pairing (reviewed in Loidl, 1990). However with the exception of meiotic telomeres (Loidl, 1990, Dernburg et al., 1995), it is not known which loci interact with the NE, particularly during interphase. Indeed, it is not known for certain if the interphase chromatin-NE contacts observed in the microscope involve NE-binding by specific chromosomal loci, a general association of chromatin with the NE, or merely

coincidental contact. If chromatin-NE interactions are site-specific, then a knowledge of precisely which sites associate with the NE in interphase could shed light on the role of such interactions in the nucleus, by allowing changes in NE association to be correlated with changes in transcriptional activity, DNA repliocation, etc. In addition, a map of NE-associated sites would facilitate identification of the molecular determinants of the interaction, and provide a basis for comparing cell-cycle dependent or developmental changes in NE association. Furthermore, such a map of NE interactions would allow manipulation, via chromosome rearrangements, of the pattern of NE contacts to test for possible functions.

One possible way to find NE-binding sites is to isolate DNA that binds to the nuclear scaffold or matrix. The nuclear scaffold is operationally defined as the insoluble fraction resulting from extraction of isolated nuclei to remove most of the chromatin (Berezney and Coffey, 1974). Specific DNA sequences, called scaffold attachment regions (SARs) coprecipitate with the scaffold after restriction endonuclease digestions, and bind the nuclear scaffold in vitro (Gasser and Laemmli, 1986). Because lamins are major components of nuclear scaffolds (Lebkowski and Laemmli, 1982), and in light of claims that a *Drosophila* SAR can bind directly to nuclear lamins (Luderus et al, 1992), it is possible that some SARs may bind the NE in vivo. However, *Drosophila* SARs have been shown by others to bind in vitro to the internal rather than the peripheral lamin-enriched component of the scaffold (Izaurralde et al., 1988). The binding of SARs to the nuclear envelope is thus a controversial question. Moreover, the relevance of the various nuclear scaffold preparations to actual nuclear structures in vivo is itself a matter of some controversy (Jackson et al., 1990).

In addition to SAR preparations, in vitro binding studies using defined components have identified proteins that may be involved in chromatin-NE interactions, including both nuclear lamins (along with associated proteins) and nuclear pores (Sukegawa and Blobel, 1993, Luderus et al., 1994, Glass and Gerace, 1990, Glass et al., 1993, Foisner and

Gerace, 1993, Worman et al., 1990, Yuan et al. 1991). However, without knowing which chromosomal loci interact with the NE in intact nuclei, these results may be difficult to interpret. In general, the propensity of proteins to adhere to each other and especially to chromatin, which contains many strongly charged repeated moieties such as DNA (in this regard, nonspecific DNA binding assays, and by extension chromatin binding assays, are to some extent exercises in ion exchange chromatography), makes it somewhat dangerous to conclude a biological interaction from an in vitro binding experiment in the absence of a functional assay. Moreover, it is always difficult to reproduce in vitro the exact conditions inside a cell. Chromatin, in particular, is known to be exquisitly sensitive to buffer conditions. Therefore, for many reaons, an alternative method for detecting chromatin-NE interactions in intact cells would be a useful complement to in vitro binding experiments.

One such alternative approach is to use microscopy to visualize the localization of specific chromosomal loci with respect to the NE. In addition to circumventing some of the difficulties inherent in strictly biochemical approaches, visualization of chromatin-NE interactions in the context of the intact nucleus will allow further investigations of the relations between these sites and other nuclear structures, such as lamin fibers (Belmont et al., 1993), the nucleolus (Manuelidis and Borden, 1988, Billia and De Boni, 1991), or foci of transcription and replication (Spector, 1993, Hassan et al., 1994). Furthermore, a microscopic approach is extremely fast and convenient, and is readily applied to a wide variety of tissues, and even to multiple cell types within a single tissue, facilitating an analysis of developmental, cell-cycle, or tissue specific changes in the pattern of NE contact.

Several groups have employed three-dimensional microscopy to ask whether or not particular genomic loci localize to the nuclear envelope in interphase nuclei. It is not sufficient merely to examine images and visually observe peripheral localization, because within a sphere, the majority of randomly localized points will fall near the periphery. Therefore, it is necessary to demonstrate that peripheral localization is significantly greater

than that expected at random. One method is to show that some loci lie on the nuclear surface more often than others (Manuelidis and Borden, 1988). Other groups have carried out a statistical analysis employing a theoretical model for the distribution of points within a nucleus, which is computed either analytically (Chung et al., 1990, Ferguson and Ward, 1992, Vourc'h et al. 1993) or using a Monte Carlo method (Van Dekken et al., 1990, Hoefers et al., 1993). Using these methods, localization of centromeres and telomeres with respect to the NE has been analyzed, but the NE association of euchromatic loci in general has not been specifically addressed.

In this report, we describe a light-microscopy based assay for NE association to identify interactions between specific loci and the nuclear envelope in cycle 13 *Drosophila* embryos. This method has been applied to map the position of a series of probes in the euchromatin of chromosome 2 as well as a number of heterochromatic satellite sequences, revealing a number of specific NE contacts. Comparison of the NE contact sites with known SARs (Gasser and Laemmli, 1986), boundary elements (Udvardy et al., 1985), and intercalary heterochromatin (Zhimulev et al., 1982) suggests that NE association may involve a novel type of DNA element. Remarkably, these data also reveal strong positioning of different loci within the interphase nucleus.

MATERIALS AND METHODS

Preparation of genomic FISH probes

Our mapping effort takes advantage of a library of genomic clones currently employed by the Berkeley Drosophila Genome Project for their large scale mapping and sequencing of whole *Drosophila* chromosomes. Bacteria containing specific P1 genomic clones were provided by Gerald Rubin. These P1 clones originated from a library developed by Hartl and coworkers (Hartl et al., 1994) who mapped the genomic location of many of the clones

by hybridization to polytene chromosomes. All clones used in the experiments described here were previously mapped on polytene chromosomes by Hartl et al. Only P1s that were reported to give a single hybridization signal in the genome on polytene squashes (Hartl et al., 1994) were used. Each P1 contains approximately 80kb of Drosophila genomic DNA. Use of DNA spanning such a large region has proven to be essential for obtaining high signal-to-noise ratios in the FISH procedure. 2mL LB-Kan medium were inoculated with 2 μL of an overnight culture of P1-containing bacteria and grown for 3 hours at 37 °C. Then 2 μL of 1M IPTG was added and the culture grown another 3 hrs before harvesting cells. P1 DNA was obtained by alkaline lysis miniprep from 1 ml of this culture (Sambrook et al., 1989), and amplified using degenerate oligonucleotide primed PCR (Telenius et al., 1992). Amplification by DOP-PCR was necessary because the yield of DNA from a P1 prep is generally low due to the low copy number of the P1 plasmid. Probe DNA was then digested with 4-base cutting restriction enzymes and end-labeled with rhodamine-4-dUTP (FluoroRed, Amersham Corp., Arlington Heights, IL) using terminal transferase (Ratliff Biochemical, NM). Direct labelling using fluorescent nucleotide was found to produce a cleaner FISH signal than when using nucleotides labelled with biotin or digoxygenin. While use of direct label did not necessarily reduce the intensity of the background staining, the background appeared much smoother and less punctate, making it easier to distinguish the true hybridization signal from spurious background intensity. For double-label experiments, one probe was labeled with rhodamine-4-dUTP (FluoroRed) and the other with fluorescein-dUTP (FluoroGreen, Amersham Corp.) Probes were checked by hybridization to polytene chromosome squashes to verify detection of the correct locus. Some P1s, approximately 10% of those tested, hybridized to more than one site in the genome in polytene squashes. Presumably this was due to regions of limited homology or else to the presence of middle-repetitive repeat DNA. These P1 probes were not used in embryos. Probes specific for heterochromatic repeats were made directly from cloned satellite DNA or synthetic oligonucleotides, using the same labeling procedure. The Rsp

probe was a kind gift of Dr. C.-I. Wu. Dr. A. Villasante generously provided a cloned dodecasatellite probe.

Fixation, hybridization, and staining.

Drosophila embryos (Oregon-R) collected from population cages were bleach dechorionated and fixed in 3.7% formaldehyde as described in (Paddy et al., 1990). Approximately 40 µl packed volume of embryos were then placed in 500 ml eppendorf tubes for all subsequent steps. In situ hybridization was then carried out using a modification of a published method that preserves the structural integrity of the embryos and chromosomes (Hiraoka et al., 1993). Pretreatment of embryos with RNase has no effect on the resulting images indicating that FISH signals represent hybridization to DNA (Hiraoka et al 1993). Following hybridization, embryos were washed four times in 2xSSCT (0.3M NaCl 0.03M Na3citrate 0.1% Tween-20). All subsequent steps were carried out at room temperature. Immunofluorescence was carried out on hybridized embryos with anti *Drosophila* lamin monoclonal T40 (Paddy et al., 1990) as follows. Embryos were blocked by incubating with 6 mg/ml normal goat serum (Jackson Immunoresearch Laboratories, West Grove, PA) in 2xSSCT for four hours on a rotating plate mixer. Goat serum was found to produce less background than BSA. Embryos were then washed three times in 2xSSCT. Embryos were then incubated overnight with T40 ascites fluid diluted 1:40 in 2xSSCT and then washed three times in 2xSSCT for 10 min, 1 hr, and 1.5 hrs. Next, embryos were incubated for 4 hours with fluorescein conjugated goat anti-mouse secondary antibodies (Jackson Immunoresearch Laboratories, West Grove, PA) at 7 µg/ml in 2xSSCT. For double-label experiments in which FISH probes were labeled with rhodamine and fluorescein, Cy-5 conjugated goat anti-mouse secondary antibodies were employed (Jackson Immunoresearch Laboratories). After incubation with secondary antibodies, embryos were washed twice quickly in 2xSSCT, then once for 3 hours, and then washed overnight. Embryos were then stained with 0.5 µg/ml DAPI, a

DNA specific stain, in 2xSSCT for 10 min. Finally embryos were washed twice in 50mM TRIS-Cl pH 8.0 and pipetted onto a glass slide between two #0 coverslip spacers. Use of spacers was essential, as it was found that in the absence of spacers, nuclei on the top surface of the embryo (the surface that was imaged) were deformed by the pressure of the coverslip which not only changed the shape of the nuclei making any results obtained less trustworthy, but also this deformation caused the nuclear envelope to become less clearly visible in certain parts of the nucleus. Buffer was aspirated away, and embryos were overlaid with antifade mounting medium (Vectashield, Vector Laboratories Inc. Burlingame CA). A #1.5 coverslip was then placed over the embryos and sealed with clear nailpolish. In order to ensure that all embryos analyzed were at the same developmental stage, only embryos in interphase of the 13th embryonic division cycle (as judged by number of nuclei per field of view) were imaged. DAPI imaging was used to ensure that only interphase nuclei were imaged. For analysis of telophase nuclei, telophase was distinguished by several features. First, in DAPI, the nuclei appeared small, smooth, and featureless, distinct from either anaphase when the individual chromosome arms can be seen, or interphase where the nuclei are relatively larger and the chromatin staining is not uniform. Second, lamin immunofluorescence in telophase is quite distinctive, with the nuclei appearing elongated in the plane of the embryo surface, arranged in oppositely oriented pairs, and with a clear spot of non-nuclear lamin staining at the spindle midbody. Nuclei satisfying all these criteria were chosen as telophase nuclei.

Three-Dimensional Wide-field Fluorescence Microscopy

Data collection was carried out using multiwavelength wide-field 3D microscopy (Hiraoka et al., 1991) in which a scientific grade cooled CCD camera is used to acquire images, and in which all shutters, filter wheels, stage motion, and image acquisition are under computer control. Embryos were imaged using a 60x 1.4 N.A. lens (Olympus Inc.) and n=1.5180 immersion oil (R.P. Cargille Laboratories Inc., Cedar Grove NJ). Three-

dimensional datasets, each containing 40-60 nuclei, were acquired by moving the stage in 0.5 μm intervals. Under these conditions, the pixel size is 0.1117x0.1117 μm in the XY plane and 0.5 μm in the Z axis. At each focus position, an image was acquired at each of three wavelengths (605 nm, 540 nm, 460 nm) corresponding to the three fluorophores used (rhodamine, fluorescein, and DAPI). Out of focus light was removed by constrained iterative deconvolution using an experimentally determined point-spread function (Agard et al., 1989). Use of deconvolution-wdiefield microscopy has a major advantage over confocal microscopy for such experiments in that the photon collection efficiency is very high, so that for equivalant ammounts of photobleaching, a much greater number of photons (by at least an order of magnitude) can be imaged, thus improving the signal to noise ratio. For the detection of small, somewhat dim FISH signals, a high signal to noise ratio is essential. Examples of such images are given in Figure 1. NE association of the FISH signals were analyzed based on these images, using the following procedure, which is summarized in Figure 2.

Interactive location of FISH signals

An interactive 3D visualization package (Chen et al., 1995) was used to interactively pick the 3D location of FISH signals (Figure 2A). When picking FISH spots, some hybridization signals are seen to consist of two closely adjacent smaller spots, in which case the approximate center of mass of both smaller spots taken together is chosen for the location of the signal. Once the approximate location of a FISH spot is interactively picked, the intensity-weighted center of mass is found in a 5x5x3 pixel region centered on the manually chosen point. This refined FISH spot location is used for all subsequent analysis. By using the intensity-weighted center of mass, we are able to measure the position of the center of the FISH spot to a precision exceeding the resolution limit of the microscope. This type of analysis is the basis of single-particle tracking experiments and is now commonly employed to study nanometer scale displacements of individual molecules.

Both this fitting procedure, and the procedure used to fit the nuclear surface, take advantage of averaging data from several pixels to obtain a more precise measure of the position of the spot or the surface. Because the precision of such measurements is independent of the resolution, depending only on the signal to noise ratio of the signals, optical resolution does not, place an absolute limit on our ability to detect NE associations. We note moreover that resolution does not affect our ability to detect the FISH spot even when it is close to the NE, because the FISH and the lamin immunofluorescence employ two different wavelengths of emitted light. Resolution only affects the ability to discrimiate two nearby objects when they are of the same wavelength.

Detecting and fitting the nuclear surface

Our basic approach for detecting nonrandom NE association is to model the expected distribution of points in the nucleus and then compare this expected distribution with the measured distribution of the FISH signals for a given probe. The shape of the nucleus plays a critical role in determining the expected distribution of points within it, and thus, an essential prerequisite for this approch is a computational representation of the nuclear surface. We employ a surface harmonic expansion (discussed below) which is fit to the lamin immunofluorescence signal.

Pixels belonging to the NE are automatically extracted by locating local intensity peaks in the lamin image. Local maxima are found within adjacent non-overlapping 15x15x5 pixel boxes, and their coordinates recorded. Only local-maxima whose intensity exceeds a user-specified threshold are included in the fit.

Each intensity peak is assigned to a particular nucleus, creating, for each nucleus, a set of points on the NE to which a surface will be fitted. The approximate center of each nucleus is chosen interactively. All lamin intensity peaks falling within a cylindrical region around each nucleus are assigned to that nucleus. The height h_{cut} and radius r_{cut} of this

cylinder are chosen interactively for each dataset to best match the radius and height of the nuclei (Figure 2B).

Once a set of points has been assigned to each nucleus, a surface is fit to this set of points (Figure 2C). We employ a surface harmonic expansion to represent the surface (Purcell et al., 1991). This representation is simple to calculate, can represent a wide variety of nuclear shapes, and can be fitted to a set of points of arbitrary number, placement, and ordering. The surface harmonic expansion describes the surface in spherical coordinates and takes the form:

$$r(\theta,\phi) = \sum_{n=0}^{N}[a_n P_n(\cos\theta) + \sum_{m=1}^{n}(a_{nm}\cos m\phi + b_{nm}\sin m\phi)P_n^m(\cos\theta)] \qquad (1)$$

where P_n^m are Legendre polynomials, and r is the radial distance from the origin to the surface at the angles θ and ϕ. For nuclei of Drosophila embryos, only terms up to N=4 are included in the expansion.

The surface for a nucleus is found by least-squares fitting the surface harmonic expansion to the set of NE points assigned to that nucleus. The centroid (x_0,y_0,z_0) of the set of NE points is calculated and is used to define the origin of the spherical coordinate system for that nucleus. Next, a set of equations is set up, one for each point to be fit. These are of the form:

$$r_i = r(\theta_i,\phi_i) \qquad (2)$$

The unknown parameters to be estimated are a_n , a_{nm} , and b_{nm} ,the coefficients of the surface harmonic expansion, which determine the function r(), and hence the shape of the

nucleus, by equation (1). The position of each point (x_i, y_i, z_i) to which the surface will be fitted is converted into spherical coordinates (r_i, θ_i, ϕ_i). Given N_p such points to fit, we seek the coefficients that minimize the quantity:

$$\varepsilon^2 = \frac{1}{N_p} \sum_{i=1}^{N_p} [r_i - r(\theta_i, \phi_i)]^2 \tag{3}$$

This linear least squares problem is solved using a singular-value decomposition routine (NAG FORTRAN Library Mark 15, NAG Inc., Downers Grove, IL). As illustrated in Figure 3, the surface generated by this surface harmonic fitting matches the NE shape quite well, and smoothly spans gaps in the lamin signal. When the residual fitting error ε defined by equation (3) is averaged for 256 nuclei taken from five randomly chosen datasets, the average fitting error ε is 0.28 μm. Because the lamin in these images is approximately 0.5 μm thick (see below), and because points throughout this thick lamin image are used to fit the surface, we expect a residual fitting error on the order of half the thickness of the lamin image, or 0.25 μm, which is close to what is observed. Although a deviation in the surface of 0.28 μm will have some effect on the measured distances to the NE, these effects will be comparable (and to some extent due to) the uncertainty of where the actual surface of the nuclear envelope is within the lamin image.

To compute the distance of a FISH signal to the surface, the position $(r_{fish}, \theta_{fish}, \phi_{fish})$ of the manually chosen FISH spot is first determined in spherical coordinates. The radial distance from the FISH spot to the surface is then given by

$$d_r = r(\theta_{fish}, \phi_{fish}) - r_{fish} \tag{4}$$

Monte Carlo Analysis

To test for nonrandom association of a FISH signal with the NE, a set of randomly distributed points is generated within each individual nucleus (Figure 2D). The surface defined by equation (1) is used to define a volume within which to generate points. We compensate for the effect of the Rabl orientation by generating random points whose positions are distributed in the z axis with the same distribution as the observed FISH signals. To determine the distribution of z positions due to the Rabl orientation, the vertical offset between each FISH spot and the center of the nucleus is measured. The sample average and variance of these vertical offsets are computed. Then randomly localized points are generated in a system of Cartesian coordinates with origin at the center of the nucleus. The z (vertical) position of each point is a Gaussian-distributed random variable generated by the Box-Muller normal approximation (Press et al., 1989) with mean and variance equal to the sample mean and variance in the vertical position of the observed FISH spots relative to z0. The x and y positions are uniform random variables with range $\pm$ r_{cut} (defined above). For each point thus generated, the radial distance d_r to the surface as defined by equation (4) is computed. If $d_r<0$, the randomly generated point would lie outside the surface and is not to be considered, so that point is discarded and a new point is generated, this process being repeated until a point inside the surface is generated. For telophase nuclei, in which the nuclei are not all oriented the same way, FISH using a dodecasatellite probe was used to detect the centromeric region. A vector from the center of the nucleus to the center of the dodecasatellite signal was taken as the orientation of that nucleus. This vector was then used instead of the z axis to define the vertical axis for that nucleus, and all calculations of mean vertical position and random point generation were carried out in this frame of reference.

The set of random points is used to determine if a given FISH spot is unusually close to the NE. We define "close" as follows. For a given FISH spot, the above procedure is used to generate 5000 random points within the nucleus. These points are divided into two sets; those that are closer to the NE than the observed FISH spot (Sclose), and those that

are farther from the NE (Sfar). To compensate for non uniform distribution of bulk chromatin within the nucleus (Chung et al., 1990), the DAPI intensity at each point in each set is summed (yielding the sums Dclose and Dfar, respectively). A ratio is then computed

$$\rho = \frac{\text{Dclose}}{\text{Dclose} + \text{Dfar}} \qquad (5)$$

Note that ρ represents the fraction of chromatin that is closer to the NE than the observed FISH signal. If $\rho < 0.5$ then the FISH spot is declared "peripheral", since less than half of the chromatin is closer to the NE than the FISH spot. If $\rho > 0.5$ the FISH spot is classified as being "internal" from the NE, since more than half of the chromatin is closer. By this definition, without interaction with the NE, a random locus should be classified as "peripheral" approximately 50% of the time. Therefore a test is necessary to determine if in a large population of FISH points, the frequency of peripheral points is significantly greater than 50% (figure 2E). Note that classification of points as peripheral if they are closer to the NE than 50% of chromatin is arbitrary. As discussed below, if peripheral is redefined to include only those FISH spots closer to the NE than 80% of chromatin, the results of the analysis for the probes examined here is essentially the same. The reason that the choice of percentile for defining peripheral is not critical is that the statistical test takes this value into account, and simply looks for deviations from the expected frequency of a point being "peripheral". Attachment to the NE in some fraction of nuclei will cause a nonrandomly large number of FISH signals to be located near the periphery and will thus produce a deviation in the frequency of peripheral spots no matter what percent of chromatin is chosen for the definition. We note that the test is based on looking for subtle deviations in distribution, rather than simply scoring the frequency of actual NE contact, in order to increase the sensitivity of the search: FISH probes hybridizing to regions near, but not actually containing, an NE binding site will probably

not be localized exactly on the NE, but their distribution will still be biased to a more peripheral distribution.

Let there be a total of n FISH spots, out of which c are classified as "peripheral", and let the expected frequency of peripheral spots under the hypothesis that the locus is not interacting with the NE, and hence is distributed the same as a randomly chosen point, be p, where p=0.5 according to the above definition (note that, as noted above, other values for the expected frequency p can be used, in which case a different ρ would be taken as the cutoff for the definition of peripheral). The null hypothesis we wish to test is that the frequency of peripheral points is the same as that predicted for random points. We seek a critical value k* which is the maximum number of "peripheral" spots that we expect if the locus is in fact randomly localized with respect to the NE. Then if c>k* we would reject the hypothesis of randomness. For a significance level of α the critical value k^* can be expressed as:

$$k^* = np + 0.5 + Z_{1-\alpha}\sqrt{npq} \qquad (6)$$

where $Z_{1-\alpha}$ is the 1-α-percentile of the standard normal, and q=1-p. Equation (6) is the standard method for comparison of an observed frequency with an expected frequency given by p (Papoulis, 1990). The critical value is determined by choosing α = 0.001. Thus, if for a given FISH probe, more than k^* out of n spots are classified as "peripheral" we reject the hypothesis of randomness with P<0.001, and conclude that the locus in question is associated with the nuclear envelope. Loci for which the hypothesis of randomness has been rejected will henceforth be referred to as "close".

If we consider the fraction of points classified as "internal" relative to the NE, it is possible to formulate a similar test to detect loci that are nonrandomly targeted to the nuclear interior. In this case, the same statistical test applies, except that in this case if more than k* out of n spots are "internal" , we conclude a nonrandomly interior localization. Such

regions will henceforth be referred to as "far" from the NE. Loci which are classified as neither "close" nor "far" will be classified as "random", because their localization cannot be distinguished from that of a random point by this test. We note that although a relatively stringent value of α (0.001) was used in the test, for the loci classified as random in Table 1, the null hypothesis of randomness could not be rejected even when setting α=0.01, a much less stringent test. Thus, the discrepancy between close and random loci was quite large and the danger of false positives is small. As a test of the self-consistency of the algorithm, we used the random-point generation scheme outlined above to generate, in each nucleus of an actual dataset, one or two point (depending on the number of FISH spots observed in the actual data). In order to bias the choice of random points according to the DAPI intensity distribution, initially 1000 points were generated for each nucleus and their positions, along with the DAPI intensity at that position, stored as records in an array. A random number X was then generated between 0 and the total sum of the DAPI intensities for all 1000 points. The array of points was then traversed in order, and at each new element in the array the DAPI intensity was added to a running sum. When this sum exceeded the random value X, that element of the array was then chosen. In this way, the chance that a particular element of the array would be chosen was proportional to the DAPI intensity at that point. These random points were then fed back into the Monte Carlo test routine, and the test performed. For a dataset of 49 FISH spots, this procedure was carried out five times using a different initialization of the random number generator for each run. The results were a number c of peripheral spots of 17,26,24,22,26 out of 49. In no case were these number significantly different from random. By contrast, the actual FISH data showed a highly significant association with the NE. Thus the algorithm is consistent in that random points generated artificially are indeed classified as random.

As mentioned above, the results presented here do not depend on the choice of p. If p=0.2 is used instead, the result is essentially the same, with the exception that DS00178, DS00277, DS05247, and DS07049, which are classified as close when p=0.5, are

classified as random when p=0.2. Note that of these four sites, only one showed a highly significant (α=0.001) association with the NE, and this result only affects the apparent extent of the NE associated regions, not their number or location. Finally, we reiterate that this test is designed to detect sites whose localization is biased towards the NE. This should include sites near but not actually including an NE binding site. The test was designed in this way in order to allow mapping of NE association sites using coarsely spaced probes, so that a large region of a chromosome can be covered without having to use a contiguous set of probes, and still detect most if not all NE association sites. For this reason, however, we should expect that many loci tested will show a peripheral bias in their localization, without actually touching the NE in the majority of nuclei.

Analysis of double-label experiments

Embryos labeled with two different probes in two different colors were analyzed to determine which probe of the pair was closer to the NE. Nuclear surfaces were represented as above, and distances measured using equation (4). Only pairs of FISH spots for which one or both spots were within 0.3 μm of the NE were used for analysis. Distances to the NE were compared between the two adjacent spots. When tabulating Table 2.3, pairs of spots for which the difference between the two distances is less than 0.1 μm were counted as being equidistant from the NE, so that only relatively major differences in distance were counted when determining which spot is closer.

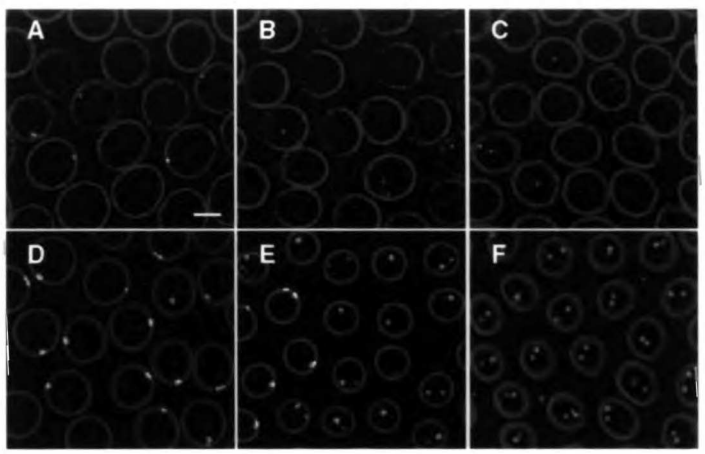

Figure 2.1

Figure 2.1. Single optical sections taken from 3D multiwavelength images of cycle 13 embryos. Specific chromosome regions are localized using FISH (in pink) followed by lamin immunofluorescence (in green) to visualize nuclear envelope. In this figure, not all nuclei appear to contain FISH spots because these images are only single optical sections. (A-C) Probes made from P1 clones of euchromatic sequences, (D-F) probes made from heterochromatic satellite sequences. (A) DS03071 is NE associated. (B) DS00861 is randomly localized. (C) DS08107 is nonrandomly far from the NE. (D) AATAC satellite, NE associated. (E) AACAC satellite, randomly localized. (F) Rsp, nonrandomly far from NE. Bar, 4 μm.

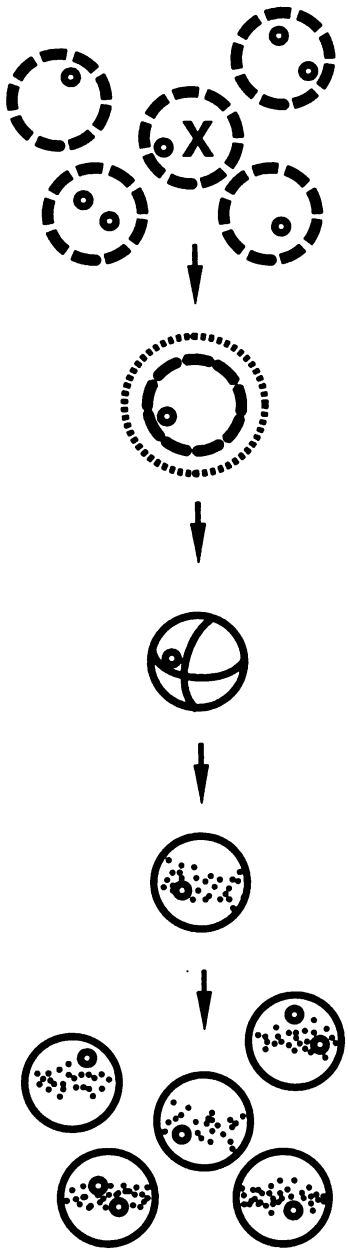

(a) Pick center of nucleus interactively. Center of current nucleus denoted by X; small circles (●) denote FISH signals.

(b) Cut out cylindrical region of image surrounding each nucleus

(c) Fit mathematically defined 3D surface (surface harmonic expansion) to lamin intensity pattern

(d) For each nucleus, compare localization of FISH spot with randomly generated points (small dots)

(e) In a population of nuclei, are the FISH spots significantly closer to the NE than the randomly generated spots? If so, conclude NE association

Figure 2.2. Diagram of image analysis procedure

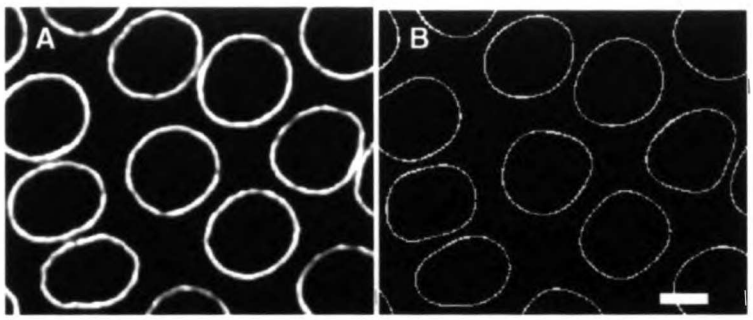

Figure 2.3. Fitting of NE using surface harmonic expansion fit to lamin signal

Figure 2.3. Fitting of NE using surface harmonic expansion fit to lamin signal. (A) single optical section through 3D lamin image. (B) surface harmonic expansions for the nuclear surfaces in (A), plotted in the corresponding plane only. Notice that the lamin signal is punctate and that the nucleus is not, in general, ellipsoidal. As illustrated in (B) the surface harmonic expansion fits a smooth closed surface to such irregular shapes. Bar, 4 μm.

RESULTS

Strategy for detecting NE association

A novel statistical test for NE association has been developed in which the positions of specific loci are determined by fluorescence in situ hybridization (FISH) followed by anti-lamin immunofluorescence to visualize the NE (see Figure 1 for examples). The DNA in-situ hybridization method employed here has been carefully optimized to preserve large-scale chromosome structure, based on a number of criteria including direct comparison with live chromosome structure (Hiraoka et al. 1993). Following three-dimensional data collection using wide-field fluorescence microscopy, the images are analyzed using the procedure summarized in Figure 2. Nuclei and FISH signals are located within the image and the nuclear surfaces are computationally modeled using the anti-lamin immunofluorescence image data (Figure 3). A large number of randomly localized points are then generated within the nucleus, and the distribution of distances from each point to the surface is computed. This distribution is then compared with the observed distances to the surface to determine if the locus is nonrandomly associated with the NE. This statistical analysis, described in Materials and Methods, is unique in that it takes into account the effects of variation in nuclear shape, large-scale chromosome organization, and nonuniform distribution of bulk chromatin, thus representing a significant advance over previous statistical techniques for detecting NE association (van Dekken et al., 1990, Hoefers et al., 1993). The large variations in nuclear shape such as we observe in Drosophila embryos can result in significantly altered distributions of points within the nuclei, indicating that it is essential to explicitly model nuclear shape as done here, and not merely assume that all nuclei are spheres or ellipsoids. Loci which are NE associated will henceforth be referred to as "close". Loci for which an NE association is not apparent fall into two classes. One class is localized nonrandomly to the nuclear interior (which will be referred to as "far")

and the other has a distribution matching that of a random point, and is hence termed "random". Formal definitions of "close", "random", and "far" are given in Materials and Methods.

Detection of specific chromatin-NE interactions

The procedure described above has been applied to a number of loci, primarily on chromosome arm 2L, with results listed in Table 2.1, and diagrammed schematically in Figure 4. All results presented here were obtained from cycle 13 Drosophila embryos. 14 out of 32 probes to euchromatic loci showed a nonrandomly peripheral localization, which we interpret as indicating an interaction with the NE. Out of 6 heterochromatic loci probed, only two (the AATAC satellite and the rDNA locus) were NE associated, while four (the AACAC satellite, Rsp, dodecasatellite, and the 359bp repeat) were not. Peripheral localization of a particular probe does not necessarily imply that an NE attachment site resides within the region of hybridization, because an NE attachment site near, but not actually inside, the region could be sufficient to recruit the flanking region to the nuclear periphery. For this reason, although clusters of linked probes (for example DS07167, DS00178, DS06189, and DS02634) all show peripheral localization, the actual attachment site does not necessarily span such a large region. The fact that most attachment sites are detected by several adjacent probes simply reflects the design of the test for NE localization, which, as detailed in Materials and Methods, is expected to detect loci near enough to an actual NE binding site to have their localization biased towards the periphery, even if the loci probed are not themselves bound to the NE. In many cases in Table 2.1, one probe may be strongly NE associated while a neighboring probe has a completely random localization. These drastic differences in localization of neighboring probes is actually not surprising in that the probes used here are spaced roughly 200 kb apart on the genome based on their location on polytene squashes. While we do not know how genomic distance corresponds to physical distance in Drosophila, work in mammalian cells

(Yokota et al., 1995) has indicated that loci 100 kb apart are roughly 0.4 μm apart in interphase. Thus, probes 200 kb apart can potentially have quite significant differences in nuclear position. In Table 1 it is apparent that for random probes, approximately 50% of the FISH spots are classified as "peripheral". This is due directly to the definition of peripheral spots as those which are closer to the NE than 50% of randomly generated points. For a randomly localized point, this will occur approximately 50% of the time. Thus the result in Table 1 for random points is exactly what we would expect a priori. For most of the probes used here, data were collected from two or more embryos. In all such cases, the results for any one probe are the same in different embryos. Representative probes were tested on different batches of fixed embryos and the results were consistent between batches of embryos.

Direct analysis of NE contact frequencies supports the conclusions of the statistical analysis. In these images, the apparent width of the lamin signal is 0.5 μm and the apparent diameter of the FISH signal is approximately 0.6 μm. These dimensions are significantly greater than the lateral resolution of the microscope (approximately 0.1-0.2 μm) and thus probably represent the actual size of the fluorescent region. Distances used for this analysis are measured from the center of the FISH spot to the center of the lamina, as described by equation 4 in Materials and Methods. However, if chromatin on the edge of the FISH spot were to touch the edge of the lamina, the distance between centers would be the sum of the radius of lamina and FISH spot, which is 0.55 μm. Thus, any spot whose center is within approximately 0.55μm of the center of the lamina is close enough to potentially be in contact with the NE. Table 1 tabulates the frequency with which probes fall within 0.6 μm of the surface, as determined by equation 4. Summing the data in Table 2.1 for the individual classes of loci, the average frequencies with which a close, random, or far FISH spot is close enough to the NE to be touching it are 0.47, 0.31, and 0.05, respectively, verifying that spots which are NE associated according to the Monte Carlo test are indeed more frequently near the NE than random or far points.

Table 2.1. Probes Tested for NE Association

Probe	Locus	Result	n	c	f_c	d_{av} (μm)	z_{av} (μm)
DS05785	97D1-97D2	random	35	17	0.51	0.61	0.1
DS03117	90C7-90C8	random	49	30	0.37	1.0	-0.2
DS04383	87B1-87B2	CLOSE	126	91	0.48	0.8	0.5
DS00189	84A6-84B2	random	38	20	0.16	1.2	0.6
histone	39D-39E	FAR	114	9	0.01	2.0	1.8
histone*	39D-39E	FAR	135	24	0.04	1.8	-0.7
DS08107	39B3-39B3	FAR	50	9	0.06	1.8	1.4
DS00861	35F1-35F2	random	97	41	0.12	1.4	0.4
DS01406	35E1-35E2	random	39	17	0.23	1.4	-0.3
DS08880	35C4-35C4	random	62	31	0.23	1.3	0.3
DS01695	35B3-35B6	CLOSE	215	156	0.42	0.9	0.2
DS03792	35A1-35A2	CLOSE	197	127	0.36	0.9	0.6
DS00889	34F3-34F4	CLOSE	138	94	0.36	1.0	0.2
DS03933	34F2-34F3	CLOSE	82	56	0.51	0.8	0.3
DS05899	34F1-34F2	CLOSE	220	166	0.43	0.8	0.5
DS02809	34F1-34F2	random	98	51	0.28	1.1	0.5
DS00428	34E4-34E5	random	32	21	0.47	0.8	0.2
DS03232	34E1-34E2	random	55	29	0.29	1.2	0.4
DS04191	34D1-34D6	random	19	10	0.16	1.3	0.8
DS01386	34C4-34D2	random	47	27	0.28	1.1	0.3
DS00576	34A5-34A11	CLOSE	117	80	0.44	0.8	0.3
DS03455	34A1-34A2	random	35	24	0.49	0.8	0.0

DS04289	33D4-33E2	random	24	11	0.29	0.9	-1.3
DS07167	33D3-33D4	CLOSE	68	50	0.49	0.8	-0.1
DS00178	33C1-33C6	CLOSE	128	82	0.38	1.0	0.1
DS06189	33A3-33A8	CLOSE	40	32	0.55	0.7	-0.8
DS02634	32E1-32E2	CLOSE ($p<0.01$)	37	27	0.41	1.0	-0.2
DS07149	23B2-23C1	random	43	27	0.37	0.7	-1.4
DS00244	23A1-23A2	CLOSE	52	38	0.58	0.7	-1.5
DS00330	22F1-22F2	random	29	20	0.48	0.8	-1.1
DS00350	22E1-22E2	random	77	48	0.48	0.6	-1.5
DS08106	22C1-22C2	random	63	32	0.37	0.8	-1.6
DS06378	22B3-22B9	CLOSE ($p=0.01$)	86	54	0.49	0.7	-1.4
DS05247	22A4-22B1	CLOSE ($p=0.01$)	110	70	0.53	0.7	-1.0
DS00277	22A1-22A2	CLOSE ($p=0.01$)	78	49	0.55	0.5	-1.5
DS03071	21E3-21E4	CLOSE	76	59	0.72	0.4	-2.1
DS07049	21B2-21B8	CLOSE ($p<0.01$)	119	74	0.56	0.5	-1.8
rDNA	h20 & h29	CLOSE	131	89	0.26	1.0	0.1
dodeca	h53	FAR	65	16	0.03	1.4	1.7
AACAC	h45	random	53	26	0.32	0.9	3.1
AATAC	h6	CLOSE	31	28	0.87	0.3	-0.2
359bp	h31-h32	FAR	32	6	0.00	1.2	1.7
Rsp	h39	FAR	100	9	0.13	1.0	1.9

---

* Position of histone locus in lt^{x13} homozygotes.

Abbreviations: number of FISH spots used in analysis (n), number of spots classified as "peripheral" (c), fraction on FISH spots within 0.6μm of the surface (f_c), average distance from FISH spot to surface (d_{av}), average vertical position relative to nuclear center of mass (z_{av}).

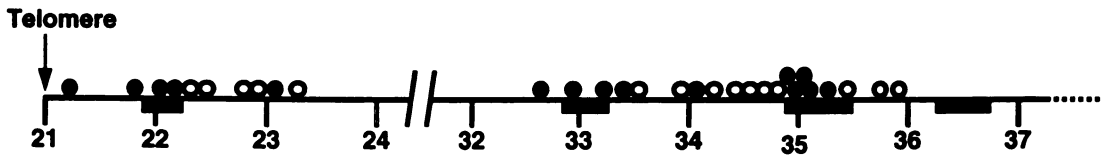

Figure 2.4. Map of NE association sites for the left arm of chromosome 2.

Figure 2.4. Map of NE association sites for the left arm of chromosome 2 in cycle 13 embryos. Numbered subdivisions given below line. Each numbered subdivision is approximately 1 Mb. Black rectangles below line indicate sites of frequent NE contact in polytene nuclei (Hochstrasser et al., 1986). Localization of specific regions as determined by FISH using P1 derived probes followed by statistical test for NE association (see Table 1) plotted above line: (●), P1 probes hybridizing to NE associated regions, (o), P1 probes hybridizing to randomly localized regions.

Why do most NE associated sites only contact the NE in a fraction of nuclei? First of all, the statistical test is designed to detect loci near but not actually containing an NE binding site, and such loci are not expected to contact the NE in most nuclei, even if their localization is peripherally biased. Results presented below using a set of neighboring probes in one particular peripheral region will further reinforce this point. Secondly, as demonstrated below, at the beginning of interphase, most NE associated sites are randomly arranged within the nucleus, and some time will be required for the chromatin to diffuse to the NE before any interaction is possible. Because interphase in cycle 13 embryos is so short (less than 20 minutes, see Foe et al., 1993), and diffusion of a large polymer like chromatin is slow, in a significant fraction of nuclei a given NE interaction site will simply not have time to reach the NE, and thus will not be able to make contact with it.

Table 1 also lists the average distance from each probe to the NE. Overall average distances to the NE for the three groups of loci classified as close, random, and far are, respectively, 0.78±0.2 μm, 1.03±0.25 μm, and 1.52±0.41 μm. The differences in these averages are highly significant, with $P<0.001$. Thus, classification based on the Monte Carlo test reflects statistically significant differences in distance to the NE. Note that the contact frequency and average distance differences do not take into account effects due to differences in nuclear shape or chromatin distribution, thus the fact that the results of the Monte Carlo analysis are mirrored in these simpler comparisons increases our confidence that the specific details of the Monte Carlo procedure are not leading to erroneous results, and also suggests that the NE associations seen are not so subtle as to be missed by simpler measurements. Note also that the comparison of contact frequencies has the been the most frequently applied criterion for NE association used by other workers (Hochstrasser et al., 1986, Manuelidis and Borden, 1988). Differences in contact frequency are also qualitatively evident by direct inspection. Visual inspection (Figure 1) reveals that probes which, by the Monte Carlo test, are NE associated, appear more frequently to contact the NE than randomly localized probes.

Some loci, such as the histone locus or the dodecasatellite (see Table 1) are nonrandomly located in the interior of the nucleus. This localization is statistically highly significant ($P<0.001$) and is reproducible in different embryos. As indicated in Table 1, both heterochromatic (e.g.. dodecasatellite) and euchromatic (e.g.. histone locus) regions can show this localization pattern.

NE associations are established later than telophase

If the NE interactions described here are the remnants of interactions primarily involved in NE reassembly following mitosis, then these sites would have been bound to NE vesicles following anaphase, and should already be NE associated during telophase. FISH and lamin immunofluorescence were carried out, and data collected from telophase nuclei, as shown in Figure 5. All images were acquired from nuclei in which NE assembly was complete but in which nuclei had not yet rotated into their interphase orientation (reviewed in Foe et. al. 1993). Orientation was determined by carrying out FISH using dodecasatellite probes to localize the centromeric regions, as described in Experimental Procedures. As listed in Table 2.2, the NE association pattern in telophase is dramatically different. Loci which are NE associated during interphase are generally not NE associated during telophase, while other loci, such as dodecasatellite itself, appear NE associated in telophase but not in interphase. These changes are reflected in differences in frequency (f_c) of NE contact and average distance (d_{av}) to the NE. The most extreme example is the AATAC satellite which is strongly NE associated in interphase but is in fact nonrandomly far from the NE in telophase. Although the nucleus increases in size between telophase and interphase, the AATAC site actually becomes closer to the NE (d_{av} goes from 0.9 μm to 0.3 μm). Thus, the interphase NE interactions tabulated in Table 2.1 do not appear to be involved in NE assembly during telophase, but are in fact established later.

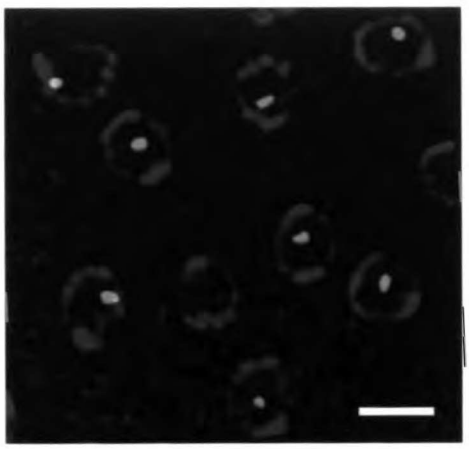

Figure 2.5. Example of FISH and lamin immunofluorescence in telophase.

Figure 2.5. Example of FISH and lamin immunofluorescence in telophase preceding cycle 13. (Pink) FISH signal from AATAC satellite probe, (Green) Lamin immunofluorescence signal. It is important to note that the AATAC satellite block is strongly NE associated during interphase of cycle13. This figure thus demonstrates the dramatic rearrangements taking place following telophase. Bar, 4μm.

Table 2.2. Changes in NE association between telophase and interphase

	Telophase			Interphase		
Probe	Localization	f_c	d_{av} (μm)	Localization	f_c	d_{av} (μm)
DS00861	random	0.59	0.4	random	0.12	1.4
DS01695	random	0.58	0.5	CLOSE	0.42	0.9
DS00576	random	0.31	0.7	CLOSE	0.44	0.8
AATAC	FAR	0.14	0.9	CLOSE	0.87	0.3
dodeca	CLOSE	1.0	0.02	FAR	0.03	1.4
histone	random	0.65	0.6	FAR	0.01	2.0

Abbreviations: fraction on FISH spots within 0.6μm of the surface (f_c), average distance from FISH spot to surface (d_{av}).

Delimiting an NE binding region using pairs of probes

Figure 4 indicates that relatively large regions, defined by several adjacent FISH probes, show some degree of NE association. For example, the entire region 34F - 35B shows a nonrandomly peripheral localization. Based on the size scale of the Drosophila cytological map, where one division (e.g. 35) spans approximately 1Mb, the region from 34F-35B is roughly 500 kb in size. Does this reflect a general adhesion over a large region, or is there a discrete binding site which recruits flanking chromatin to the periphery? In order to locate the actual NE interaction site within such a large region, embryos were hybridized simultaneously with pairs of probes, one labeled with fluorescein and one labeled with rhodamine. An image of such an embryo is given in Figure 6A. In each nucleus, the distance from the NE to each FISH spot in each color was measured, allowing us to ask if one spot was consistently closer than another. If one FISH probe hybridizes nearer to, or within, the actual NE binding site, then it will tend to be closer to the NE than a FISH probe hybridizing further away. However, note that because in some nuclei the locus may not actually be bound to the NE but merely coincidentally near the periphery, it is possible for the probe that is farther from the binding site to actually be closer to the NE in some nuclei. For this analysis, only pairs of FISH spots for which at least one spot was within 0.3 μm of the NE were employed, so that only pairs which could be in contact with the NE were scored. The results for four pairs of probes are given in Table 3, and summarized graphically in Figure 6B. It thus appears that probe DS03933 is closer to the NE than any other probe in this region, which is consistent with the frequencies of NE contact tabulated in Table 2.1. This result suggests that a single NE binding site is in or near the region spanned by DS03933, with the remaining flanking probes recruited to the periphery because they are near to this site on the chromosome.

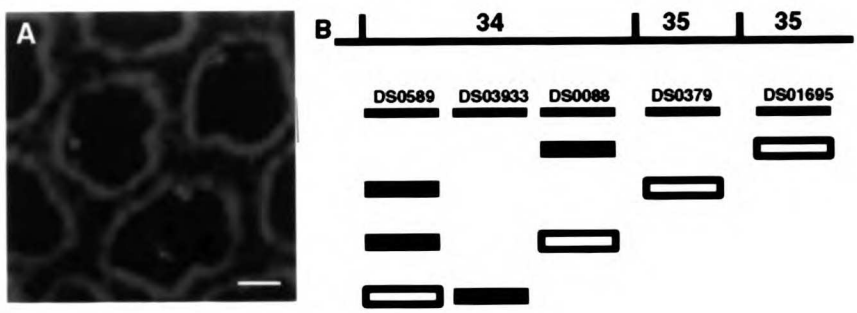

Figure 2.6. Mapping the NE association site at 34F–35B using pairs of FISH probes.

Figure 2.6. Mapping the NE association site at 34F-35B using pairs of FISH probes labeled in two different colors. (A) Single section from one such double-label dataset, rendered in pseudocolor to visualize lamin fluorescence along with two different FISH colors. (Pink) DS00889 probe labeled with rhodamine, (Yellow) DS01695 probe labeled with fluorescein, (Green) anti-lamin staining using Cy-5 conjugated secondary antibodies. Scale bar, 2 μm. (B) Result of double label experiment, as tabulated in Table 2.3. Probes are aligned to cytogenetic map at top of figure. Pairs of rectangles below probes indicate pairs of probes compared. Black rectangles indicate probes which were closer in the majority of nuclei, white rectangles represent probes which were farther.

Table 2.3. Comparison of distance to NE between pairs of neighboring probes

Red Probe	Green Probe	$d_R<d_G$	$d_R=d_G$	$d_R>d_G$
DS01695	DS00889	9	4	19
DS00889	DS01695	9	4	4
DS03792	DS05899	12	16	26
DS05899	DS03792	4	2	0
DS05899	DS00889	11	11	6
DS05899	DS03933	4	6	10

Abbreviations: Distance measured from the red FISH spot to the NE (d_R). Distance measured from the green FISH spot to the NE (d_G). Columns list number of nuclei in which red spot is closer, equidistant, or farther from the NE than the green spot. See Materials and Methods for precise definition of distances. Pairs for which the difference in distance to the NE was less than 0.1 μm were counted as equidistant.

Polarized configuration of interphase chromosomes

In many cell types, chromosomes are polarized, with telomeres clustered at one end of the nucleus, and centromeres clustered at the other. This polarized configuration is known as the Rabl orientation (reviewed in Comings 1980). An outstanding question, though, has been to what extent is the entire chromosome linearly polarized? Does the chromosome follow a meandering path down through the nucleus, looping back on itself, or is it strung more directly, with vertical position a monotonicaly decreasing function of genomic distance from the centromere? The answer to this question will, to some extent, reflect the degree of decondensation of the mitotic chromosome. The reason this question has been difficult to address in general is that while both telomeres and centromeres can be shown to be clustered, this provides no informatino about the path the rest of the chromosome is taking. Chromosome painting can be used to delineate the whole chromosome, but again the path of the chromosome fiber within the painted domain cannot be determined. The key is to use FISH together with an external frame of reference to define the vertical axis. In *Drosophila* embryos all nuclei have the same orientation relative to the embryo surface (Hiraoka et al., 1990a, Hiraoka et al., 1993, Foe and Alberts, 1985), with centromeres grouped outward, on the top of the nucleus nearest to the surface of the embryo, and telomeres pointing inwards. When 3D images are collected, all nuclei in the embryo lie in a plane perpendicular to the optical axis (z-axis) of the microscope. For each locus, the average vertical position of the FISH signal relative to the center of mass of the nucleus was measured and compared to its genomic location in order to test for a Rabl chromosome orientation. The vertical position of the FISH signal for given locus is quite consistent, having a standard deviation in the range 0.4-0.8 μm, so that within a nucleus approximately 7 μm in height, the loci are constrained to lie within a disk-like region 1-2 μm thick. We have listed in Table 1, and plotted in Figure 7, the average vertical positions (z_{av}) of each probe, from which the Rabl orientation is generally evident: loci near the telomere are lower in the nucleus than loci near the centromere.

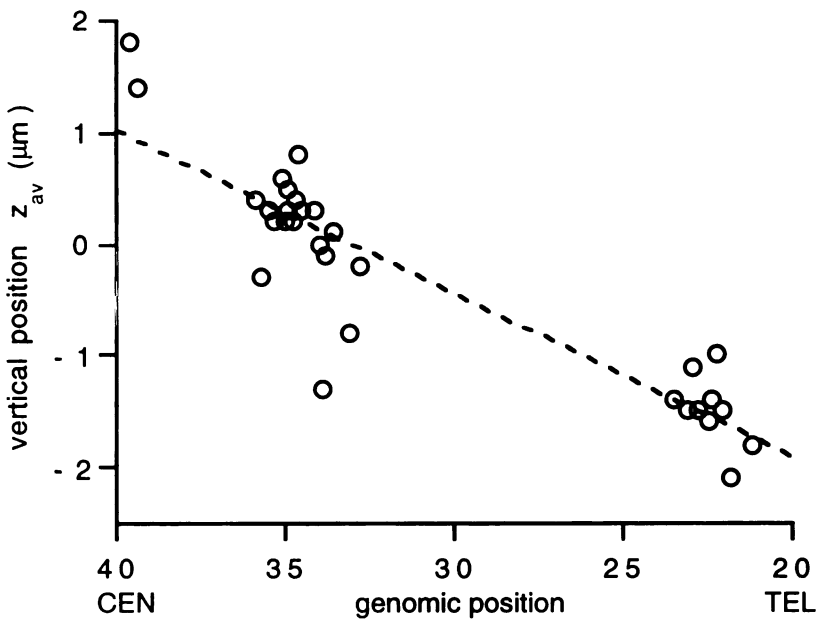

Figure 2.7. Polarized (Rabl) configuration of chromatin in interphase nucleus. Vertical position taken from Table 1 plotted versus position on chromosome arm 2L, along with best-fit line. Larger values of z_{av} correspond to the end of the nucleus nearest to the surface of the embryo.

Different loci occupy defined positions in the nucleus

An outstanding question in nuclear organization has been the extent to which a given locus occupies a predetermined position in the nucleus. We can measure position of a FISH spot by two values, the vertical position (z) and the radial distance to the surface (d). These two coordinates are illustrated in Figure 8A, and defined more precisely in Materials and Methods. Presumably, the Rabl configuration sets the vertical position of a particular locus and localization relative to the NE determines the average distance from the locus to the NE, thus setting the radial position. The average values of these two positional coordinates, listed in Table 1, are plotted for several loci in Figure 8B. The striking result of Figure 8B is that different loci do in fact consistently occupy different territories within the nucleus. Furthermore, these coordinates can be specified independently. The position of one site (the histone locus) was analyzed in embryos homozygous for the lt^{x13} translocation (Wakimoto and Hearn 1990), which translocates the left arm of chromosome 2 to a distal position on the right arm of chromosome 3 (see Figure 8C) with the effect that the histone locus is now shifted to a much more distal position. Figure 8D plots the localization of the histone locus in lt^{x13} as compared to wild type. As expected from its more distal position, and as has been previously demonstrated (Hiraoka et al., 1993), the vertical position of this locus is now more than 2 μm lower in the nucleus, which is what a Rabl configuration would predict. However, the average distance from the locus to the NE is the same as in wild type, indicating that the radial position is unaffected. The breakpoint of lt^{x13} on 3R is located in region 97D, and as shown in Table 1 the 97D region is much closer to the NE than the histone locus. Thus, in lt^{x13} the highly internal radial position was indeed conferred by the histone locus or its flanking regions on 2L, and was not a feature of the adjacent region on 3R.

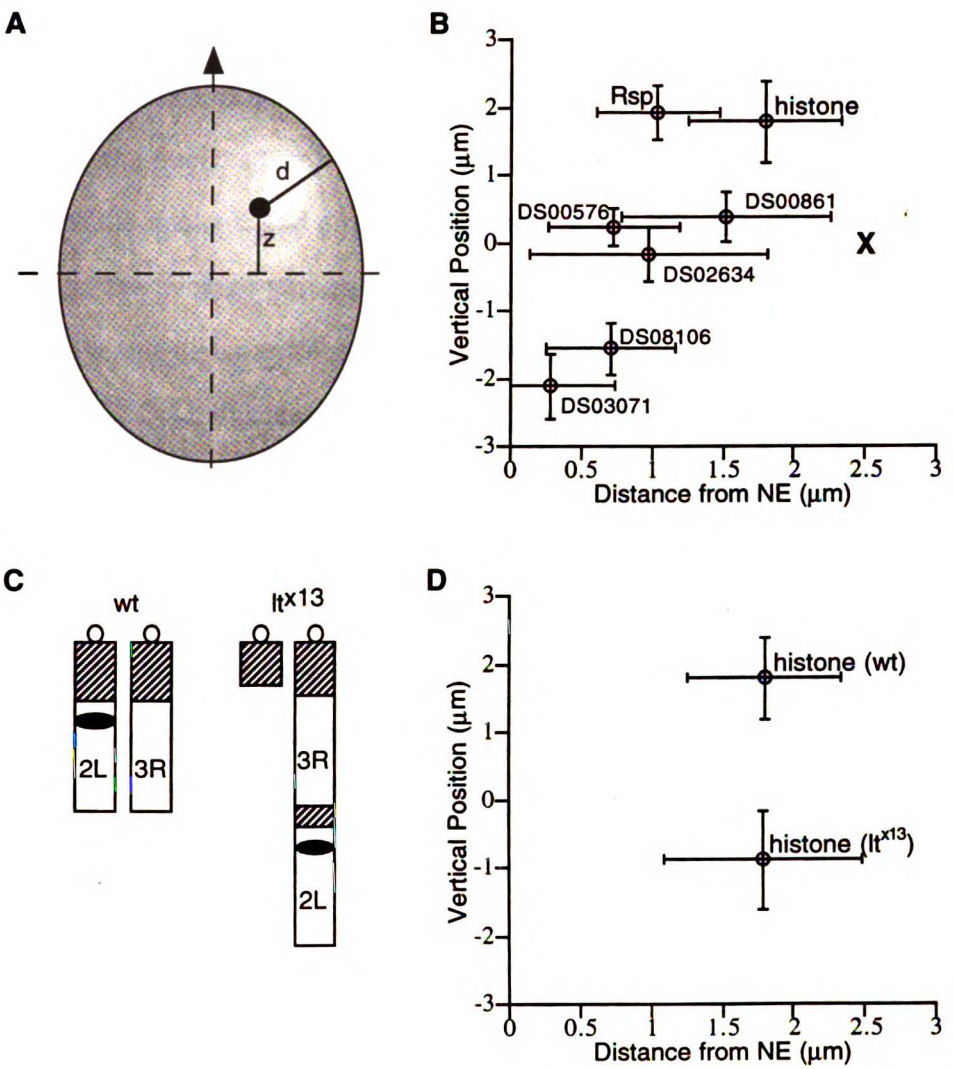

Figure 2.8. Defined positioning within the nucleus

Figure 2.8. Defined localizations of different loci to specific regions within the nucleus. (A) Position within the nucleus can be described by two coordinates, a vertical height z above the center of the nucleus, and a radial distance d to the NE, given by equation (4). (B) For each locus, the average vertical position relative to the center of the nucleus is plotted versus the average distance from the NE. Error bars indicate one standard deviation in each measurement. (X) indicates the average position of the center of the nucleus. (C-D) Vertical position and distance from NE specified independently. (D) Diagram of translocation. Chromosome arrangement in wild type and lt^{x13} translocation; the histone locus is represented by a filled ellipse; hatched and open boxes represent heterochromatin and euchromatin, respectively; the open circle represents the centromere.(D) The localization of the histone locus is plotted as in (B) for wild type embryos and for embryos homozygous for the lt^{x13} translocation. Shifting histone locus to a more distal position alters vertical position without affecting radial position.

DISCUSSION

Distribution of NE association sites

Three-dimensional FISH in conjunction with a semiautomated statistical method has been developed to detect specific chromatin-NE associations, and this approach has been used to demonstrate the existence of site-specific chromatin-NE interactions in nuclei in intact cycle 13 Drosophila embryos. One important caveat of this work is that in the cycle 13 embryo zygotic transcription has not yet reached maximum levels, and thus it will be interesting in the future to examine NE interactions in later embryos and adult tissues to determine the effects of transcription and differentiation. Based on these results, in which NE contacts have been mapped along a region covering approximately one third of chromosome arm 2L, we estimate that there are on the order of 15 NE interaction sites per arm, or a total of 150 NE association sites per diploid nucleus. Note that this value has been extrapolated from a relatively small portion of the genome, and the density of NE contact sites may differ in other regions. These NE-associated sites would be spaced, on average, 1-2Mb apart, and could thus define the boundaries of large loop domains tethered to the NE in interphase. Evidence for large chromosome loops on the order of 1Mb in human interphase nuclei has recently been reported (Yokota et al., 1995). We propose that large chromosome loops could be tethered by attachment either to the NE or to an internal structure. Existence of distinct peripheral and internal chromatin anchoring sites has previously been proposed on the basis of in vitro experiments (Lebkowski and Laemmli, 1982). In addition to forming large loops, NE attachment could potentially have direct effects on the NE associated loci. It is apparent in Figure 4 and from the results given in Figure 6B that a large region (100-500 kb, assuming 1Mb per division) flanking each interaction site can be brought to the periphery by a relatively discrete NE association site, so that NE binding at one site could influence the subnuclear localization of a relatively

large flanking region. An NE binding site can thus exert an influence on surrounding DNA by targeting it to the NE.

The specificity of NE association is interesting in light of recent work suggesting that the primary molecular interaction between chromatin and the NE may be binding of lamin protein to the core histones (Taniura and Gerace, 1995). Since this interaction does not involve DNA it should not be sequence specific. However, it is entirely possible that local variations in chromatin structure could bring about specific spatial arrangements of nucleosomes which would be able to interact cooperatively with the nuclear lamin lattice. If this turns out to be the case, it will be difficult to isolate a small DNA sequence that confers NE association. Rather, association will be dictated by the chromatin context.

Only a fraction of heterochromatin is associated with the NE in these nuclei. This is in contrast with a common assumption that all heterochromatin is NE associated, and suggests that specific DNA sequences, rather than the heterochromatic state in general, are required to confer NE attachment to heterochromatin. It is, however, probable that in the cycle 13 embryo, the heterochromatic state is not yet fully established (Hiraoka et al., 1993). Comparative studies of NE association in cycle 14 embryos and more developmentally advanced tissues should resolve this issue.

Some regions (the histone locus, dodecasatellite, and Rsp) are not only not associated with the NE, but are in fact nonrandomly far from the NE. This type of localization has been previously described in other cell types (Lawrence et al., 1988, Hoefers et al., 1993, Vourc'h et al., 1993), and may reflect an association with an internal matrix or scaffold. This implies that the nucleus may contain at least two types of subnuclear neighborhoods, a peripheral NE associated neighborhood, and an internal, possibly matrix associated, neighborhood.

Other loci are classified as randomly localized. However, this is based solely on distance to the NE, and does not imply that the loci occupy completely random positions in

the nucleus with respect to other criteria. Indeed, with respect to vertical positioning (the Rabl orientation) the localization of these loci is clearly nonrandom.

Having identified several NE associated loci, it should now be possible to test their effects by inserting reporter genes into these regions, or using chromosome rearrangements to alter the pattern of attachment. Furthermore, the door is now open for a directed search for the molecular components of these interactions. In particular, the method illustrated in Figure 6 of comparing the localization of pairs of nearby probes should allow specific NE binding sites to be pinpointed more precisely. The probes used in Figure 6B fall in a region spanned by a contiguous set of overlapping P1 genomic clones (Berkeley Drosophila Genome Project, personal communication), which should allow us, in the near future, to map the NE binding site to within a single P1 clone. Such experiments are currently underway.

Comparison with previous studies of nuclear organization

Three dimensional reconstructions of polytene nuclei from *Drosophila* salivary glands (Hochstrasser et al., 1986) revealed a number of loci which were found near the NE with an unusually high frequency. These frequent NE contacts were observed at the same loci in other polytenized tissues (Hochstrasser and Sedat, 1987) suggesting they may be a general feature of nuclear organization. The presence of sites with relatively high frequency of peripheral localization relative to other sites could, however, reflect either an NE association of the former sites or a nonrandomly internal localization of the latter sites. In those studies, four significant NE contact sites were observed on chromosome 2L, at regions 22A-B, 32F-33A, 34F-35C, and 36C-E. (Hochstrasser et al., 1986). Figure 4 reveals that of the three regions tested so far (22A-B, 32F-33A, and 34F-35C) all three regions are also associated with the NE in the embryo, suggesting that these interactions can be maintained over long developmental times, and further implying that the high frequency surface contacts seen in the polytene nuclei are indeed due to NE associations.

However, several regions that are associated with the NE in the embryo, such as 23A, 34A, and 87B, are not in particularly frequent contact with the NE in polytene nuclei (Hochstrasser et al., 1986), suggesting that these associations may be lost during polytenization. This is consistent with studies of NE-chromosome contact in polytene chromosomes of *Chironomus* and *Acricotopus* (Quick, 1980) in which a progressive loss of NE contact was found to accompany polytenization.

Telomere-NE interactions have been proposed to play a role in meiosis (Loidl, 1990) and telomeric silencing (Palladino et al., 1993). Peripheral localization of telomeres during interphase has previously been reported (Manuelidis and Borden, 1988, van Dekken et al., 1989, Chung et al., 1990) while in other cell types telomeres are more internally located (Ferguson and Ward, 1992). Initial reports that telomeres in yeast were NE associated in a SIR4 dependent manner (Palladino et al, 1993) have subsequently been retracted following more careful three-dimensional analysis (Gasser 1996 ??????). While we have not used telomeric probes in this study due to difficulties with secondary hybridization to non-telomeric sites, the most distal probe employed thus far, DS07049, is indeed associated with the NE. This is in agreement with the observation than during prophase in the *Drosophila* embryo, telomeres often appear to be in contact with the NE (Hiraoka et al., 1990b).

In contrast to telomeres, centromeres are almost certainly not NE associated in the *Drosophila* embryo. Cytological and genetic studies have indicated that the heterochromatic Rsp and dodecasatellite blocks are closely linked to the centromeres of chromosomes 2 and 3, respectively (Wu et al. 1988, Pimpinelli and Dimitri, 1989, Carmena et al., 1993). Figure 4 reveals that both Rsp and dodecasatellite are, in fact, nonrandomly far from the NE, implying that centromeres are not NE associated, and may interact with an internal nuclear structure. Such a nonrandomly internal localization of centromeres has previously been reported in vertebrate cells (Hoefers et al., 1993, Zalensky et al., 1995) although other groups have reported peripheral localization of centromeres (Manuelidis and Borden,

1988, van Dekken et al., 1989, van Dekken et al., 1990, Ferguson and Ward, 1992, Vourc'h et al., 1993).

Relation to SARs and other known chromosomal elements

Scaffold attachment regions have been described in *Drosophila* embryos (Gasser and Laemmli, 1986). As discussed above, SARs were potential candidates for NE association sites because of the presence of large quantities of nuclear lamin proteins in the scaffold preparations. Four regions containing known SARs were probed in the present work. Of these, two, the Adh (35B3) and hsp-70 (87A7) loci were indeed within NE associated regions (see Table 1). However, another SAR, contained in the ftz locus (84B1), was in a randomly localized region, while a fourth , the histone locus (39D-E), was in fact nonrandomly far from the surface. This last result is particularly interesting in light of claims that naked DNA containing the *Drosophila* histone SAR can specifically bind lamin paracrystals in vitro (Luderus et al., 1992, Luderus et al., 1994). It has, however, previously been demonstrated that while Drosophila SAR DNA can bind nuclear scaffolds in vitro, if scaffolds are prepared which are highly enriched for lamins, and lacking the internal protein network usually seen in other scaffold preparations (Lebkowski and Laemmli, 1982), SAR DNA no longer binds (Izaurralde et all, 1988). The inability of SAR DNA to bind the NE-associated scaffold component in vitro is consistent with our data from intact cells, and implies that SARs do not confer NE association either in vitro or in vivo. In the two cases where a SAR is found in an NE associated region, there is no evidence that the SAR sequence itself is required for NE association. There is moreover a great deal of controversy surrounding the SAR preparation, and there remains a strong possibility that the nuclear scaffold is an artifact produced by the highly specific conditions employed during its preparation. For instance, scaffold preparations typically include both lamins and topoisomerase II, proteins which do not colocalize within the cell, implying that perhaps any large insoluble protein structures aggregate together during the scaffold

preparation. Thus, scaffold associated sequences could be binding to just one of these separate components, and thus have nothing to do with the nuclear envelope. On the other hand, evidence for some sort of intranuclear skeletal structure in vivo is gradually accumulating. Recently we have shown that two centrosomal proteins, CP60 and CP190, enter the nucleus in Drosophial embryos and form an insoluble protein network that can be observed in living cells injected with labelled protein (K. Oegema, W.F. Marshall, J. Sedat, and B. Alberts, manuscript submitted, see appendix ?????). During prophase and metaphase, when the nuclear envelope breaks down, these proteins remain inside the nucleus implying that they are actually assembled into some sort of large structure that could in fact represent a nuclear matrix (K. Oegema, W.F.Marshall, J. Sedat, and B.Alberts, manuscript submitted, see appendix ?????). How this structure relates to the usual scaffold preparations remains to be determined. At any rate, though, the CP60/CP190 network is uniform throughout the nucleus and thus would not be likely to be the basis for peripheral localization of specific chromatin regions.

One role of NE associated chromatin could be to form boundaries between independent chromatin domains. A class of loci , known as scs (specialized chromatin structure) elements, have been described that may act as boundaries between chromatin domains (Udvardy et al., 1988, Kellum and Schedl, 1992). Genes flanked by scs elements are insulated from euchromatic position effect and from the action of upstream enhancers, suggesting that these sites function as boundaries of chromatin domains, perhaps by anchoring chromatin to the NE to form topologically independent loops. While one scs-containing locus, hsp-70 (87A7), is in an NE associated region, another, the 90BC tRNA locus, located at position 90B-C, is not. Thus there is no strict correlation between NE associated sites and scs-like elements. We further note that while topologically independent loop domains have been observed in *Drosophila* (Benyajati and Worcel, 1976) they are only 85kb in length, on average, far smaller than the 1-2Mb loops defined by the NE associations described here.

Genetic studies have led to the discovery of many chromosomal proteins that are thought to influence chromatin structure and activity. If NE binding requires particular chromosomal proteins, it is possible that genetic identification of such proteins may eventually reveal the proteins involved in NE association. In *Drosophila*, the binding sites of many chromatin proteins have been determined, revealing a limited number of regions on each chromosome that bind different chromatin proteins. However, NE associations do not appear to correlate strictly with any of these binding sites. For example, the 23A NE associated region contains binding sites for Su(z)2, Psc, and z, but not ph, Pc, or HP-1, while the 33B NE associated region contains binding sites for ph and Pc, but not Su(z)2, Psc, z, or HP-1 (James et al., 1989, Rastelli et al., 1993). Therefore, NE association does not appear to require binding sites for z, Su(z)2, Psc, ph, Pc, or HP-1.

Recently, an interaction has been demonstrated in vitro between the mammalian lamin B receptor and a mammalian homolog of HP-1 (Ye and Worman 1996). Although we saw no correlation between the positions of HP-1 binding sites and NE association, the possibility remains that HP-1 binding sites may be different in the embryo than in salivary glands where they have been determined. We have made extensive attempts to demonstrate a loss of NE association in HP-1 null mutant embryos, but have not seen any difference (data not shown). However, because HP-1 is essential in Drosophila, we were forced to study the homozygous embryos produced by parents heterozygous for a null allele of Su(var)205 (the gene coding for HP-1 protein), and thus we cannot rule out the possibility that NE association is rescued by maternally contributed protein. Production of germ-line clones (R. Kellum, personal communication) should allow this question to be addressed in the future.

Finally, NE association sites were compared to the locations of intercalary heterochromatin (IH). Intercalary heterochromatin (Zhimulev et al., 1982) refers to a set of loci found in the euchromatic arms of Drosophila polytene chromosomes which share several characteristics suggestive of a heterochromatic state, including late replication, high

frequency of chromosome breaks, and formation of ectopic fibers. On 2L, IH is found in regions 22A, 25A, 25E-F, 33A-B, 34E-35A, 35C-F, 36D, and 39E, as judged primarily by frequency of ectopic fiber formation (Zhimulev et al., 1982). As seen in Table 1, three of these IH-containing regions coincide with NE associated regions, while one, 39E, is in a region that is nonrandomly far from the NE. Thus, while many IH regions are NE associated in embryos, some are not. In addition, it is clear that some NE associated regions (for example 34A or 87B) are clearly not IH by any criterion. Thus, IH is neither strictly necessary nor sufficient for NE association. However, IH has been cytologically defined only in polytene nuclei, and it is possible that the exact distribution of regions with IH properties is different in diploid interphase nuclei. In spite of these differences, the fact that three of the most significant IH sites on 2L (Zhimulev et al., 1982) correspond exactly to NE associations seen there is suggestive of some underlying relation between IH and NE association. This is also supported by the fact that essentially all polytene NE contact sites (see above) correspond to IH regions (Hochstrasser et al., 1986).

Relation to lamin-fiber associated chromatin

In vitro binding studies have suggested that lamins may bind chromatin, either directly (Glass and Gerace, 1990, Yuan et al., 1991, Glass et al., 1993, Luderus et al., 1992, Luderus et al., 1994) or via lamin-associated proteins (Foisner and Gerace, 1993). Interactions of specific loci with nuclear lamins could be the basis for the associations observed here. The nuclear lamina in *Drosophila* embryos appears in the light microscope to consist of a reticular basketlike structure composed of large fibers (Paddy et al., 1990). Previous studies have revealed that approximately 20-30 chromosomal sites, as detected by DAPI staining, are close enough to one of these large lamin fibers to potentially be in contact with it (Paddy et al., 1990). While the number (20-30) of such sites is significantly less than the number of specific NE associated sites reported here, it is possible that a fraction of the NE associated sites do indeed bind to the regions of heavy lamin staining ,

while the remainder interact with more diffusely organized lamins, or with some other NE components, such as nuclear pore complexes. In support of this latter possibility, some nuclear pore components contain DNA binding motifs (Sukegawa and Blobel, 1993).

A putative lamin-associated DNA region has been identified in Drosophila (Baricheva et al., 1996) using an in vitro binding assay. FISH using probes made with this clone indicated a peripheral localization in polytene nuclei from the salivary gland, however, these results are difficult to interpret because the clone maps to the centric heterochromatin. In salivary gland nuclei, the centric heterochromatin from all chromosomes coalesces together to form a compact chromocenter, which is known to be NE associated (Hochstrasser et al ??????). Thus, any probe mapping to the centric heterochromatin will appear NE associated in salivary gland nuclei, but this does not necessarily mean that this clone actually is responsible for this localization. We feel that rather than start with in vitro binding, a much more productive approach to finding specific NE-association elements in the genome is to progressively narrow down the site by using the two-probe method developed here (Figure 6), and then eventually to transform the Drosophila genome with subclones from this region.

Alternative models for apparent NE association

This work is based on the assumption that the FISH procedure employed does not strongly affect the position of chromatin within the nucleus. Comparison of hybridized chromosomes with both living and fixed non-hybridized chromosomes does not indicate any significant rearrangement due to the FISH procedure (Hiraoka et al., 1993). The minor structural differences between hybridized and unhybridized chromatin are likely to be significant only at much higher resolution than currently available in the light microscope, and should not affect the statistical test employed, which tests for an overall bias in localization rather than actual contact with the NE, and is thus only affected by relatively large displacements. The precise vertical positioning reported here is also not consistent

with a scrambling of nuclear organization following hybridization. Ultimately, however, analysis of nuclear organization in living cells will be required to completely settle this point.

We have tacitly assumed that the strongly peripheral localization observed is due to an interaction of chromatin with the NE. While this interpretation is the simplest, and is consistent with a significant body of literature supporting the existence of such interactions, nevertheless several alternate models must be considered.

First, since we know that some sites are nonrandomly localized to the nuclear interior, it is possible that the remaining chromosome regions could become peripheral due to either excluded volume effects or rigid loops extending outward. If such a large fraction of the inner 50% of the nucleus was occupied by "internal" sites as to produce the strong peripheral localizations seen here, then all other sites, not just some, should appear nonrandomly peripheral. This is obviously not the case, as many sites appear randomly localized. Moreover, an excluded volume effect would not explain why only certain loci appear consistently peripheral.

A second possibility is that extended loops may run outward from internally anchored points, thus directing some loci to a peripheral location. This model requires the existence of internal anchor points between any two peripheral sites. Such internal anchor regions should appear nonrandomly far from the NE. However, as seen in Table 1, far points do not in general occur between peripheral sites. Thus, peripheral localization is unlikely to be a consequence of internal localization of other sites, either by excluded volume or rigid loops.

Finally, it remains a formal possibility that the peripheral sites are associated, not with the NE per se, but with some unknown peripheral structure which may or may not be anchored to the NE. With regards to the role these interactions may play in nuclear organization and chromosome dynamics, the nature of the peripheral structure to which

they are attached may be less important, and in any event, this question will certainly be resolved once the molecular determinants of the interactions described here are identified.

Interphase NE interactions are not remnants of NE reassembly

One interesting function for chromatin-NE interaction would be to mediate NE reassembly following mitosis by binding NE vesicles to anaphase chromosomes. If such binding interactions were to persist until interphase, then at telophase, when the NE has reassembled, the interactions should already be established, which as seen in Table 2, is not the case. Therefore, the specific interactions seen between chromatin and the NE in interphase are not the same as the interactions that bind NE vesicles to chromosomes following mitosis. We note that changes in nuclear positioning of centromeres have recently been demonstrated in vivo in mammlian cells using a GFP-centromere binding protein fusion. Thus, extensive nuclear rearrangement following chromosome decondensation is likely to be a universal feature of the cells cycle in all species. This result also illustrates that chromatin can undergo rather substantial large-scale motions during interphase, a result we have obtained more directly by visualizing chromosome motion in vivo (see Chapter 4).

Rabl orientation in interphase

The Rabl orientation, with centromeres at one end of the nucleus and telomeres at the other (reviewed in Comings 1980), is evident in Drosophila embryos during prophase (Hiraoka et al., 1990b) and following anoxia-induced premature chromosome condensation (Foe and Alberts, 1985). In interphase, FISH has revealed that subtelomeric sequences are located near the bottom of the nucleus facing the embryo interior (Hiraoka et al., 1990a). Furthermore, Hoechst staining in interphase reveals brightly fluorescing heterochromatic blocks located near the top of the nucleus in Drosophila virilis embryos (Ellison and Howard, 1981). However, the extent to which the chromosome arms themselves follow

this arrangement along their entire length is unknown. In salivary nuclei the path of the chromosomes is not particularly straight, and often loops back before eventually reaching the other side of the nucleus (Hochstrasser et al., 1986). Diploid interphase chromosomes are more flexible than polytene chromosomes, and might be expected a priori to follow an even more meandering path through the nucleus. FISH studies of the histone locus(Hiraoka et al., 1993) revealed it to be constrained to a defined vertical region. As described above, this holds true for all loci investigated here, with each locus lying in an approximately 1μm wide vertical position defined relative to the center of the nucleus (see Figure 8B). Moreover, as listed in Table 1, and plotted in Figure 7, the average vertical position is correlated with genome position exactly as expected from a Rabl configuration. Loci near the centromere are found near the top of the nucleus, while loci near the telomere are near the bottom of the nucleus. Apparent exceptions to this rule (such as DS00889 vs. DS02809) are for the most part minor differences between nearby loci, and are probably due to embryo to embryo variation in nuclear size. However, we cannot rule out, from this study, the possibility of deviations from the strict Rabl configuration due to chromosome arms looping back within the nucleus. It is clear that in addition to the clustering of telomeres and centromeres at opposite ends of the nucleus, other loci on the chromosome arm are similarly constrained according to the general polarization of the nucleus. This high degree of constraint is likely to require anchoring of chromosomes to a rigid structure of some sort, and the NE interactions reported here could serve such a role.

Positional Determination of Chromosomal Loci within the Interphase Nucleus

An important result of this study is that different loci reproducibly occupy defined regions of the nucleus, as detailed in Figure 8B. This is true even for loci not associated with the NE. Some aspects of this positioning are maintained in a translocation (Figure 8D). Furthermore, even loci classified as random with respect to NE association appear to

have a specific nuclear sublocalization on the vertical axis and possibly also the radial axis, consistent with the idea that as the chromosome loops in from the NE, loci along the loop occupy preferred radial positions. The size of the error bars could reflect variation in nuclear size, cell cycle-dependent or developmental changes (including apoptosis), or interphase chromosome motion. Regarding the latter point, we have developed methods to track interaphse chromatin motion in living cells, with the result that this motion is constrained, in at least some cases, to a small sub-region of the nucleus (see Chapter 4). This constraint may be the temporal reflection of the spatial confinement observed here.

Specific positioning within the nucleus could have a strong effect on processes such as transvection or recombination that involve physical interactions between loci, since loci in two completely disparate regions would not be able to interact. The data in Figure 8D demonstrate that it is possible to use chromosome rearrangements to alter the vertical position of a particular locus within the nucleus. Similarly, we have recently demonstrated (Dernburg et al 1996) that a chromosome region can be targetted to the NE, without affecting its vertical position, by the insertion of an NE associated heterochromatic satellite block. By manipulating nuclear organization in this manner, it should be possible to test whether or not this defined nuclear positioning plays a functional role.

The data in Figure 8D also imply that vertical positioning is determined primarily by location within the genome, in accordance with the Rabl configuration, while radial distance to the NE is a more local property of a particular region. This is consistent with the result that NE associations are established after chromosome decondensation in telophase.

This is, to our knowledge, the first clear evidence for specific positioning of multiple different euchromatic loci within the interphase nucleus. Prior studies of 3D nuclear organization (Manuelidis and Borden, 1988, Van Dekken et. al., 1990, Ferguson and Ward, 1992, Hoefers et al., 1993, Vourc'h et al., 1993) have focused on only one or two, generally heterochromatic, loci such as centromeres or telomeres. It is likely that a

more extensive analysis of the localization of a large number of sites would reveal a similar degree of positioning as that seen here. The *Drosophila* embryo proved particularly well suited to these studies, however, since all nuclei in one dataset are highly synchronized and oriented the same way relative to the surface of the embryo, which allowed a vertical axis to be defined. We predict that in the future, the radial and vertical positioning demonstrated here will turn out to be a general feature of nuclear organization in other cell types. The functional significance of such positioning now remains to be determined.

ACKNOWLEDGMENTS

The authors would like to thank Dr. H. Bass, J. Fung, Dr. M. Gustafsson, and S. Parmelee for critical reading of the manuscript. The statistical test was suggested by Dr. C.W. Marshall, Dept. of Mathematics, Polytechnic University, Farmingdale, NY. We also acknowledge Gina Dailey and Dr. Gerald Rubin, University of California, Berkeley, CA, for providing P1 genomic clones. This work was supported by a Howard Hughes Medical Institute Predoctoral Fellowship (W.F.M.), National Institutes of Health grants R01-GM-225101-16 and R01-GM-331627-12 (J.W.S. and D.A.A., respectively), and stages of this work were supported by the Howard Hughes Medical Institute (D.A.A. and J.W.S.). D.A.A. is currently an investigator of the Howard Hughes Medical Institute.

REFERENCES

Agard, D.A., Hiraoka, Y., Shaw, P., and Sedat, J.W. (1989). Fluorescence microscopy in three dimensions. Meth. Cell Biol. *30*, 353-378.

Baricheva, E.A., Berrios, M., Bogachev, S.S., Borisevich, I.V., Lapik, E.R., Sharakhov, I.V., Stuurman, N., and Fisher, P.A. (1996). DNA from Drosophila melanogaster beta-heterochromatin binds specifically to nuclear lamins in vitro and the nuclear envelope in situ. Gene *171*,171-176.

Belmont, A.S., Zhai, Y., and Thilenius, A. (1993). Lamin B distribution and association with peripheral chromatin revealed by optical sectioning and electron microscopy tomography. J. Cell Biol. *123*, 1671-1685.

Benyajati, C., and Worcel, A. (1976). Isolation, characterization, and structure of the folded interphase genome of Drosophila melanogaster. Cell *9* , 393-407.

Berezney, R., and Coffey, D. (1974). Identification of a nuclear protein matrix. Biochem. Biophys. Res. Commun. *60*, 1410-1419.

Billia, F., and De Boni, U. (1991). Localization of centromeric satellite and telomeric DNA sequences in dorsal root ganglion neurons, in vitro. J. Cell Sci. *100*, 219-26.

Blobel, G. (1985). Gene gating: a hypothesis. Proc. Natl. Acad. Sci. U.S.A. *82*, 8527-9.

Carmena, M., Abad, J.P., Villasante, A., and Gonzalez, C. (1993). The Drosophila *melanogaster* dodecasatellite sequence is closely linked to the centromere and can form connections between sister chromatids during mitosis. J. Cell Sci. *105*, 41-50.

Chen, H., Swedlow, J.R., Grote, M., Sedat, J.W., and Agard, D.A. (1995). The collection, processing, and display of digital three-dimensional images of biological

specimens. In *Handbook of Biological Confocal Microscopy*, J.B. Pawley ed. (New York, New York: Plenum), pp197-210.

Chung, H.M., Shea, C., Fields, S., Taub, R.N., Van der Ploeg, L.H.T., and Tse, D.B. (1990). Architectural organization in the interphase nucleus of the protozoan Trypanosoma brucei: location of telomeres and mini-chromosomes. EMBO J. *9*, 2611-2619.

Comings, D.E. (1980). Arrangement of chromatin in the nucleus. Hum. Genet. *53*, 131-143.

Cremer, T., Kurz, A., Zirbel, R., Dietzel, S., Rinke, B., Schroeck, E., Speicher, M.R., Mathieu, U., Jauch, A., Emmerich, P., Scherthan, H., Ried, T., Cremer, C., and Lichter, P. (1993). Role of chromosome territories in the functional compartmentalization of the cell nucleus. Cold Spring Harbor Symposium on Quantitative Biology *58*, 777-792.

Dernburg, A.F., Sedat, J.W., Cande, W.Z., and Bass, H.W. (1995). Cytology of telomeres. In *Telomeres*, E.H. Blackburn and C.W. Greider, eds. (Cold Spring Harbor,New York: Cold Spring Harbor Laboratory Press), pp. 295-338.

DuPraw, E.J. (1965). The organization or nuclei and chromosomes in honeybee embryonic cells. Proc. Natl. Acad. Sci. U.S.A. *53*, 161-168.

Ellison, J.R., and Howard, G.C. (1981). Non-random position of the A-T rich DNA sequences in early embryos of Drosophila virilis. Chromosoma *83*, 555-561.

Ferguson, M. and Ward, D.C. (1992). Cell cycle dependent chromosomal movement in pre-mitotic human T-lymphocyte nuclei. Chromosoma *101*, 96-106.

Foe, V.E. and Alberts, B.M. (1985). Reversible chromosome condensation induced in Drosophila embryos by anoxia: visualization of interphase nuclear organization. J. Cell Biol. *100*, 1623-1636.

Foe, V.E., Odell, G.M., and Edgar, B.A. (1993). Mitosis and morphogenesis in the Drosophila embryo: point and counterpoint. In *The Development of Drosophila melanogaster*, M. Bate and A. Martinez Arias, eds. (Cold Spring Harbor, New York: Cold Spring Harbor Laboratory Press), pp. 149-300.

Foisner, R. and Gerace, L. (1993). Integral membrane proteins of the nuclear envelope interact with lamins and chromosomes, and binding is modulated by mitotic phosphorylation. Cell *73*, 1267-1279.

Gasser, S.M. and Laemmli, U.K. (1986). Cohabitation of scaffold binding regions with upstream/enhancer elements of three developmentally regulated genes of D. melanogaster. Cell *46*, 521-530.

Glass, C.A., Glass, J.R., Taniura, H., Hasel, K.W., Blevitt, J.M., and Gerace, L. (1993). The α-helical rod domain of human lamins A and C contains a chromatin binding site. EMBO J. *12*, 4413-24.

Glass, J.R., and Gerace, L. (1990). Lamins A and C bind and assemble at the surface of mitotic chromosomes. J. Cell Biol. *111*, 1047-1057.

Hartl, D.L., Nurminsky, D.I., Jones, R.W., and Lozovskaya, E.R. (1994). Genome structure and evolution in Drosophila: applications of the framework P1 map. Proc. Natl. Acad. Sci. U.S.A. *91*, 6824-6829.

Hassan, A.B., Errington, R.J., White, N.S., Jackson, D.A., and Cook, P.R. (1994). Replication and transcription sites are colocalized in human cells. J. Cell Sci. *107*, 425-34.

Hilliker, A.J., and Appels, R. (1989). The arrangement of interphase chromosomes: structural and functional aspects. Exp. Cell Res. *185*, 267-318.

Hiraoka, Y., Minden, J.S., Swedlow, J.R., Sedat, J.W., and Agard, D.A. (1989). Focal points for chromosome condensation and decondensation revealed by three-dimensional in vivo time-lapse microscopy. Nature *342*, 293-296.

Hiraoka, Y., Rykowski, M.C., Lefstin, J.A., Agard, D.A., and Sedat, J.W. (1990a). Three-dimensional organization of chromosomes studied by *in* situ hybridization and optical sectioning microscopy. Proc. SPIE *1205*, 11-19.

Hiraoka, Y., Agard, D.A., and Sedat, J.W. (1990b). Temporal and spatial coordination of chromosome movement, spindle formation, and nuclear envelope breakdown during prometaphase in Drosophila melanogaster embryos. J. Cell Biol. *111*, 2815-2828.

Hiraoka, Y., Swedlow, J.R., Paddy, M.R., Agard, D.A., and Sedat, J.W. (1991). Three-dimensional multiple-wavelength fluorescence microscopy for the structural analysis of biological phenomena. Sem. Cell Biol. *2*, 153-165.

Hiraoka, Y., Dernburg, A.F., Parmelee, S.J., Rykowski, M.C., Agard, D.A., and Sedat, J.W. (1993). The onset of homologous chromosome pairing during Drosophila melanogaster embryogenesis. J. Cell Biol. *120*, 591-600.

Hochstrasser, M., Mathog, D., Gruenbaum, Y., Saumweber, H., and Sedat, J.W. (1986). Spatial organization of chromosomes in the salivary gland nuclei of Drosophila melanogaster. J. Cell Biol. *102*, 112-123.

Hochstrasser, M. and Sedat, J.W. (1987). Three-dimensional organization of Drosophila melanogaster interphase nuclei. II. Chromosome spatial organization and gene regulation. J. Cell Biol. *104*, 1471-1483.

Hoefers, C., Baumann, P., Hummer, G., Jovin, T.M., and Arndt-Jovin, D.J. (1993). The localization of chromosome domains in human interphase nuclei. Three-dimensional distance determinations of fluorescence in situ hybridization signals from confocal laser scanning microscopy. Bioimaging *1*, 96-106.

Hutchison, N. and Weintraub, H. (1985). Localization of DNAase I-sensitive sequences to specific regions of interphase nuclei. Cell *43*, 471-482.

Izaurralde, J., Mirkovitch, J., and Laemmli, U.K. (1988). Interaction of DNA with nuclear scaffolds in vitro. J. Mol. Biol. *200*,111-125.

Jackson, D.A., Dickinson, P., and Cook, P.R. (1990). Attachment of DNA to the nucleoskeleton of HeLa cells examined using physiological conditions. Nuc. Acids Res *18*, 4385-93.

James, T.C., Eissenberg, J.C., Craig, C., Dietrich, V., Hobson, A., and Elgin, S.C.R. (1989). Distribution patterns of HP1, a heterochromatin-associated nonhistone chromosomal protein of Drosophila. Eur. J. Cell Biol. *50*, 170-180.

Kellum, R. and Schedl, P. (1992). A group of scs elements function as domain boundaries in an enhancer-blocking assay. Mol. Cell. Biol. *12*, 2424-2431.

Lawrence, J.B., Villnave, C.A., and Singer, R.H. (1988). Sensitive high-resolution chromatin and chromosome mapping in situ: presence and orientations of two closely integrated copies of EBV in a lymphoma line. Cell 52, 51-61.

Lebkowski, J.S. and Laemmli, U.K. (1982). Non-histone proteins and long-range organization of HeLa interphase DNA. J. Mol. Biol. *156*, 325-344.

Lohe, A.R., Hilliker, A.J., and Roberts, P.A. (1993). Mapping simple repeated DNA sequences in heterochromatin of Drosophila melanogaster. Genetics *134*, 1149-1174.

Loidl, J. (1990). The initiation of meiotic chromosome pairing: the cytological view. Genome *33*, 759-70.

Luderus, M.E., den Blaauwen, J.L., de Smit, O.J., Compton, D.A., and van Driel, R. (1994). Binding of matrix attachment regions to lamin polymers involves single-stranded regions and the minor groove. Mol. Cell. Biol. *14*, 6297-305.

Luderus, M.E., de Graaf, A., Mattia, E., den Blaauwen, J.L, Grande, M.A., de Jong, L, and van Driel, R. (1992). Binding of matrix attachment regions to lamin B. Cell *70*, 949-959.

Manuelidis, L. and Borden, J. (1988). Reproducible compartmentalization of individual chromosome domains in human CNS cells revealed by in situ hybridization and three-dimensional reconstruction. Chromosoma *96*, 396-410.

Mathog, D., Hochstrasser, M., Gruenbaum, Y., Saumweber, H., and Sedat, J. (1984). Characteristic folding pattern of polytene chromosomes in Drosophila salivary gland nuclei. Nature *308*, 414-421.

Murray, A.B. and Davies, H.G. (1979). Three-dimensional reconstruction of the chromatin bodies in the nuclei of mature erythrocytes from the newt Triturus cristatus: the number of nuclear envelope-attachment sites. J. Cell Sci. *35*, 59-66.

Paddy, M.R., Belmont, A.S., Saumweber, H., Agard, D.A., and Sedat, J.W. (1990). Interphase nuclear envelope lamins form a discontinuous network that interacts with only a fraction of the chromatin in the nuclear periphery. Cell *62*, 89-106.

Palladino, F., Laroche, T., Gilson, E., Axelrod, A., Pillus, L., and Gasser, S.M. (1993). SIR3 and SIR4 proteins are required for the positioning and integrity of yeast telomeres. Cell *75*, 543-555.

Papoulis, A. (1990). *Probability & Statistics.* (Eagle Cliffs, New Jersey: Prentice-Hall), p. 332.

Pimpinelli, S. and Dimitri, P. (1989). Cytogenetic analysis of segregation distortion in Drosophila melanogaster: the cytological organization of the Responder (Rsp) locus. Genetics *121*, 765-72.

Press, W.H., Flannery, B.P., Teukolsky, S.A., and Vetterling, W.T. (1989). Numerical Recipes in Pascal. (Cambridge, U.K: Cambridge University Press), pp 224-226.

Purcell, C., Mashiko, T., Odaka, K., and Ueno, K. (1991). Describing head shape with surface harmonic expansions. IEEE Trans. Biomed. Eng. *38*, 303-305.

Quick, P. (1980). Junctions of polytene chromosomes and the inner nuclear membrane. Experientia *36*, 456-457.

Rastelli, L., Chan, C.G., and Pirrotta, V. (1993). Related chromosome binding sites for zeste, suppressors of zeste, and Polycomb group proteins in Drosophila and their dependence on Enhancer of zeste function. EMBO J. *12*, 1513-1522.

Sambrook, J., Fritsch, E.F., and Maniatis, T. (1989). Molecular Cloning. (Cold Spring Harbor, New York: Cold Spring Harbor Laboratory Press).

Spector, D.L. (1993). Macromolecular domains within the cell nucleus. Ann. Rev. Cell Biol. *9*, 265-315.

Sukegawa, J. and Blobel, G. (1993). A nuclear pore complex protein that contains zinc finger motifs, binds DNA, and faces the nucleoplasm. Cell *72*, 29-38.

Telenius, H., Carter, N.P., Bebb, C.E., Nordenskjold, M., Ponder, B.A., Tunnacliffe, A. (1992). Degenerate oligonucleotide-primed PCR: general amplification of target DNA by a single degenerate primer. Genomics *13*, 718-25.

Udvardy, A., Maine, E., and Schedl, P. (1985). The 87A7 chromomere. Identification of novel chromatin structures flanking the heat shock locus that may define the boundaries of higher order domains. J. Mol. Biol. *185*, 341-355.

van Dekken, H., Pinkel, D., Mulliken, J., Trask ,B., van den Engh, G., and Gray J. (1989). Three-dimensional analysis of the organization of human chromosome domains in human and human-hamster hybrid interphase nuclei. J. Cell Sci. *94*, 299-306.

van Dekken, H., van Rotterdam, A., Jonker, R., van der Voort, H.T.M., Brakenhoff, G.J., and Bauman, J.G.J. (1990). Confocal microscopy as a tool for the study of the intranuclear topography of chromosomes. J. Microscopy *158*, 207-214.

Vourc'h, C., Taruscio, D., Boyle, A.L., and Ward, D.C. (1993). Cell cycle-dependent distribution of telomeres, centromeres, and chromosome-specific subsatellite domains in the interphase nucleus of mouse lymphocytes. Exp. Cell Res. *205*, 142-151.

Wakimoto, B.T., and Hearn, M.G. (1990). The effects of chromosome rearrangements on the expression of the heterochromatic genes in chromosome 2L of Drosophila melanogaster. Genetics *125*, 141-154.

Wiese, C. and Wilson, K. (1993). Nuclear membrane dynamics. Curr. Opin. Cell Biol. *5*, 387-94.

Worman, H.J., Evans, C.P., and Blobel, G. (1990). The lamin B receptor of the nuclear envelope inner membrane: a polytopic protein with eight potential transmembrane domains. J. Cell Biol. *111*, 1535-1542.

Wu, C.I., Lyttle, T.W., Wu, M.L., and Lin, G.F. (1988). Association between a satellite DNA sequence and the Responder of Segregation Distorter in D. melanogaster. Cell *54*, 179-89.

Yokota, H., van den Engh, G., Hearst, J.E., Sachs, R.K., and Trask, B.J. (1995). Evidence for the organization of chromatin in megabase pair-sized loops arranged along a random walk path in the human G0/G1 interphase nucleus. J. Cell Biol. *130*,1239-1250.

Yuan, J., Simos, G., Blobel, G., and Georgatos, S.D. (1991). Binding of lamin A to polynucleosomes. J. Biol. Chem. *266*, 9211-15.

Zalensky, A.O., Allen, M.J., Kobayashi, A., Zalenskaya, I.A., Balhron, R., and Bradbury, E.M. (1995). Well-defined genome architecture in the human sperm nucleus. Chromosoma *103*, 577-590.

Zhimulev, I.F., Semeshin V.F., Kulichkov, V.A., and Belyaeva, E.S. (1982). Intercalary heterochromatin in Drosophila I. Localization and general characteristics. Chromosoma *87*, 197-228.

Chapter 3. Interphase Chromatin Undergoes Large-Scale Diffusional Motion in Living Cells

SUMMARY

While many essential biological processes require large-scale chromosomal motion, the dynamic behavior of interphase chromatin is not known. Indeed, the high concentration and large size of the chromatin polymer, along with the possibility of interactions with the nuclear envelope or nuclear matrix, would suggest that interphase chromatin might be relatively immobile. To address this issue experimentally, we have, for the first time, been able to directly measure chromatin motion and diffusion in living cells of Saccharomyces cerevisiae and Drosophila melanogaster. The diffusion constant was found to be similar in both organisms but unlike in Drosophila, diffusion of chromatin in yeast cells appears constrained at long time scales, providing the first direct in vivo evidence for attachment of chromatin to an immobile nuclear superstructure. The diffusion constant was found not to depend strongly on chromosome size, which is consistent with predictions for a tethered polymer model. The diffusive behavior is likely to be due to Brownian motion because it is largely unaffected when cellular metabolism is poisoned with azide. The diffusion constant of chromatin is sufficiently high to permit chromosomal interactions to occur by large-scale diffusive motions on a reasonable time-scale, while the fact that chromatin diffusion can be constrained implies that nuclear architecture will play a determining role in such interactions.

INTRODUCTION

Chromatin motion is intrinsic to many essential processes in molecular biology, including homologous recombination, meiotic homolog pairing, chromosome condensation, and enhancer looping. These processes all require that two initially separated chromosome regions come together and interact. The rates at which these interactions can take place depends on how fast the necessary segments of chromatin can move. Therefore, knowing the rate at which chromatin diffuses is essential for understanding the mechanism and kinetics of these processes. It has been argued that since chromatin is such a large polymer, its diffusion might not be fast enough for many processes, particularly meiotic homology searches (Maguire, 1984), to take place by diffusion alone. This has led to the proposal of more elaborate active mechanisms that would not be diffusion limited (Smithies and Powers, 1986). Clearly, a quantitative measurement of chromatin mobility would help to settle this point. Here we report the direct measurement of the diffusive motion of chromatin within nuclei in living cells of *Saccharomyces cerevisiae* and *Drosophila melanogaster*, which indicates that diffusive motion of chromatin is sufficiently fast for motion-requiring processes to be able to occur by diffusion alone.

Of direct relevance to the question of chromatin motion is the question of chromatin positioning. Our work (Marshall et al 1996) has directly demonstrated that different chromosomal loci occupy defined positions within the nucleus. If chromatin is able to undergo diffusional motion, how could such positioning be maintained? One explanation could be that chromatin may be anchored to large, relatively immobile nuclear structures such as the nuclear envelope or nuclear matrix. If chromatin were to be tethered to such a structure at a few discrete sites, as suggested for the NE by (Marshall et al 1996), then the chromatin in between tethering sites would form mobile loops which could diffusive within a limited region of the nucleus, thus allowing limited diffusional search within the context of an overall nuclear organization. In principle, measurement of chromatin

motion could distinguish this type of constrained motion from free diffusion, and thus test for interactions of chromatin with an immobile structure in living cells.

Chromatin is also of interest from the standpoint of polymer dynamics. The behavior of large polymers is currently the subject of intense research in the physics community. Recently, significant progress has been made in the study of DNA as a polymer (Chu refs, etc.) which has revealed insights into basic polymer physics. The extension of such polymer-dynamics studies of macromolecules to the study of molecules in vivo remains a challenging and fascinating problem. How do interactions with structural components and enzymes within the cell affect polymer conformation and dynamics? In particular, topoisomerase II is likely to have profound effects on DNA behavior. Direct quantitative measurements of chromatin motion in vivo will provide a basis for comparing the dynamics of isolated polymers with those of a large polymer in a living context.

The main technical challenge in measuring chromatin motion is developing a method to visualize the position of a discrete chromosome site in living cells. Fluorescence in situ hybridization (FISH) can be used to detect the position of an arbitrary DNA sequence in the nucleus, but requires the cells to be fixed and denatured, thus making it impossible to measure the motion of the spot under in vivo conditions. While DNA stains can be used to visualize the chromatin in vivo, it is impossible to distinguish individual chromosomes during interphase by such means. Thus, we need to rely on more elaborate means to track interphase chromosome motion.

Materials and Methods

Visualizing chromosome motion in yeast using GFP-lac repressor

Cells were grown and mounted as described (Straight et al., 1996; Robinett et al., 1996). Cells mounted in this way continue to grow and divide normally. Time-lapse 3-dimensional images were collected at rates of one 3-dimensional data set every 12s, 24s, or 96s, using wide-field deconvolution 3-dimensional microscopy (Agard et al., 1989)

using a 60x N.A. 1.4 objective and 1.5180 oil. At each time point, 14 256x256 pixel images were collected at focal plane increments of 0.25 μm per plane. For high-speed data collection (one dataset every 12 seconds) only 7 sections were acquired.

Simulation of random walk motion

Random walks were simulated on a cubic lattice (Lee et al., 1991; Kao and Verkman, 1994) for two particles. At the start of each run, the particles were set 2.0 μm apart (initial distance did not affect the outcome significantly). For each time step (τ=50 ms), the x,y, and z coordinates of the particle were independently incremented or decremented (with equal probability) by $\delta=2D\tau$ (Lee et al., 1991). We note that while at a short time scale, this algorithm generates a uniform step size, in contrast to the Gaussian step size expected for Brownian motion, at larger time-scales, the net displacement becomes Gaussian as a consequence of the central limit theorem approximation, provided that the number of discrete uniform steps is fairly large. This is why we employ a very short time intervals (50ms) relative to the time intervals actually reported at the end (5 s). To represent confinement, any step causing either particle to exceed a fixed confinement distance R from its initial position was rejected, and a new step chosen. The distance d(t) between the two particles was stored every 5 seconds of simulation, with 1800 steps stored per run. Finally, 200 runs were averaged to compute $\langle\Delta d^2\rangle$ vs. Δt. To find the values of D and R that best fit the observed data, simulations were run for different values of D and R, changing D in increments of 0.5×10^{-12} cm^2/s and R in 0.025 μm increments. For each set of values, the mean-squared difference between the observed data and the simulation for corresponding values of Δt was computed, and the D and R which together resulted in the least squared error were chosen.

Estimation of measurement precision

We approximate the observed distance d(t) as the actual distance d'(t) plus a zero-mean random offset δ such that δ is uncorrelated between successive measurements, and define the rms error in distance measurement to be $\sqrt{<\delta^2>}$. Clearly $<\Delta d(\Delta t)^2>$ approaches $2<\delta^2>$ when Δt becomes small. For the smallest measured time interval Δt_{min} (in this case, 12 sec) $<\Delta d'(t_{min})^2>$ is still nonzero (approximately 0.004 μm^2 for the fixed cells in Figure 2B), thus $2<\delta^2>$ must be less than $<\Delta d(\Delta t_{min})^2>$, from which we conclude the distance measurement precision $\sqrt{<\delta^2>} \leq 0.04$ μm.

Arrest of metabolism with sodium azide

Cells were grown and GFP-LacI expression induced under identical conditions to those used for the non-azide treated cells. Following induction of GFP-LacI, sodium azide was added from a 10% stock solution to a final concentration of 0.02%. Cells were then incubated for 20 minutes at room temperature to allow depletion of cellular ATP. Cells were then mounted and observed in the continuous presence of azide. Data from a total of 30 cells with an average of 31 time points per data record were combined and plotted in Fig. 2B. To verify the toxic effect of azide on these cells, growth curves were carried out in the presence and absence of azide and indicated a complete arrest of cell division in the azide treated cells. The effect of azide on metabolism is likely to be very rapid: addition of 0.02% azide to cells undergoing mitotic division results in an immediate arrest (Aaron Straight, personal communication). Addition of azide has been shown to block movement of cortical actin patches (Doyle and Botstein, 1996) within 30 min, and azide causes a loss of endonuclease activity in yeast within 15 minutes (James Haber, Personal Communication.

Topoisomerase II visualization in living Drosophila embryos

Wild-type (Oregon-R) flies were maintained in population cages. Embryos were collected on cornmeal agar plates. Embryos were bleach dechorionated and injected with

rhodamine-labelled topoisomerase II (prepared by J. R. Swedlow) as previously described (Swedlow et al., 1993). Rather than staging embryos prior to injection as had previously been done (H. Itoi and J. Swedlow, pers. comm.), we found it more convenient to simply inject all embryos and then select only those at the approrpriate stage. Three dimensional images were collected from cycle 12 or 13 embryos, using wide-field deconvolution microscopy (32), using a 60x N.A. 1.4 objective lens and 1.5180 oil. At each time point, a set of 16 256x256 pixel images were collected at focal plane increments of 0.5 μm. One 3-dimensional dataset was collected every 20 s.

Measuring position of the topoisomerase II focus

The nuclear center was defined as the centroid of the nuclear boundary traced from the outline of the nuclear image. In order to compute the centroid, we first fit the surface points with a surface harmonic expansion (Marshall et al 1996). Then, the spherical coordinate angles theta and phi are stepped in uniform increments, and then the average x,y, and z coordinate of all points thus generated is taken as the center of the nucleus. This surface resampling procedure was used in order to make the method insensitive to any nonuniformities in the interactive point picking (for example, more points picked on one side of the nucleus than the other). The topoisomerase II focus position was defined by interactively picking the spot and taking an intensity-weighted center of mass around the chosen point.

RESULTS

Constrained Diffusion of Chromatin in Yeast

In order to track the diffusion of chromatin in the yeast *Saccharomyces cerevisiae*, we take advantage of a recently developed method (Straight et al., 1996; Robinett et al., 1996) to visualize arrays of Lac operator sites inserted in the yeast genome, by expressing a fusion of the Lac repressor protein with the green fluorescent protein (GFP-LacI).

Diploid yeast homozygous for an insertion of the Lac operator array into the LEU2 locus near the centromere of chromosome III were imaged in three dimensions as shown in Fig. 1. Only unbudded (and hence in the G1 phase of the cell cycle) cells were examined in order to avoid motion caused by the mitotic spindle. Cells remained alive during imaging as judged by their ability to successfully undergo mitotic nuclear division. Once we have imaged the position of the Lac operator array over time, its diffusion constant can be computed. This approach is known as single-particle tracking (Gelles et al., 1988; Qian et al., 1991), and relies on the fact that by locating the center of mass of the image of an object, very small displacements can be measured with a precision limited only by the signal to noise ratio of the image, and not by the resolution limit of the microscope. At each time point, the three dimensional distance d(t) between the two GFP spots was measured. Distance between two spots, rather than the position of a single spot, is used to compensate for drift or rotation of the nucleus (Parvinen and Soderstrom, 1976; De Boni and Mintz, 1986) which might otherwise lead to apparent motion. A typical plot of d(t) for one nucleus is given in Fig 2A. Denoting a time interval by Δt and the change in distance d during this interval Δd, we compute the mean-squared change in d(t) as $\langle \Delta d^2 \rangle = \langle [d(t)-d(t+\Delta t)]^2 \rangle$. All computation is carried out in terms of Δd^2 rather than Δd because the hallmark of random-walk diffusive motion is that unlike ordinary linear motion, in which distance changes linearly with time, distance for a diffusing particle changes, on average, linearly with the square root of time (Berg 1983). Thus, by plotting Δd^2 we can obtain a measure of motion that is expected to be linear with time. In particular, for two particles undergoing three-dimensional random walks with diffusion constant D, it can be shown that a plot of $\langle \Delta d^2 \rangle$ vs. Δt should be linear with a slope of 4D (Van Kampen, 1992). We note that this expression is not the same as the usual expression for displacement versus time (6Dt) due to the fact that we are measuring change in distance between two points, rather than change in position for a single point. We further note that if the motion of the two particles is not diffusive, but rather a

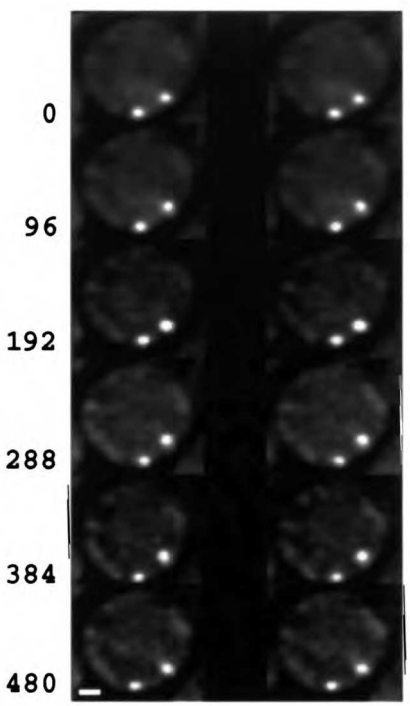

Figure 3.1. Visualizing interphase chromatin in living yeast cells.

Figure 3.1. Visualizing interphase chromatin motion in living yeast cells in three dimensions. Stereo pairs show successive time lapse 3-dimensional images of a diploid yeast cell homozygous for an insertion of a Lac operator array at the LEU2 locus and expressing a GFP-Lac repressor fusion protein (Straight et al., 1996). Yeast cells imaged under these conditions remain viable as judged by their ability to successfully bud and undergo mitotic divisions. Elapsed time since beginning of experiment given in seconds to left of each image. Scale bar 2 μm.

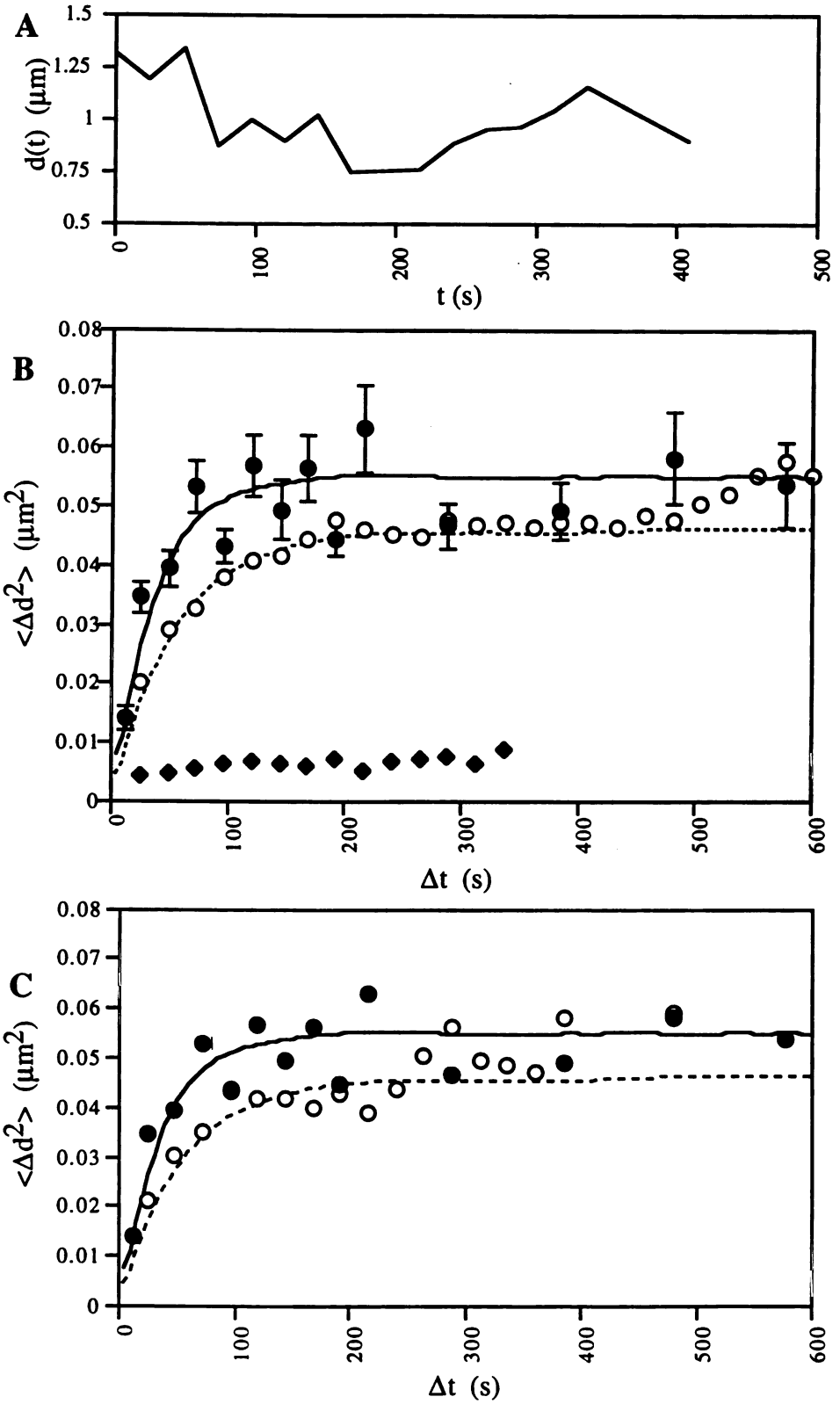

Figure 3.2. Constrained Diffusion of Yeast Chromatin

Figure 3.2. Constrained diffusion of chromatin in yeast. (A) typical data record showing the distance between GFP spots versus time. (B) Overall mean squared change in distance between GFP spots $<\Delta d^2>$ versus time interval Δt. (•) Living yeast cells. A total of 110 data records, each containing an average of 13 time-points were combined in this plot. (——) Result of computer simulation using parameters $D=5x10^{-12}$ cm^2/s and R=0.3 μm. (♦) GFP expressing yeast cells fixed in 3.7% formaldehyde and imaged under identical conditions. Motion seen in non-fixed cells is much greater than in fixed cells, and is thus not due merely to stage drift or insufficient measurement precision. (o) Chromatin motion in azide-treated yeast cells showing only slightly reduced motion relative to living cells. (- - -) Result of simulation with $D=3x10^{-12}$ cm^2/s, R=0.25 μm which best fits azide-treated data. (C) Diffusion of a CEN plasmid compared to a chromosome. (•) Motion of the centromere of chromosome III (reproduced from panel B for comparison). (o) $<\Delta d^2>$ versus time interval Δt for CEN plasmid. (- - -) Result of simulation with $D= 3x10^{-12}$ cm^2/s, R= 0.25 μm.

persistent directed motion such as that produced by a typical motor protein, we expect that $<\Delta d^2>$ vs. Δt will no longer be linear, but rather will curve upwards. This has been demonstrated in many cases where particle motion is measured in the presence of flow. A total of 110 data records, each from a different cell, were averaged and plotted in Figure 2B. At short time intervals, we do indeed observe a monotonic increase of $<\Delta d^2>$ with increasing Δt, suggesting diffusive motion. Because the plot does not curve upwards, we rule out flow or directed motion.

For long time intervals, in contrast, the plot is horizontal, implying that the average displacement is independent of the time interval. This behavior at long time intervals is the expected result if the diffusion of the two particles is constrained, that is, each particle is confined to diffuse within some limited region of confinement from which it cannot escape. Confinement would be expected if, for example, the chromatin was tethered to the nuclear envelope. The plateau height depends on the size of the confinement region, while the steepness of the plot at shorter time scales depends on the diffusion constant. We have used computer simulations to model this process. Based on these simulations, the experimental data are best described by a particle with $D=5\times10^{-12}$ cm^2/s confined to a region of radius $R=0.3$ μm (rms fitting error in $<\Delta d^2>$ is 4×10^{-3} μm^2). This radius is significantly smaller than the radius of the diploid nucleus (about 1.5 μm), and reflects confinement of the chromatin to a small nuclear sub-region, less than one tenth the volume of the nucleus, which could reflect anchorage to the nuclear envelope or an internal nuclear skeleton.

To rule out the possibility that the observed motion was caused by random error due to imprecision in measurement of the position of the two GFP spots, we measured the apparent motion in formaldehyde-fixed yeast cells that were imaged under identical conditions to those of the live cells (intensities, and hence signal to noise ratios, were the same as for live cells, leading to equivalent measurement precision). As plotted in Figure 2B, motion in living cells was much greater than in fixed cells, and was thus not due to

limited measurement precision. Using data from fixed cells, the error of the individual position measurements is estimated to be less than 0.04 μm, which is small relative to the displacements observed in living cells. This result emphasizes that, as with all single particle tracking experiments, it is possible to measure displacements much smaller than the resolution limit of the microscope, because resolution does not affect the precision of position measurements.

The constrained motion observed here could, in principle, be explained without invoking diffusion if the chromatin was fixed within a nucleus that was itself undergoing elastic deformations. These deformations would cause proportional displacements between any pair of points embedded in the nucleus, and would give rise to an apparent constraint if the deformations were limited in extent. This model predicts that the displacement between two points resulting from an elastic deformation of the entire nucleus will be proportional to the distance between the points. However, when the average magnitude of the displacements $\langle |d(t)-d(t+\Delta t)| \rangle$ was plotted versus the distance d(t), for a fixed time interval Δt=24s, no such correlation was seen (data not shown). Hence, the motions are unlikely to result from a simple elastic deformation.

Chromatin Movement Is Predominantly Brownian

The random walk motion observed could in principle be due either to Brownian motion, involving collisions with thermally excited solvent particles, or else it could be driven by enzymes or motor proteins whose direction of motion is uncorrelated over the time-scales we examine, thus leading to an apparent random walk. This question is important because if the motion is actively driven, then mutations in the motile machinery would be expected to have effects on a wide variety of processes involving chromosome motion. The idea that chromosome motion could be an active process is not unreasonable. In addition to the enzymes of DNA metabolism, which can act as motors (Yin et al., 1996), a number of potential motor proteins including the SMC family of

proteins (Hirano et al., 1995; Koshland and Strunnikov, 1996) and possibly myosin/actin-related nuclear proteins (Weber et al., 1995) have been identified in the nucleus. To test for a requirement of metabolic activity, we repeated the experiment described above in the presence of 0.02% azide which poisons cellular metabolism by blocking the respiratory electron transport chain. As plotted in Figure 2B, diffusion of chromatin is only slightly reduced in the presence of a lethal dose of azide. This small reduction might reflect the involvement of active motors in moving the chromatin. However, it is clear that most if not all the chromatin motion we observe continues in the absence of active metabolism, and is thus likely to reflect true Brownian motion.

Chromatin Diffusion Is Size-Independant

The diffusion of tracer molecules in cytoplasm depends strongly on the size of the molecules, which is thought to reflect an effective mesh size of a protein network in the cytoplasm (Luby-Phelps et al., 1988). To similarly determine how a chromosome's size affects its diffusion in the nucleus, we measured the motion of a small circular centromere-containing plasmid. We used a 15 kb CEN plasmid of which 10 kb was Lac operator repeats, thus most of the plasmid was visualized. Because CEN plasmids have a low copy number it was possible to locate cells with two distinct spots corresponding to a copy number of two, and these were used to compute $<\Delta d^2>$ vs. Δt as plotted in Figure 2C. Because the plasmid is much smaller than the chromosome we expected that D should be much higher for the plasmid. Surprisingly, D for the plasmid was 3×10^{-12} cm^2/s, which is actually slightly less than for the chromosome. Thus, contrary to expectation, loci on shorter pieces of chromatin do not necessarily diffuse any faster than loci on longer ones. If confinement of diffusion in fact reflects tethering of discrete chromosome sites to an immobile structure, then the surprising lack of size dependence of the diffusion constant can be explained, because the diffusion constant would depend not on the overall size of the chromosome, but rather on the length of chromatin between

successive tethering points. If the spacing of tethering points is similar for all chromatin, then the diffusion constant would be independent of chromosome size.

Chromatin Diffusion In Drosophila Embryos

For comparison we measured chromatin motion in *Drosophila melanogaster* by exploiting a novel localization pattern of topoisomerase II. In *Drosophila*, topoisomerase II shows diffuse localization along all chromosome arms, but in addition accumulates at 1-2 discrete foci per nucleus (Swedlow et al., 1993). To test if these foci reflect site-specific chromosome binding, topoisomerase II immunofluorescence was carried out in *Drosophila* embryos (Mitchison and Sedat, 1983) using anti-topoisomerase II polyclonal antibodies, following fluorescence in situ hybridization (FISH) using DNA probes to different heterochromatic satellite regions (Dernburg et al., 1996). The topoisomerase II spot did not correlate with the rDNA locus or the Rsp heterochromatin block, but colocalized precisely with the 359bp repeat block (Hsieh and Brutlag, 1979; Lohe et al., 1993) on the X chromosome (Fig 3). The positions and shapes of the FISH and immunofluorescence signals exactly coincide, implying that topoisomerase II binding is co-extensive with the entire 359bp repeat region. In agreement with these findings, the most common topoisomerase II-specific drug-stimulated cleavage site in the *Drosophila* genome is found in the 359bp repeat sequence (Kas and Laemmli, 1992). Thus, topoisomerase II is one of a growing number of proteins known to bind to specific heterochromatic regions (Masumoto et al., 1989, Raff et al., 1994). This provides a means to track a specific chromosome region: by injecting fluorescently labeled topoisomerase II into living embryos the accumulation foci can be imaged, revealing the motion of the underlying chromatin (Fig 3I). Embryos remained alive during imaging as judged by normal synchronized nuclear divisions and subsequent successful hatching. To compensate for nuclear drift, we compute the distance r(t) from the topoisomerase II spot to the center of the nucleus . For a particle with diffusion constant D, $\langle \Delta r^2 \rangle$ vs. Δt

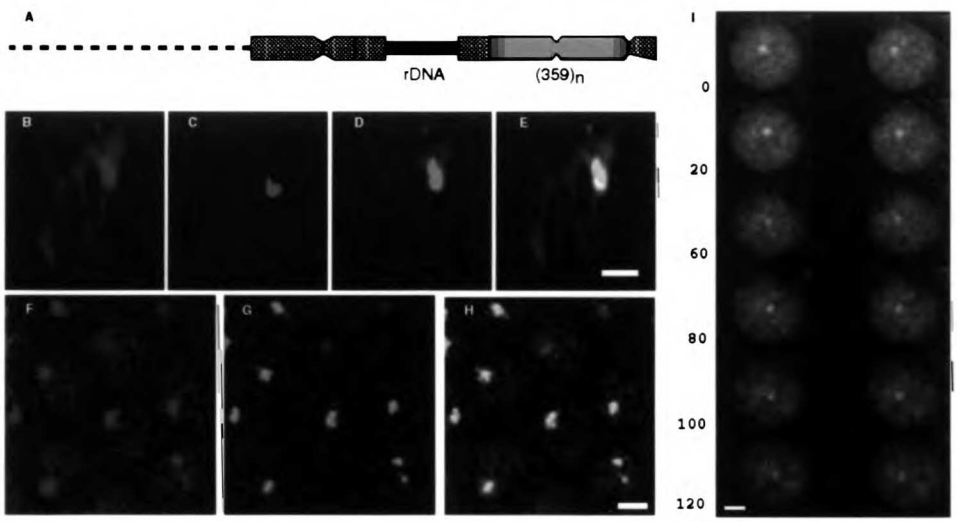

Figure 3.3. Visualizing interphase chromatin motion in Drosophila.

Figure 3.3. Visualizing interphase chromatin motion in Drosophila: topoisomerase II binds at the 359bp repeat region on the X chromosome in *Drosophila* embryos. (A) heterochromatin of the X chromosome (Lohe et al., 1993). (B-E) simultaneous FISH and immunofluorescence demonstrating topoisomerase II accumulation at 359bp repeat in anaphase. (B) anti-topoisomerase II immunofluorescence, (C) FISH using probe to rDNA locus, (D) FISH using probe to 359bp repeat, (E) overlay of B,C, and D. Clearly the topoisomerase II signal completely coincides with the 359bp signal but not the neighboring rDNA. Bar 2.0 μm. (F-H) topoisomerase II localization in interphase. (F) topoisomerase II, (G) 359bp repeat, (H) overlay showing complete coincidence of the two signals. Bar 2.0 μm. (I) Injection of rhodamine labeled topoisomerase II allows visualization of the 359bp repeat region in vivo in three dimensions. Times corresponding to each stereo pair given in seconds. Bar 2.0 μm. Embryos imaged under these conditions remain viable: after imaging embryos were maintained in humidified chambers until hatching. Embryos that were imaged hatched with the same frequency as embryos injected with buffer and not imaged. During imaging, synchronized mitoses occurred on schedule and no chromosome segregation defects (anaphase bridges, etc.) were observed.

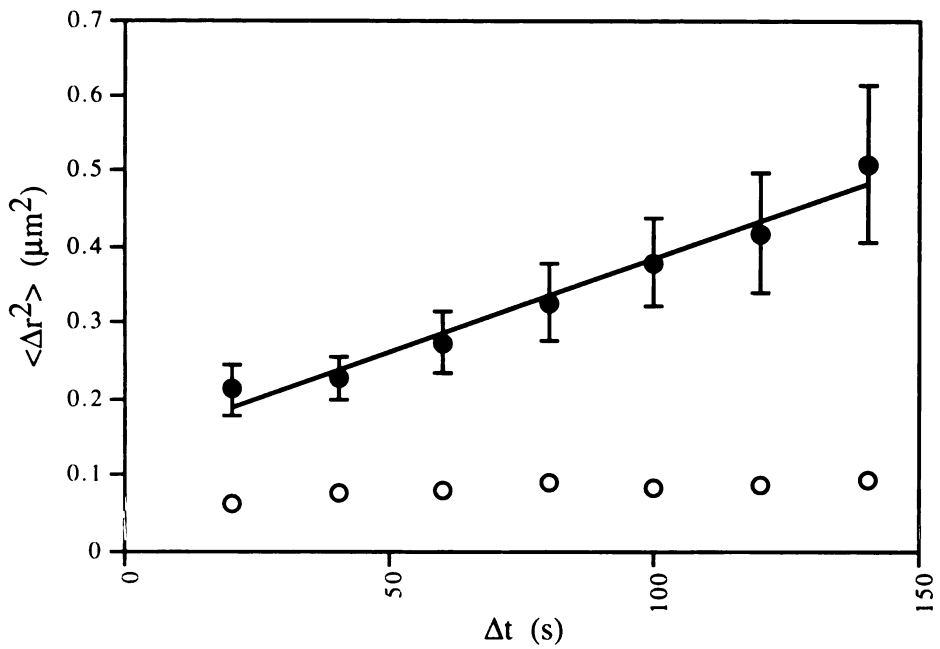

Figure 3.4. Chromatin diffusion in *Drosophila*. (•) Data from living embryos. A total of 27 data records, each containing an average of 9 time-points, were combined in this plot. (——) best-fit line with slope 0.0025 $\mu m^2/s$ corresponding to $D=1.25 \times 10^{-11}$ cm^2/s. Linear plot implies free diffusion on the time-scale examined. (o) fixed embryos stained with anti-topoisomerase II antibodies and imaged under identical conditions.

should be linear with slope 2D. We computed $<\Delta r^2>$ vs. Δt for 27 nuclei from 6 different *Drosophila* embryos (Fig. 4). The data fit a line of slope 0.0025 $\mu m^2/s$ (correlation coefficient r=0.987). From the slope we estimate $D=1.25x10^{-11}$ cm^2/s, a slightly larger value than in yeast. The plot does not plateau, so the diffusion appears unconstrained. This apparent lack of confinement is interesting in light of evidence that this region is a scaffold-associated region (SAR) in Drosophila (Kas and Laemmli, 1992). One would have anticipated that interaction with a large insoluble nuclear scaffold spanning the nuclear interior, such as that visualized in electron microscopy of nuclear matrix preparations (Capco et al., 1982), should result in strong confinement of diffusion. If, however, the scaffold in vivo actually represents a flexible chromosome backbone or some other highly dynamic structure, then the presence of SARs in the 359bp repeat need not necessarily lead to a diffusion constraint. Moreover, the present Drosophila data only covers a relatively fast time-scale, and hence our results do not address confinement on longer time scales. Indeed, we have demonstrated by FISH that in fact different loci in Drosophila, including the 359bp repeat, reproducibly localize to particular regions of the nucleus (Marshall et al 1996), which strongly implies that some sort of confinement will indeed be observed on a longer time scale.

DISCUSSION

We have developed a methodology to measure the motion of chromatin in interphase nuclei of living cells. Such measurements reveal that diffusive motion of chromatin does indeed occur, but this motion is constrained in some cases.

Comparison With Other Studies of Chromatin Motion

Previous studies of chromatin in living cells have generally indicated rotational motion of the nucleus as the predominant type of chromatin motion (6). Our study differs from this earlier work in that we have deliberately chosen to use rotationally invariant

measures (d and r) so that changes of position within the nucleus, rather than overall nuclear rotation, can be measured directly. Apart from nuclear rotation, apparent Brownian motion of chromosomes within the nucleus has not previously been reported (Cremer et al., 1982; De Boni and Mintz, 1986; Shelby et al., 1996). The small magnitude of the diffusion constants measured here, together with the fact that chromatin diffusion is constrained in some cases, predicts that the diffusive motion we observe is unlikely to be noticed unless explicitly tested for, using the type of analysis employed here. Indeed, one recent paper used a centromere-localized GFP fusion protein and concluded that Brownian motion of the centromeres was not taking place (Shelby et al 1996), but in fact their data appeared very similar to that in Figure 2A, and it may well be that if they had in fact plotted the mean-squared change in position versus time interval, rather than position versus time, a similar constrained diffusion might have been observed.

We also note that several studies have used time-resolved fluorescence spectroscopy to study chromatin motion on a very short time scale. Notably, Selvin et al (1990) have used time-resolved polarized fluorescence recovery after photobleaching (a measure of rotational diffusion) to measure the small-scale motion of chromatin on the millisecond time scale in intact isolated nuclei, with the result that under physiological conditions, very little movement was observed. However, we note that these spectroscopic methods employ a much faster time-scale than the particle-tracking method employed by us. It is very difficult to predict the diffusive behavior on one time-scale from the behavior measured on a vastly different time-scale. This does, however, provide a cautionary note: the results obtained here only apply to processes that require large motions on the order of a micron. Our results make no predictions regarding the rate of very small scale processes such as looping of enhancer regions to contact promotor regions.

Comparison with Other Biological Macromolecules

These results indicate that chromatin moves with a diffusion constant much lower than that previously reported for biological macromolecules. For proteins D is generally around 10^{-6} cm^2/s in aqueous solution and 10^{-8} to 10^{-7} cm^2/s in cytoplasm (Luby-Phelps et al., 1985). This difference is, of course, to be expected given the vastly greater size of the chromosome polymer. Chromatin also diffuses more slowly than DNA in dilute solution, for which D ranges from 10^{-8} to 10^{-9} cm^2/s for DNA 4-300 kb in length (Smith et al, 1996). This result was not obvious a priori, since presumably interphase chromatin is more compact than naked DNA and thus its intrinsic diffusion constant should be higher. Presumably the more tangled conditions in the nucleus lead to the vastly decreased motion that is observed.

Comparison With Predictions From Polymer Dynamics

Having characterized chromatin motion as diffusive, we consider how the diffusion constant compares with that expected for a large polymer undergoing thermal motion in free solution (Doi and Edwards, 1986), $D_{free} = 0.2\ kT\ /\eta R$ where $kT = 4x10^{-14}$ ergs at room temperature, η is the viscosity, and R is the average end-to-end length of the polymer. For the CEN plasmid, because the Lac operator array constitutes the majority of the DNA, we approximate the end-to-end length R as the radius of the observed GFP signal. The GFP signal radius is less than 0.5 μm, so taking this as an upper bound on R yields a lower bound for D_{free}. Nucleoplasm viscosity is reported to be in the range 1.0 - 10.0 cP based on the diffusion of tracer molecules in the nucleus (Lang et al., 1986; Fushimi and Verkman, 1991). We assume a reasonable value η = 5 cP. This gives a minimum $D = 3x10^{-9}$ cm^2/s, three orders of magnitude larger than the experimental value. This discrepancy is difficult to make up with reasonable changes in R or η, but can be explained if we consider that the chromatin is not in a dilute solution. As with cytoplasmic molecules (Lubh-Phelps et al., 1988), crowding and entanglement will impede chromatin motion. If the chromosome is entangled at n loci, a conservative

estimate based on the theory of reptation (Grosberg and Khokhlov, 1994) indicates that the diffusion constant is reduced to $D_{entangled} = D_{free}/n^{3/2}$. We briefly derive this result here. We assume chromatin behaves as an ideal polymer chain (Van den Engh et al., 1992). According to the reptation model the set of entanglements provide obstacles which delimit a tube within which the polymer diffuses with diffusion constant D_t. The n entanglement sites divide the chain into n subchains, each with average radius $R_{subchain}=R/(n^{1/2})$ so each subchain has a diffusion constant of $D_{free}n^{1/2}$. A string of n subchains thus diffuses through the tube with a diffusion constant $D_t \sim (1/n)D_{free}n^{1/2} = D_{free}/n^{1/2}$. The time for the chain to diffuse out of the tube is $\tau^*=L^2/D_t$ where the total contour length of the tube is $L=nR_{subchain}$. During this time the center of mass of the polymer diffuses over a distance R. Hence, $D_{entangled} \sim R^2/\tau^* = R^2D_t/L^2 = D_t/n$ (since $L^2=nR^2$). Thus $D_{entangled} \sim D_{free}/n^{3/2}$. A modest number (~20) of entanglements would slow the diffusion constant by two orders of magnitude, and motion could be further impeded by other nuclear components. The observed magnitude of D is thus roughly consistent with that expected from Brownian motion. However, the fact that azide slightly reduces chromatin motion in yeast (Fig. 2B) may suggest additional contributions to chromatin motion from active processes. Additionally, the fact that D does not necessarily increase with decreasing chromosome size (Fig. 2C) further suggests a more complicated picture, although, as discussed above, this may simply be a consequence of the tethering of chromatin to a substrate.

Magnitude of the Diffusion Constant Relative to Rates of Biological Processes

If we assume the magnitude of D measured here for these particular sites is representative of chromatin in general, we can reconsider the question of whether or not chromatin diffusion is fast enough for motion-requiring processes to take place by diffusion alone. A process such as meiotic homolog pairing will generally require chromatin to move over distances of several microns. Given D in the range 10^{-12} to 10^{-}

^{11} cm^2/s, it would take roughly 1-10 min for chromatin to diffuse 1 μm in a given direction, which is sufficiently fast compared to the duration of interphase (>1hr) for such process to be able to occur via diffusion. On the other hand, because this diffusion time is slow relative to the time-scale of most molecular interactions, diffusion is likely to be rate-limiting in these processes.

Implications of Constrained Diffusion

The fact that chromatin diffusion is constrained (Fig. 2B) has strong implications for processes involving motion. For two loci to interact, their confinement regions must overlap, otherwise the interaction will be prevented because the loci will never be sufficiently close. On the other hand, if the confinement regions of two loci do overlap, the frequency of collisions between the loci will actually be higher than if the loci were unconfined, because they are forced to remain in the same general vicinity. Thus, in cases of constrained diffusion, nuclear architecture (i.e.. where a locus is positioned in the nucleus) is of paramount importance and will determine whether a particular interaction can or cannot occur. Moreover, the diffusional constraint observed in yeast provides the first direct evidence that chromatin is anchored to a relatively immobile superstructure in vivo. Whether this anchoring structure is the nuclear envelope or some internal nuclear matrix will be the subject of future investigation.

Conclusions

The picture thus emerges that interphase chromatin is able to diffuse within the nucleus, but only to a limited extent. The result that a given locus may not be free to explore the entire nucleus is consistent with our recent studies of nuclear positioning in interphase which indicated that for 42 different loci examined, each was consistently found in approximately the same position in all nuclei, and this reproducible nuclear position was locus-specific (Marshall et al., 1996). The present work indicates that

within its region of localization, the chromosome locus is nevertheless able to undergo substantial diffusive motion.

These studies illustrate the power of quantitative motion analysis for time-lapse three-dimensional microscopic data. This approach of inferring mechanistic behavior from analysis of three dimensional motion should be applicable to a broad range of problems in cell biology.

References

Agard, D.A., Hiraoka, Y., Shaw, P., Sedat, J.W. 1989. Fluorescence microscopy in three dimensions. *Meth. Cell Biol.* **30**, 353-377.

Berg, H.C. 1983. Random walks in biology. Princeton University Press, Princeton.

Capco, D.G., Wan, K.M., and Penman, S. 1982. The nuclear matrix: three-dimensional architecture and protein composition. *Cell* **29**,847-858.

Cremer, T., Cremer, C., Baumann, H., Luedtke, E.K., Sperling, K., Teuber, V., and Zorn, C. 1982. Rabl's model of the interphase chromosome arrangement tested in chinese hamster cells by premature chromosome condensationnand laser-UV-microbeam experiments. *Hum. Genet.* **60**,46-56.

De Boni, U., Mintz, A.H. 1986. Curvilinear, three-dimensional motion of chromatindomains and nucleoli ni neuronal interphase nuclei. *Science* **234**,863-6.

Dernburg, A.F., Broman, K.W., Fung, J.C., Marshall, W.F., Philips, J, Agard, D.A., and Sedat, J.W. 1996. Perturbation of nuclear architecture by long-distance chromosome interactions. *Cell* **85,** 745-759.

Doi, M., and Edwards, S.F. 1986. *The Theory of Polymer Dynamics* . Oxford University Press, NY. Chapter 4.2.

Fushimi, K. and Verkman, A.S. 1991. Low viscosity in the aqueous domain of cell cytoplasm measured by picosecond polarization microfluorometry. *J. Cell Biol.* **112**,719-725.

Gelles, J., Schnapp, B.J., Sheetz, M.P. 1988. Tracking kinesin-driven movements with nanometre-scale precision. *Nature* **331**,450-453.

Grosberg, A.Y., and Khokhlov, A.R. 1994. *Statistical Physics of Macromolecules.* Am. Inst. of Physics Press, NY. pp. 257-266.

Hirano, T., Mitchison, T.J., Swedlow, J.R.. 1995. The SMC family: from chromosome condensation to dosage compensation. *Curr. Opin. Cell Biol.* **7**,329-36.

Hsieh, T., Brutlag, D. 1979. Sequence and sequence variation within the 1.688 g/cm^3 satellite DNA of Drosophila melanogaster. *J. Mol. Biol.* **135**,465-481.

Kao, H.P., Verkman, A.S. 1994. Tracking of single fluorescent particles in three dimensions: use of cylindrical optics to encode position. *Biophysical J.* **67**, 1291-1300.

Kas, E. andLaemmli, U.K. 1992. In vivo topoisomerase II cleavage of the Drosophila histone and satellite III repeats: DNA sequence and structural characteristics. *EMBO J.* **11**, 705-716.

Koshland, D., Strunnikov, A. 1996. Mitotic chromosome condensation. *Ann. Rev. Cell Dev. Biol.* **12**,305-333.

Lang, I., Scholz, M., and Peters, R. 1986. Molecular mobility and nucleocytoplasmic flux in hepatoma cells. *J. Cell Biol.* **102**,1183-90

Lee, G.M., Ishihara, A., Jacobson, K.A. 1991. Direct observation of Brownian motion of lipids in a membrane. *Proc. Natl. Acad. Sci. U.S.A.* **88**, 6274-8.

Lohe, A.R., Hilliker, A.J., Roberts, P.A. 1993. Mapping simple repeated DNA sequences in heterochromatin of Drosophila melanogaster. *Genetics* **134**, 1149-1174.

Luby-Phelps, K., Lanni, F., Taylor, D.L. 1988. The submicroscopic properties of cytoplasm as a determinant of cellular function. *Ann. Rev. Biophys. Biophys. Chem.* **17**,369-96.

Luby-Phelps, K., Lanni, F., and Taylor, D.L. 1985. Behavior of a fluorescent analog of calmodulin in living 3T3 cells. *J. Cell Biol.* **101**,1245-56.

Maguire, M.P. 1984. The mechanism of meiotic homolog pairing. *J. Theor. Biol.* **106**,605-15.

Marshall, W.F., Dernburg, A.F., Harmon, B., Agard, D.A., Sedat, J.W.. 1996. Interactions of chromatin with the nuclear envelope: positional determination within the nucleus in Drosophila melanogaster. *Mol. Biol. of the Cell* **7**,825-842.

Masumoto, H., Masokata, H., Muro, Y., Nozaki, N., and Okazaki, T. 1989. A human centromere antigen (CNEP-B) interacts with a short specific sequence in alphoid DNA, a ahuman centromeric satellite. *J. Cell Biol.* **109**,1963-73.

Milankov, K., De Boni, U.. 1993. Cytochemical localization of actin and myosin aggregates in interphase nuclei. *Exp. Cell Res.* **209**,189-99.

Mitchison, T.J., Sedat, J. 1983. Localization of antigenic determinants in whole Drosophila embryos. *Dev. Biol.* **99**,261-4.

Parvinen, M., Soderstrom, K.O.. 1976. Chromosome rotation and formation of synapsis. *Nature* **260**,534-535.

Qian, H., Sheetz, M.P., Elson, E.L.. 1991. Single particle tracking. *Biophys. J.* **60**,910-921.

Raff, J.W., Kellum, R., and Alberts, B. 1994. The Drosophila GAGA transcription factor is associated with specific regions of heterochromatin throughout the cell cycle. *EMBO J.* **13**,5977-83.

Robinett, C.C., Straight, A.F., Murray, A.W., and Belmont, A. 1996. In vivo localization of DNA sequences and visualization of large-scale chromatin organization using lac operator/repressor recognition. *J. Cell Biol.* **6**,1685-1700.

Selvin, P.R., Scalettar, B.A., Langmore, J.P., Axelrod, D., Klein, M.P., and Hearst, J.E. 1990. A polarized photobleaching study of chromatin reorientation in intact nuclei. *J. Mol. Biol.* **214**,911-922.

Shelby, R.D., Hahn, K.M., Sullivan, K.F.. 1996. Dynamic elastic behavior of alpha-satellite DNA domains visualized in situ in living human cells. J. Cell Biol. ***135***,545-558.

Smith, D.E., Perkins, T.T., Chu, S. 1996. Self-diffusion of long DNA molecules. *Macromolecules* **29**,1372-1373.

Smithies, O. and Powers, P.A. 1986. Gene conversions and their relation to homologous chromosome pairing. *Phil. Trans. Royal. Soc. London Ser. B* **312**,291-302.

Straight, A.F., Belmont, A.S., Robinett, C.C., Murray, A.W.. 1996. GFP tagging of budding yeast chromosomes reveals that protein-protein interactions can mediate sister chromatid cohesion. *Curr. Biol.* **6**,1599-1608.

Swedlow, J.R., Sedat, J.W., Agard, D.A.. 1993. Multiple chromosomal populations of topoisomerase II detected in vivo by time-lapse, three-dimensional wide-field microscopy. *Cell* **73**, 97-108.

Van den Engh, G., Sachs, R., Trask, B.J. 1992. Estimating genomic distance fromDNA sequence location in cell nuclei by a random walk model. *Science* **257**,1410-2.

Van Kampen, N.G. 1992. *Stochastic Processes in Physics and Chemistry* North Holland, Amsterdam. p. 203.

Weber, V., Harata, M., Hauser, H., Wintersberger, U.. 1995. The actin-related protein Act3p of Saccharomyces cerevisiae is located in the nucleus. *Mol. Biol. of the Cell* **6**,1263-70.

Yin, H., Wang, M.D., Svoboda, K., Landick, R., Block, S.M., and Gelles, J. 1996. Transcription against an applied force. *Science* **270**,1653-1657.

Chapter 4. Chromosome mechanics in vivo: quantitative analysis of biological structure and motion in four dimensions

Summary

Mitosis is an essentially mechanical process, and for this reason we need to understand the mechanical properties of the components involved if we are to understand the mechanism of chromosome segregation and cell division. Ideally, we would like a way to measure the mechanical properties of spindle components and chromosomes in a noninvasive way inside living cells. To this end, we have developed a suite of computational tools for visualization and analysis of motion in four dimensions, from which a number of important mechanical properties of the system can be deduced based solely on time-lapse 3D microscopic imaging.

Recent developments in microscopy have made the acquisition of such four dimensional (three-dimensions as a function of time) image data a routine process. However, the vast quantities of data included in these four dimensional image series leads to a general need for methods to analyze the data and rapidly extract useful information without becoming overwhelmed. In particular, direct visual examination of time lapse 3D data rarely provides much information, since the images are complicated and constantly changing. Clearly a computational approach is called for. Here we present a model-based nonrigid motion estimation algorithm for tracking the motion of chromosomes in vivo. We then present a series of computational tools for extracting information about chromosome mechanics from the motion data. These tools are then applied to the prometaphase congression of chromosomes in the Drosophila embryo. We demonstrate that chromosomes approach the metaphase plate in a direction perpendicular to the long axis of the chromosomes, and the motion is sometimes led by the kinetochores, and sometimes by

the arms, as if the forces exerted by the polar ejection force and those exerted at the kinetochore are roughly equivalent.

INTRODUCTION

Two recent trends in microscopy point towards the need for computational analysis of motion of cellular structures. One major trend is the use of microscopy and optical techniques to study the mechanics of cells. For example, diffusion of fluorescent tracer molecules has been used to probe the pore size of the cytoskeletal protein network (Luby-Phelps et al., 1988). Another example is the measurement of microtubule flexibilty from the fluctuations of microtubule shape images (Gittes et al., 1993). These approaches are gradually leading to an understanding of cytomechanics in some detail, but one crucial aspect has for the most part been missing, namely, the direct measurement of the mechanical behavior of cellular structures in 3D in vivo. The second important trend in microscopy has been the increasing use of time-lapse three-dimensional imaging to study the behavior of living cells (Thomas et al, 1996). These four-dimensional (three spatial dimensions plus time) microscopy methods lead to a large volume of data from which meaningful conclusions must be drawn. One of the most obvious applications of four-dimensional imaging lies in the mechanics of cellular structures. The key is to realize that the motion and conformational dynamics of cellular components reflects their mechanical properties and the forces acting upon them. In order to exploit this connection, and thus combine the twin technological developments of in vivo cytomechanics and four-dimensional imaging, we need a methodology that will allow properties of cellular structures that are relevant to cytomechanics (such as flexibility, mobility, etc) to be extracted from complex four-dimensional datasets. Ultimately we would like such tools to be very general, capable of analysis of membrane-bound vesicles, protein filaments such as microtubules, chromosomes, mitochondria, and so forth. This overarching goal will

involve a major development effort in the areas of computer vision, visualization, and computational geometry. As a first step in this direction, we have developed a toolkit of algorithms for the measurement and analysis of chromosome motion. Many of these tools could, of course, be applied to other cellular structures as well. In order to maintain a goal-oriented focus in this work, we have geared the suite of analysis tools towards the aim of measuring chromosome mechanics during prometaphase congression.

A major question in cell biology is how does the spindle position chromosomes on the metaphase plate. This process clearly involves an interplay between forces applied directly at the kinetochore and forces exerted along the chromosome arms by the polar ejection force. This polar ejection force refers to a tendency for chromosomes or chromosome fragments toe driven away from the spindle poles. One model for the polar ejection force is that the chromosomes are pushed by polymerizing microtubules "like a knight being repelled by a lance" (Murray and Hunt, 1994). Another possibility, however, is that microtubule motor proteins localizing to the chromosome arms cause the arms to move along non-kinetochore microtubules (Afshar et al., 1995). At any rate, the kinetochore forces and the polar ejection forces together result in proper alignment of the chromosome in metaphase. As our initial goal we thus seek to analyze the mechanical features of the polar ejection force indirectly by visualizing its effect on chromosomes. In effect, we wish to use the motion of chromosomes as an indicator of the forces acting on them, just as aeronautical engineers use dust particles to visualize the flow of air around an airplane wing in a wind tunnel. Drosophila is a particularly useful system in this regard because its chromosome are relatively long and flexible, unlike those of vertebrates which are short rigid rods. As a consequence of the higher chromosome flexibility in Drosophila, differences in force (such as that applied at the kinetochore versus that applied by the polar ejection force) will result in more pronounced bending of the chromosome. Thus in principle, changes in chromosome shape will reflect changes in applied forces. Finally, Drosophila prometaphase is interesting from the point of view of nuclear architecture

because the chromosomes assume a very characteristic arrangement, in which the relatively straight chromosomes form a bundle oriented perpendicularly to the spindle axis. This is one of many examples of chromsomes forming a reproducibly specific arrangement, and it is hoped that by studying the motion of the chromosomes as they attain this configuration, we can gain insight into the mechanism by which specialized chromosome arrangements are formed. For these reason, we desired to study the conformational dynamics of Drosophila embryo chromosomes as they congressed to the metaphase plate. Specifically, we would like to determine whether kinetochores or arms lead the motion towards the plate, and try to use the shape of the chromosomes during congression to indirectly measure the relative forces exerted at the kinetochore and the forces exerted on the arms. There is already a precedent for this approach. Careful analysis of chromosome motion during prometaphase and metaphase in newt lung epithelial cells has revealed periodic oscillations in kinetochore movement along the spindle, which has important implications for spindle-chromosome interactions (Skibbens et al, 1993). However, unlike newt lung cell chromosomes, chromosomes in the Drosophila embryo are not confined to a single plane, therefore 3D motion analysis methods are required. Furthermore, because visualization of Drosophila chromosomes in 3D is a slow process compared with video DIC microscopy, the motion tracking method must be able to cope with limited temporal resolution, which is a formidable problem. Our lab has previously developed the high-speed high-resolution low-light three-dimensional fluorescence imaging system required to collect time-lapse 3D images of congressing Drosophila chromosomes, as well as a suite of image processing and visualization tools to improve image contrast and compensate for image degradation due to optics and to noise. Methods to model and analyze the three dimensional conformation of chromosomes have also been the focus of past development efforts. This chapter focusses on the next step, the analysis of chromosome motion from time-lapse 3D fluorescence images.

Tracking the motion of nonrigid objects from a series of images is a nontrivial image processing problem and is currently the subject of research by many groups. We present a model-based motion estimation scheme for tracking nonrigid 3D motion under conditions of limited temporal resolution. We present a scheme for using the motion estimate to deduce mechanical properties of chromosomes, such as flexibility, and for tracking the trajectories of specific regions on a chromosome. We further present algorithms for extracting the component of motion parallel to the mitotic spindle and present preliminary results obtained from metaphase chromosomes in living Drosophila embryos.

Materials and Methods

injection of embryos

Both wild-type (Oregon-R) flies and flies homozygous for the lt^{x13} translocation (Wakimoto and Hearn, 1990) were used for this study. In lt^{x13} the left arm of chromosome 2 is translocated onto the right arm of chromosome 3, resulting in one arm that is twice as long as the others. This allows identification of one particular chromosome arm in images of living embryos, which ordinarily is impossible because all arms are approximately the same length. Oregon-R embryos were collected from population cages on cornmeal-agar plates. lt^{x13} Embryos were collected from bottles using miniature cornmeal plates made by melting cornmeal-agar media and pouring into the lids of small plastic petri dishes. Scratches were made on the surface of the cornmeal-agar after cooling, to encourage egg-laying. After collecting for 30 minutes from cages or 1 hour from bottles, embryos were bleach dechorionated, mounted on a 22x35 #1.5 coverslip with double-stick tape glue dissolved in heptane, and desiccated for 13 minutes in a sealed chamber with Dri-Rite desiccant. During dessication embryos were observed to avoid over-drying. Embryos were then overlaid with halocarbon oil and injected either with Cy5-labelled histone protein (a gift of Michael Paddy, University of Florida) or with a solution of the DNA dye OliGreen (Molecular Probes Inc., Eugene, OR) diluted 20-fold in PBS

(use of OliGreen as an in vivo chromosome stain in Drosophila embryos was first demonstrated by William Theurkauf, SUNY Stony Brook). Our previous studies of chromosome motion have employed directly labeled histones, but OliGreen has the advantage that it is commercially available and relatively cheap. Because it is a small molecule, the injection solution has a low viscosity and does not form precipitates, so that the needles have good flow and never clog even when many embryos are injected. However, OliGreen tends to produce a higher background fluorescence than labelled histones, and so for the highest quality images we were forced to rely on Cy5 labelled histones. Because Cy5 fluorescence emits light in the infrared region of the spectrum it is not visible to the eye, and so we added a small ammount of OliGreen to the injection mixture, allowing visual identification of nuclei. After locating an embryo about to enter mitosis (this can be determined by noting an increase in the granularity of the nuclear chromatin signal) using the eyepieces of the microscope, all subsequent steps were carried out by using the CCD camera to detect the Cy5 fluorescence.

four dimensional fluorescence wide-field microscopy

Following injection, embryos were imaged on a wide-field epifluorescence microscope in which all filter wheels, shutters, and stage motion are under computer control[5]. The excitation light source was a mercury arc lamp coupled to the microscope by a fiber-optic light scrambler to give uniform illumination accross the entire field. This type of wide-field imaging is extremely advantageous for in vivo 3D imaging, because unlike in a confocal microscope where 90% of the photons emitted by the sample are rejected by the pinhole, and another 90% fail to be registered by the photomultiplier tube due to the inherently low quantum efficiency of the PMT, in the wide-field system essentially all the emitted photons are recorded because there is no pinhole and the detector, a cooled scientific grade CCD camera, has a very high quantum efficiency, on the order to 90%. Thus, a mercury lamp can be used as a light source rather than the much brighter laser sources used in confocal.

The use of the low excitation intensity of the mercury lamp appears essential for keeping the embryos alive during the imaging process, to avoid concerns about photodamage-induced artifacts. Imaging was done through a 60x N.A. 1.4 oil immersion lens using 1.5180 oil. 256x256 pixel images were collected at each focal position by the CCD camera, using a filterset and dichroic mirror optimized for FITC, and optical sectioning was performed by stepping the stage in 0.5 μm increments. The pixel size with this setup is 0.1117 x 0.1117 x 0.5 μm. At each focal plane, a 0.5 second exposure was collected. After 18 sections were collected, the stage was moved back 9.0 mm and the process repeated. With this arrangement, our current temporal resolution is one 256x256x18 three-dimensional dataset every 25 seconds. The time resolution is limited primarily by exposure time and time required to move the stage from one position to the next. The total overhead time required to read out an image from the CCD, convert the analog charge to digital values, write these values onto the hard drive, and move the stage by 0.5 μm, was 1.8 seconds. Taking smaller images (128x128 pixel) does not substantially increase data collection rate, and greatly increases the chances that a nucleus will drift out of the field of view before data collection is finished. Following data collection, out of focus blur is removed by three-dimensional constrained iterative deconvolution[6] using an empirically measured point spread function. Projections of four successive time-points from such a 4D dataset is given in figure 4.1. Neither the OliGreen nor the imaging process were damaging to the embryos: of 15 embryos injected, 14, including the embryo used for the analysis presented here, developed normally into larvae. These survival rates are the same as those for embryos injected with buffer alone. Moreover, during imaging, synchronized nuclear divisions occur at the appropriate rate and without any gross abnormalities, such as anaphase bridges, which would be diagnostic of DNA damage. We note that despite the fact that several labs use confocal microscopy to image chromosomes in Drosophila embryos, none have been able to keep the embryos alive during the imaging process. This is likely due to the extremely high intensity of the laser light needed in the confocal setup.

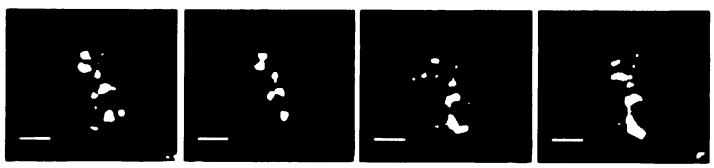

Figure 4.1. Visualizing motion of mitotic Drosophila chromosomes in vivo.

Figure 4.1. Projections of four successive 3D images taken from a time lapse 3D movie of a living Drosophila embryo injected with the DNA dye OliGreen, showing the metaphase chromosomes of a single nucleus. Scale bar 2.0 mm.

image processing

After imaging and deconvolution, images were further processed by median filtering. A median filter is an algorithm that replaces the value of each pixel with the median intensity in a 3x3 or 5x5 box of pixels surrounding the pixel in question. This is most useful for removing "salt and pepper" noise, in which the image is corrupted by scattered bright and or dark intensity spikes. This type of noise is characteristic of the photon statistical noise which is the dominant noise source in low light imaging. Another type of noise common in low-light imaging is quantization noise due to the fact that the entire inensity range of the sample may be so low as to end up being mapped by the A/D converter onto a relatively few discrete digital values. This results in a grainy image. To reduce quantization noise, we employ an analog amplifier prior to the A/D converter thus expanding the dynamic range of the signal prior to quantization, in order to spread the inensity range of the signal over more digital levels, thus making a smoother image. One other type of image degradation needs to be discussed: motion blurring. When taking an image of a moving object, if the object moves significantly during the acquisition time of a single image, it will produce a blurred image on the camera. Based on the estimates of rigid body motion discussed below, the overall translational displacement of the nuclei is on the order 0.2 μm between successive 24 second time points. This then predicts that during a 0.5 second exposure, the nucleus will move approximately 0.04 μm, which is significantly less than the size of one pixel (0.1117 in x and y), thus there will be essentially no motion blurring.

Results

Optical flow algorithms cannot track moving chromosomes

Initial attempts to track the motion of Drosophila prometaphase chromosomes employed the Block-Matching optical flow algorithm (Haralick and Shapiro, 1993), a standard

motion estimation algorithm commonly employed in the computer vision field. In block matching, the image is divided into small blocks of pixels, (tests on Drosophila used blocks ranging from 5x5x3 to 21x21x5 pixels). Then for each box, a search is done to see which block in the image at time t+1 best matches, pixel by pixel, the current block at time t. The relative spatial offset of the best-matching box at time t+1 relative to the box at time t specifies the motion estimate for the center of the box at time t. Block-matching type optical flow algorithms have been employed to track the movements of cells during Dictystelium development (Awasthi et al., 1994; Doolittle et al., 1995). Because the nonrigidity of chromosomes will allow chromosome segments to rotate and possible stretch, we also tested a variant of this approach in which the box is allowed to undergo a general affine transformation (which allows, in addition to translation, the additional operations of rotation, magnification, and shear) in order to find the best match (Fuh and Maragos, 1991). When the results of these analyses were compared with the actual images, it was found that the motion vectors produced did not correspond to the motion that was visually apparent. For example, frequently neighboring points on the same chromosome arm at time t would be mapped onto wildly disparate points on separate arms at time t+1. The failure of the block matching approach is due to a well-known flaw in block matching and all other local optical flow algorithms, which is called the "Aperture Problem". The aperture problem stems from the fact that we are examining a small window of data and trying to compare it with similar small windows in the new image. If this window of data is too small, then there will be a great many possible matches at time t+1. This is particularly true in our case, where a small region of a chromosome will look basically the same as any other small region, thus generating many false matches and making block matching impossible. If, on the other hand, the window of data is taken so large that it contains a meaningful pattern that will not generate many false matches, chances are it contains portions of more than one chromosome, which are moving relative to each other, and so the resulting best match may not reflect the motion of any individual

chromosomes. Moreover, for nonrigid objects like Drosophila chromosomes, the shape of the segment within the box is likely to change so much as to make a direct match impossible. Thus block matching was not a viable method for tracking prometaphase chromosome motion in Drosophila, and indeed I should have known from the outset that this would be the case (D. Agard, per. comm.).

The problem with block matching can best be summed up by saying that small windows of data do not contain enough information to determine the motion in the image, while large windows of data are unlikely to remain even approximately constant due to nonrigidity and limited temporal resolution. This does not however mean that motion estimation is impossible. As with many machine vision tasks, specific a priori knowledge about the objects can be used to assist the motion estimation process. In this case, we know that chromosomes are connected curve-like objects which do not break apart during mitosis. The key to chromosome motion analysis then is to find a way to take advantage of this knowledge.

Model-based nonrigid motion estimation

Most published cases of motion esimation algorithms which make use of a priori information are based on the assumption that the object moving is a rigid body and hence its motion can be described as a composition of a simple translation and a simple rotation. Estimation of the motion of nonrigid objects, such as chromosomes, is much less common. In this case, we cannot rely on absolute rigidity as an assumption, but we can make assumptions about connectivity. In other words, while neighboring points need not remain at a fixed relative position as in a rigid body, initially connected points must at the very least remain connected. In order to incorporate connectivity information into the motion estimation process, we first represent the chromosome configuration as a graph, in which vertices represent points on a chromosome arm, and edges represent continuous stretches of chromatin connecting neighboring points. This graph representation is built by

interactively picking and connecting object points within a 3D image, forming a set of wireframe models (Mathog, 1985) for the chromosomes. This interactive modelling is done using a custom interactive modelling package developed in our lab by Diana Hughes. In this system, the object is displayed in several different orientations along with a display of the current wireframe model, and the user clicks the mouse on various points in the images to specify locations along the chromosome arms, and the model is automatically updated as is the cursor position in the other viewing orientations. The wireframe models represent the arm as a set of positions versus length along the arm. Length along an arm is specified such that telomeres are at the beginning of the arm (length=0) and centromeres are at the end. Unambiguous identification of centromeres and telomeres is possible in metaphase because the centromeres cluster to form the metaphase plate while telomeres protrude out into the cytoplasm. Figure 4.2 illustrates the chromosome models obtained for one nucleus, for several successive time points. From this data it is already clear that there is considerable motion from one time point to the next. It is also clear that it is difficult to visually determine which chromosome corresponds to which between successive time points.

Once a graph is obtained for each time-point, the motion estimation problem becomes a graph-matching problem, in which we seek an optimal mapping of elements of the graph at time t onto elements of the graph at time t+1. Because vertices are chosen manually, their number and positioning along an arm are arbitrary and unlikely to be consistent from one time point to the next. Therefore, attempting to match vertices onto vertices is problematical. For this reason, we have instead chosen to first locate entire chromosomes within the graph and then set up a mapping between chromosomes, thus imposing a topological constraint that connected points remain connected under the mapping. In this implementation a chromosome is defined as a simple path in which all vertices have degree 2 except the first and last vertices. Because the Drosophila embryo chromosomes at metaphase are simple linear unbranched chromosomes, this simple definition is sufficient.

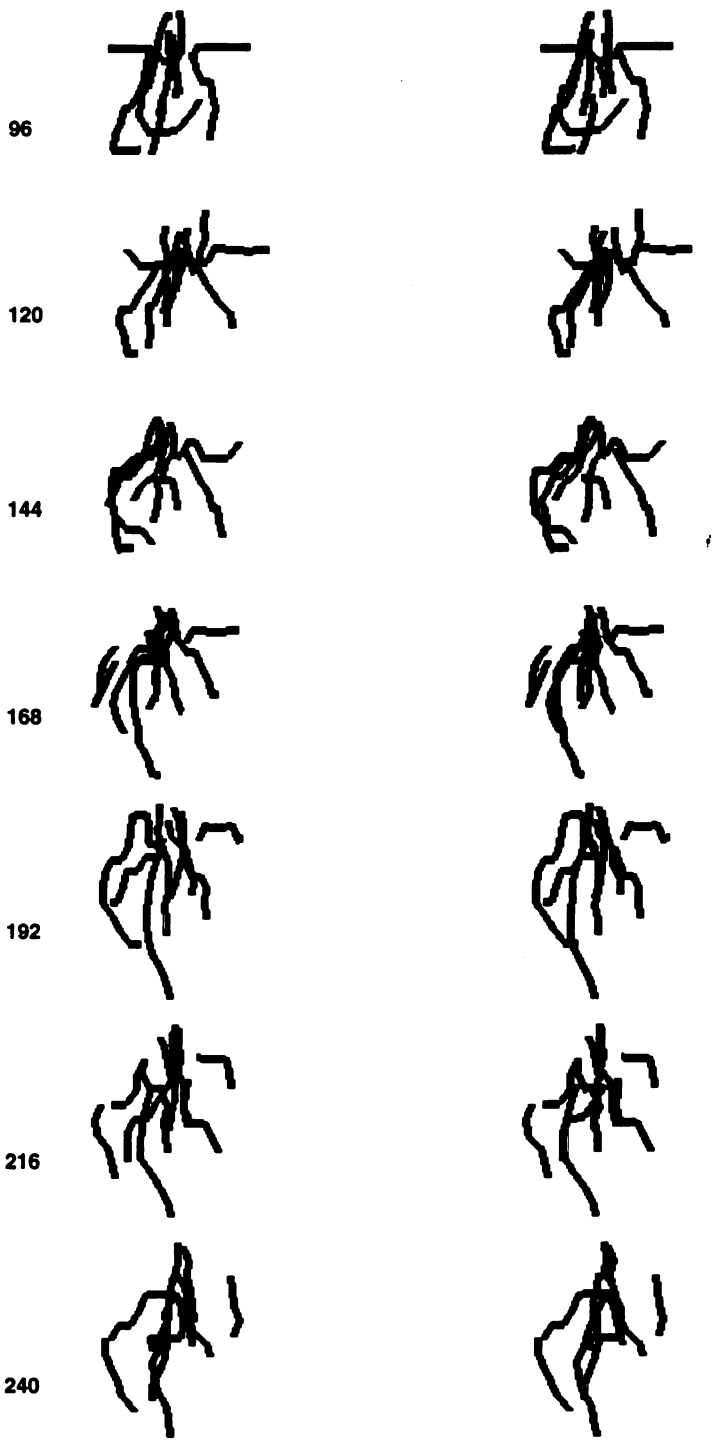

Figure 4.2. Wireframe models of metaphase chromosomes.

Figure 4.2. Wireframe 3D models of metaphase chromosome arms in living embryo, displayed as stereo pairs. Times indicated are number of seconds elapsed since beginning of data collection.

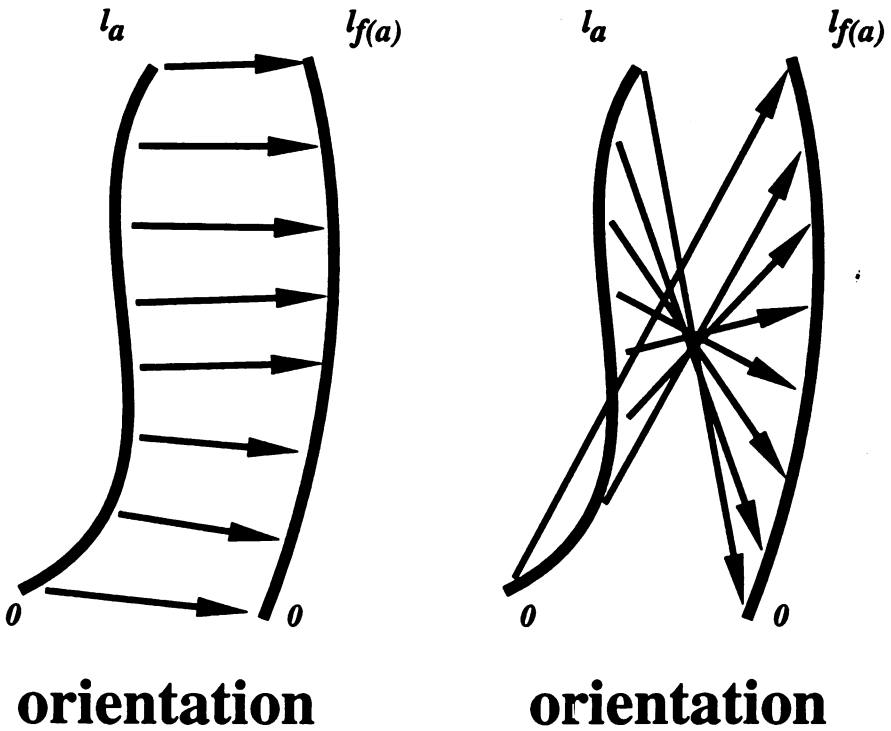

Figure 4.3. Arms can be mapped in two possible orientations.

Figure 4.3. Points on an arm at time t can be mapped onto points on corresponding arm at time t+1 in two ways.

We assume a one to one mapping and require that the number of chromosomes be the same for all time points. This is always true for the case that concerns us (e.g.. Drosophila metaphase). The set of chromosomes at time t is denoted A_t.

We now develop a measure of the distance between any two chromosomes. This measure will be used to form a cost function that will allow us to find the optimal mapping $f:A_t \rightarrow A_{t+1}$ between sets of chromosomes. Suppose under a given mapping chromosome $a_1 \in A_t$ maps onto chromosome $f(a_1) \in A_{t+1}$. Each chromosome is represented by a piecewise linear curve in 3 space formed by the union of line segments connecting adjacent points. Let this curve be denoted C_a. Each curve is parameterized by arc length, with position vectors to points on the curves given by $\mathbf{r_a}=\mathbf{C_a}(s)$ and $\mathbf{r_{f(a)}}=\mathbf{C_{f(a)}}(s)$. For each chromosome a, s varies from 0 to l_a, the total contour length of the chromosome. Note that the direction in which C_a is traversed in space as s varies from 0 to l_a, is arbitrary, but once assigned remains consistent throughout the remaining computations. Because of this, when computing the distance between from C_a to $C_{f(a)}$, it is necessary to specify the sense in which each curve is traversed. Given an arm a, and its corresponding arm under the mapping f(a), there are two possible ways to map points on a onto points on f(a), as illustrated in figure 4.3: either a and f(a) are traversed in the same sense or the opposite sense. These two relative orientations result in two possible definitions for the mean squared displacement experienced by chromosome a under the mapping f as:

$$\text{d\_direct}_{a,f(a)} = \frac{1}{l_a}\int_0^{l_a} \|\mathbf{C_a}(s)-\mathbf{C_{f(a)}}(s*\frac{l_{f(a)}}{l_a})\|^2 \, ds \qquad (1)$$

if the two arms are traversed in the same sense and

$$\text{d\_indirect}_{a,f(a)} = \frac{1}{l_a}\int_0^{l_a} \|\mathbf{C_a}(s)-\mathbf{C_{f(a)}}([l_a-s]*\frac{l_{f(a)}}{l_a})\|^2 \, ds \qquad (2)$$

if the two arms are traversed in the opposite sense. For every possible pairing of arms $a \in A_t$ and $f(a) \in A_{t+1}$, the distance from a to f(a) is defined as

$$d_{a,f(a)} = \min(d\_direct_{a,f(a)} , d\_indirect_{a,f(a)}) \quad (3)$$

Values of $d_{a,f(a)}$ are pre-computed for all possible pairs of arms, and for each case the optimal relative orientation is recorded. This mean-squared displacement between chromosomes can be used to define an overall cost function for a given mapping f at any time interval, as:

$$D = \sum_{a \in A_t} d_{a,f(a)} \quad (4)$$

Solution of motion estimation problem by simulated annealing

The graph matching problem thus becomes that of finding f to minimize D. Because there are many possible mappings f, some attention must be given to the algorithm for finding the optimal f to minimize D. Generally, one would like an algorithm for finding an exact solution to run in polynomial time, that is, the time taken to find a solution should be bounded by some polynomial function of the size of the problem. If a polynomial time algorithm for finding the solution does not exist, then it is generally better to find an approximation algorithm that can find a solution in some reasonable time at the cost of not quite getting the exact optimum. Does a polynomial time algorithm exist for graph matchine? It turns out that the graph matching problem is NP complete. The term NP complete describes a set of problems, which includes the famous Travelling Salesman

Problem, such that any NP problem can be converted into any other NP complete problem by an algorithm which runs in polynomial time. So if any one NP complete problem can be solved, the same method can be used to solve any other NP complete problem. What makes this set of problems interesting, however, is that no polynomial-time algorithm has ever been found for any NP-complete problem. It is generally assumed that no such polynomial time solutions exist for these problems, or at the very least, considering the time invested by many experts in seeking such a solution, it is clearly not worth attempting to find one. Thus, we seek instead an approximation algorithm to find the approximately optimal mapping. We therefore find the optimal mapping f to minimize D using simulated annealing (Press et al., 1989), which is a standard approach to solve large NP complete combinatorial optimization problems.

In simulated annealing, a random solution is initially generated, and then random changes are made to the solution so as to mimic the random motions that occur when a metal cools slowly (a process known as annealing). The advantages of simulated annealing are that it can avoid local minima that might trap other minimization schemes, and it can be applied to a purely combinatorial minimization in which the solution space is a set of discrete states rather than a numerical value for some parameter. Simulated annealing has been used by other groups in solving motion estimation problems in 2D (Dubois and Konrad, 1993), although their approach differs from ours in that it is fundamentally an optical flow scheme and not model-based. Our implementation proceeds as follows. After locating all chromosomes, and computing all pairwise distances between arms at time t and arms at time t+1 using equation 3, f is initialized to a random mapping. The transition operation used to generate new candidate solutions within the simulated annealing algorithm is a swapping operation, in which given a current mapping, two chromosomes a_i and a_j are chosen at random. If a_i maps onto $b_i=f(a_i)$ and a_j maps onto $b_j=f(a_j)$, the swapping operation generates a new mapping where a_i maps onto b_j and a_j maps onto b_i. Using this swapping operation to generate new candidate solutions, and the cost function

of eqn 4 to evaluate the cost of each mapping, simulated annealing is then performed using the Metropolis algorithm (Press et al., 1989) as follows. If the swapping operation would result in a lower value for D, then that swap is performed and the mapping updated accordingly. However, if the swap under consideration would lead to an increased value for D, then the swap is performed conditionally, with probability P given by:

$$P = e\{-\Delta D/\lambda\} \tag{5}$$

where ΔD is the (positive) change in D for the swap and λ is a control parameter that starts out at a very high value, greater than the maximum possible ΔD, such that all swaps proposed are automatically taken with probability very close to 1. The purpose of this probalistic update is to help the algorithm jump out of local minima as the solution gradually searches for a global minimum. λ is gradually reduced in multiplicative steps as the minimization proceeds. In our implementation, λ is reduced by a factor of 0.95 whenever a fixed number of successful swaps have been made or when a larger fixed number of swaps have been attempted. The algorithm terminates when D fails to decrease for a large, fixed number of attempted swaps, or when a fixed total number of changes in λ have taken place. We note that while the use of simulated annealing allows this algorithm to be applied to datasets with a large number of chromosomes, or even partially traced fragments of chromosomes, it is probably overkill in the case of a normal Drosophila embryo which has a diploid complement of only 12 chromosome arms (we track arms, rather than entire chromosomes, because sometimes it is difficult to determine the connectivity at the centrosomal region during later prometaphase. In principle the motion estimate can itself be used to resolve ambiguities in connectivity, as discussed below, but this has not yet been implemented). The total number of ways to map 12 arms onto 12 arms is 12! (twelve factorial) which is equal to 479,001,600 which though a large number, is not so large as to prohibit directly computing all possible solutions. However, for cases

with more chromosomes a brute-force evaluation of all solutions is impossible. For example, in yeast with 16 chromosomes there are approximately 10^{13} possible mappings. If, as a very conservative estimate, it takes ten clock cycles on a 200 MHz machine to evaluate one mapping, it would take over three years to check all solutions. In this case, simulated annealing becomes essential. Simulated annealing allows the problem to be solved because it makes a tradeoff: it finds a very good approximate solution in a reasonable time scale but at the expense of occasional errors.

Once the mapping (f) of chromosomes at time t onto chromosomes at time t+1 is found, the mapping of points on chromosome a onto points on chromosome f(a) is found by uniformly mapping each point on chromosome a onto the corresponding point on chromosome f(a), taking into account the relative orientation (fig. 4.3). This mapping is the final motion estimate, which indicates the displacement experienced by any given point. When the individual motion vectors for selected points are plotted, they generally agree with the visually observed motion. For the wireframe data in figure 4.2, the mappings at each time interval were checked with those determined by careful visual examination of the data, and generally agreed except in cases where the visual analysis did not reveal an obvious solution. Thus, the simulated annealing algorithm does as well as, or better than, tedious visual examination of the chromosome images. The automated algorithm has the advantage that it can take into account all arms simultaneously, rather than just looking at one pair of arms at a time, as a visual examination must.

Given the motion estimate, we can determine the trajectory of any given point. Starting with the point at time t=0, we determine from the motion estimate the point at t=1 onto which the current point maps. The coordinates of this point are stored, and then the corresponding point at t=2 is found. This is repeated until the position of the point has been tracked for all time intervals.

Rigid body motion compensation

Because we are primarily interested in small-scale motion of individual chromosomes, we seek to remove the effects of overall motion of the nucleus as a whole. Rotational spinning of nuclei within living cells has been extensively documented in other cell types (De Boni and Mintz, 1986; Paddock and Albrecht-Buehler, 1988). In addition, during embryogenesis in Drosophila melanogaster, the entire embryo pulsates with a constant series of actin-myosin driven contractions which cause the nuclei to wash back and forth within the syncytium. This constant flowing of nuclei produces both translational and rotation motion of the nuclei. Taken together, these overall motions will dominate the observed motion for a given chromosome, thus obscuring the conformation motion of the chromosomes themselves. Thus, in order to extract only the local conformations of the chromosomes we must first estimate the overall rigid body motion (ie. rotation plus translation) in three dimensions, and then correct for these motions.

The overall translation of the nucleus is found by computing, for each time interval, the average displacement vector $\langle \Delta \mathbf{r} \rangle_t$. The displacement vector for a single point is simply computed by taking the position of each point at time t+1 and subtracting from it the position of the corresponding point at time t. In order to find a set of points for computing this average, we resample each arm at time t in 0.1 μm intervals and then uniformly map these points onto corresponding points on corresponding arms at time t+1. We then take the average of this displacement vector over this set of points. Once we have estimated the average translational displacement vector for each time interval, we then use this estimate to compensate for the translation motion. Suppose a total of T time points, so that t=1..T. To the last time point, we apply no displacement, since there is no translation estimate available (since there is no data for T+1). To the second to last time point, t=T-1, we add to the position of each point the single displacement vector $\langle \Delta \mathbf{r} \rangle_{T-1}$ which thus puts the second to last time point into the same translation frame of reference as the last time point. For t=T-2, we apply to each point a total displacement $\langle \Delta \mathbf{r} \rangle_{T-2} + \langle \Delta \mathbf{r} \rangle_{T-1}$ which again puts

the data at time T-2 into the same frame of reference as the data of time T. Thus for any time point t, we sum the displacement vectors $\langle\Delta r\rangle_t + \langle\Delta r\rangle_{t+1} + ... + \langle\Delta r\rangle_T$ and add the total offset to the points at time t, in order to generate a new set of points that is translationally fixed with respect to the final time point. We thus remove the translational component of the overall nuclear motion.

We now seek to perform a similar compensation for the rotational motion. Given a set of points at time t , and a set of corresponding points at time t+1 (as described above for translational motion), the rotation matrix which results in a least-squares alignment of the two sets of corresponding point is computed using a singular-value decomposition method described by Kanatani (Kanatani, 1993). We start with sets of points for which translational motion has already been compensated. We have for each time interval two sets of points specified by the position vectors $\mathbf{r}_i$ at time t and $\mathbf{r'}_i$ at time t+1, where i ranges over all resampled points on all arms (let the total number of points be N). The goal is to find the rotational motion which brings these two sets of points into the closest correspondence. The rotational motion will be specified by a rotation matrix **R**. A rotation matrix is a 3x3 orthogonal matrix with determinant 1, which represents a rotation such that given the three dimensional position vector **r** of some point, the new position vector after the rotation becomes **r'=Rr**. Our goal is thus to find the nine elements of **R** which best map the points $\mathbf{r}_i$ onto the points $\mathbf{r'}_i$. Because we are concerned with rotational motion, we replace each point $\mathbf{r}_i$ with the corresponding unit vector $\mathbf{m}_i$, and now ask for the rotation matrix **R** which best maps $\mathbf{m}_i$ onto $\mathbf{m'}_i$. We formulate this as a least squares problem, where we define the optimal **R** as that which minimizes ε^2 ,the total squared distance after the rotation:

$$\varepsilon^2 = \sum_{i=1}^{N} \|\mathbf{m}_i - \mathbf{R}\mathbf{m'}_i\|^2 \qquad (6)$$

Using the least squares criterion has the advantage of robustness, in that a good approximate R can be found even when there exists no **R** that exactly maps $\mathbf{m}_i$ onto $\mathbf{m'}_i$ (which is likely to be the case if the chromosomes are flexible). How do we find **R** to minimize ε^2 ? The answer follows by expanding the squared term:

$$\varepsilon^2 = \sum_{i=1}^{N} \|\mathbf{m}_i\|^2 - 2\mathbf{m}_i \cdot \mathbf{m'}_i + \|\mathbf{R}\mathbf{m'}_i\|^2 \tag{7}$$

Some manipulation gives:

$$\varepsilon^2 = \sum_{i=1}^{N} \|\mathbf{m}_i\|^2 - 2\mathrm{tr}\left(\mathbf{R}^T \sum_{i=1}^{N} \mathbf{m}_i \cdot \mathbf{m'}_i^T\right) + \sum_{i=1}^{N} \|\mathbf{m'}_i\|^2 \tag{8}$$

Because the first and last terms do not depend on **R**, we find that to minimize ε^2 we need to maximize the quantity $\mathrm{tr}(\mathbf{R}^T\mathbf{K})$ where K is the correlation matrix (whose value can be directly found from the known points) given by:

$$\mathbf{K} = \sum_{i=1}^{N} \mathbf{m}_i \cdot \mathbf{m'}_i^T \tag{9}$$

The first step to maximize $\mathrm{r}(\mathbf{R}^T\mathbf{K})$ is to carry out a singular value decomposition (Press et al., 1990) of **K**, in which **K** is rewritten as $\mathbf{K}=\mathbf{V}\Lambda\mathbf{U}^T$, where **V** and **U** are orthogonal matrices and Λ is the matrix:

$$\Lambda = \begin{pmatrix} \sigma_1 & & \\ & \sigma_2 & \\ & & \sigma_3 \end{pmatrix} \tag{10}$$

where σ_1,σ_2, and σ_3 are the singular values. Standard algorithms exist to find **U**, **V** and Λ given **K**. For this work we employ the NAG routine F02WCF (Numerical Algorithms Group). Once we have done this, the optimal rotation matrix R can be directly computed, because it can be proven that is maximized when

$$R = \mathbf{V}\begin{pmatrix} 1 & & \\ & 1 & \\ & & \det(\mathbf{V}\mathbf{U}^T) \end{pmatrix}\mathbf{U}^T \tag{11}$$

This solution is unique if **K** is rank greater than 1 and $\det(\mathbf{V}\mathbf{U}^T)=1$. Both of these uniqueness criteria are evaluated by the program, and were found to hold for chromosome data. Indeed, the ease with which uniqueness of the solution can be demonstrated is a major advantage of the singular value decomposition approach (Kanatani, 1993). Thus, at each time point t we end up with the rotation matrix $\mathbf{R}_t$ that best describes the observed motion. This allows us to compensate for the rotational motion of the nuclei. At each time point t, we apply to all points a composite rotation matrix given by:

$$\mathbf{R}_{comp}(t)= \prod_{t=1}^{T-1}\mathbf{R}_t \tag{12}$$

That is, we apply to each time point all successive rotation matrices such that the points end up in a frame of reference rotationally fixed relative to that of the last time point. Once we have done this, the final result is a set of chromosome models for which there is no overall nuclear translation or rotation, and the only remaining motion is due to motion of one chromosome relative to another, and to the conformational flexibilty of the chromosomes themselves. It is this revised set of chromosome models that will be used for all subsequent analysis.

The rotational motion estimation is also of intrinsic interest, in light of the many published reports that nuclei in vivo undergo persistent spinning motion (De Boni and Mintz, 1986; Paddock and Albrecht-Buehler, 1988). When the time-lapse 3D images of Drosophila chromosomes are viewed as a time-lapse movie of stereo pairs, it often appears that the nuclear are rotating, but despite careful examination of these movies it was never possible to say for sure what direction they were rotating, or about what axis, or indeed to distinguish between spinning and rocking back and forth. Rocking motions back and forth could simply be an optical illusion, a case where several small random motion are percieved as a single coherent motion. However, if indeed the chromosome complement is spinning around during mitosis that would suggest a very unusual activity of the spindle. In order to resolve this issue, we turn to the rotational motion estimate described above. Euler's Theorem (Kanatani, 1993) states that any rotation matrix represents a rotation about an axis by some angle. That is, any 3D rotation can be represented by some rotation axis $\boldsymbol{l}$ and some rotation angle Ω about that axis. Spinning motion, in which the nucleus spins around and around a relatively constant axis, would be reflected in an axis $\boldsymbol{l}$ that does not change its orientation very much. On the other hand, rocking back and forth will also entail a relatively fixed rotation axis $\boldsymbol{l}$ except that the axis will flip between opposite orientations as the nucleus rocks first in one direction, then the other. Finally, if the nucleus is not undergoing any persistent rotation, but is just tumbling due to turbulent flow of the cytoplasm and or random collisions with spindle microtubules, then the rotation axis $\boldsymbol{l}$ should be uncorrelated from one time interval to the next, and will change at random. In accordance with Eulers theorem, we can compute $\boldsymbol{l}$ and Ω from the rotation matrix $\mathbf{R}$ at each time interval, using the following relations (Kanatani, 1993):

$$\Omega = \cos\text{-}1\frac{\mathrm{tr}\mathbf{R} - 1}{2} \tag{13}$$

$$\boldsymbol{l} = N\left[\begin{pmatrix} R_{32}-R_{23} \\ R_{13}-R_{31} \\ R_{21}-R_{12} \end{pmatrix}\right] \tag{14}$$

where R_{ij} are the components of R and N is the vector normalization operation defined by

$$N[\mathbf{u}] = \frac{\mathbf{u}}{\|\mathbf{u}\|} \tag{15}$$

When we carry out this computation for several time intervals we get the results illustrated in Table 4.1. Clearly, the rotation axis is not at all constant, its orientation not corresponding at all from one time point to the next. Thus, we conclude that the apparent spinning motion observed in time-lapse movies of Drosophila embryo chromosomes is in fact just random tumbling. Although this is a negative result, it illustrates the power of quantitative motion analysis to understand chromosome behavior in situations where direct visual examination is not sufficient.

Table 4.1. Apparent nuclear rotation is tumbling rather than spinning or rocking

t (sec)	W (deg)	lx	ly	lz
0	7.3	0.12	-0.34	-0.93
24	3.2	-0.12	0.96	0.23
48	12.8	-0.07	0.36	0.93

Tools for analysis of chromosome mobility

The simplest measurement of four-dimensional behavior is chromosome mobility, ie, how much does a given point move around throughout the nucleus. Chromosome mobility is interesting because if chromosome are attached to any sort of immobile superstructure, for example the nuclear envelope, it should be reflected by a reduction in chromosome mobility. Moreover, given the average chromosome mobility and a knowledge of the size of the chromosomes, it is straightforward to compute the effective viscosity of the surrounding nucleopolasm, which should provide important information about the structure of cytoplasm and nucleoplasm. Chromosome mobility is easily computed as the rms displacement experienced at each point on an arm, which is straightforward to compute given the motion estimate. For points near centromeres, mobility probably reflects mainly pushing and pulling by the spindle. For points further from centromeres, mobility reflects both Brownian motion, the polar ejection force (a force on chromosome directed away from the spindle poles, probably due to random collision with the ends of growing microtubules, see Rieder and Salmon, 1994) and force transmitted along the chromosome from the kinetochore. As can be seen in figure 4.4, the telomeres are generally more mobile than the centromeres. This implies that telomeres are not anchored to any rigid structure such as a nuclear matrix or residual nuclear envelope. Analysis of mobility during prophase when the nuclear envelope is still present (Hiraoka et al., 1990) is currently underway, and a comparison of telomere mobility in prophase and metaphase will be used to test for interactions of telomeres with the nuclear envelope in vivo.

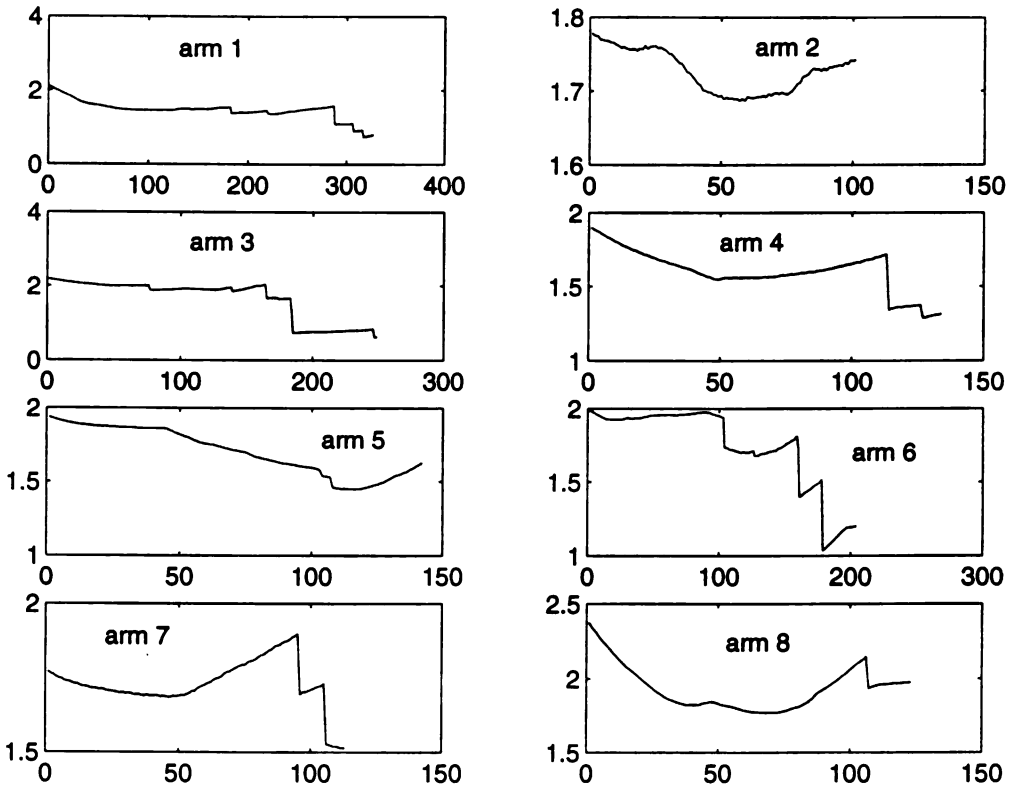
arm 1
arm 2
arm 3
arm 4
arm 5
arm 6
arm 7
arm 8

Figure 4.4. Mobility of chromosomes. RMS displacement plotted versus position along each arm (in arbitrary units). For each arm, position 0 represents the telomere, and the other end is the centromere.

Tools for analysis of chromosome conformation in four dimensions

A complete motion estimate for a four-dimensional data set is a huge volume of information, and direct inspection of the individual motion vectors is almost completely uninformative. What we really want is a way to obtain simple measures of chromosome behavior from the motion estimate, so that the mechanics and motion of the chromosomes can be represented in some easily interpretable way. There are doubtless many ways to approach this problem. We chose to build on previous work in our lab which focused on ways of analyzing three dimensional structure. Mathog et al. (Mathog, 1985) developed a set of scalar conformation descriptors, which associated with each point on a chromosome wire-frame model some scalar value describing the shape of the chromosome in the vicinity of that point. One example of such a measure is curvature. Our approach is to extend these measures to describe four-dimensional structure, by computing the scalar conformation descriptors for all points on all chromosomes at all time point, and then taking the root mean-squared change in the value of the descriptor at a given point over time. Essentially this produces a measure of the degree of temporal fluctuation in 3D conformation at the point in question. Thus, taking the case of curvature, by measuring the rms change in curvature we get a measure of flexibility, and by plotting this value versus position on the chromosome, we can in principle identify regions of higher or lower flexibility which could potentially reflect differences in chromosome structure.

Chromosome flexibility is interesting in itself because different physical models for how the chromatin is packed into the chromosome make some predictions about its flexibility. Flexibility is also of intrinsic importance in processes that require bending or looping of the chromosome. Although chromatin flexibility has been directly measured on isolated chromosomes (Castro, 1994) the notorious sensitivity of chromosome structure to isolation conditions makes it highly desirable to measure flexibility in situ in living cells.

Tools for analysis of spindle-driven motion

One major application of motion analysis is the study of interactions between chromosomes and the mitotic spindle. These interactions have been shown in other systems to include a periodic oscillation of the centromeres along the spindle axis, and the polar ejection force pushing chromosome arms away from the poles (Rieder and Salmon, 1994). Figure 4.5 plots the trajectories of centromeres and telomeres for two arms. From figure 4.5C it is apparent that the motion of the arms is largely along an axis perpendicular to the arms themselves. This implies that during metaphase there is no rigid nuclear matrix which would be expected to block such motion. Coordinated motions of entire arms may be caused by random collision with growing MT ends that push the whole arm one way or the other. Alternatively, the motion may be caused by kinetochore fibers exerting force on the kinetochore, and the rest of the arm is dragged along passively. In the latter case, the fact that the whole arm moves in a direction perpendicular to its axis would imply that the chromosome cannot rotate about the point of attachment to the kinetochore microtubules.

We are particularly interested in studying the motions of chromosomes during congression. One model for this motion would suppose that the kinetochores are the dominant motive force, and they drag the chromosomes behind them. An alternative though is that the polar ejection force acting on the chromosome arms plays a substantial role in moving the chromosomes into the correct position on the metaphase plate. In principle these can be distinguished by carefully examining the shape and motion of the chromosomes. Drosophila chromosomes have a big advantage over vertebrate chromosomes in that they are long and flexible, as opposed to the short rigid rodlike vertebrate mitotic chromosomes, and thus differences in force acting at different parts of the Drosophila chromosome should produce correspondingly larger differences in shape and motion. The main prerequisite for this analysis is to determine the component of the motion that is parallel to the spindle axis. Unlike DIC images of newt lung cells, in fluorescence 3D images of chromatin it has not been possible to directly visualize the

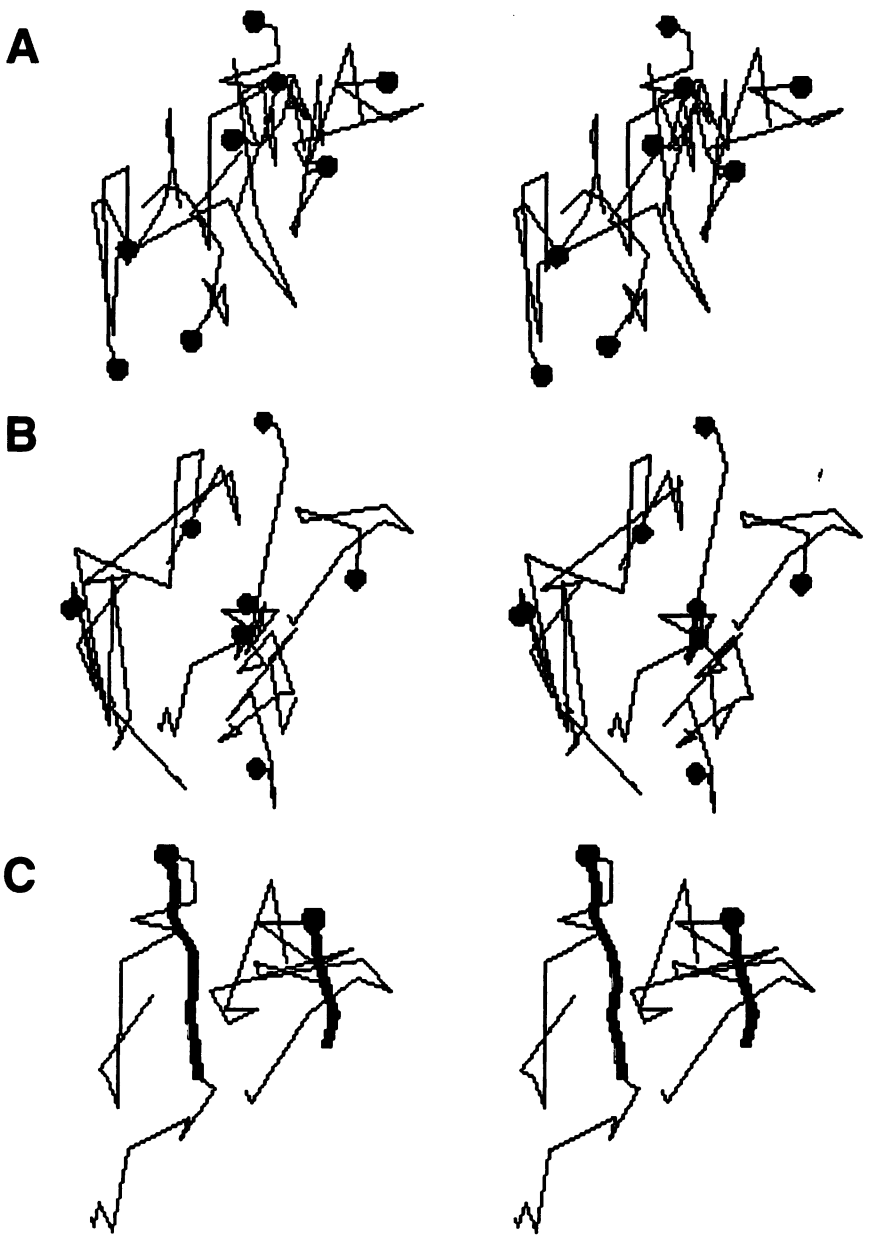

Figure 4.5. Trajectories of centromeres (A) and telomeres (B) during prometaphase.

Figure 4.5. Visualization of 3D trajectories. A. Trajectories of all centromeres. B. Trajectories of all telomeres. C. Trajectories of centromeres and telomeres for two selected arms. Spherical markers indicate initial position of centromere or telomere

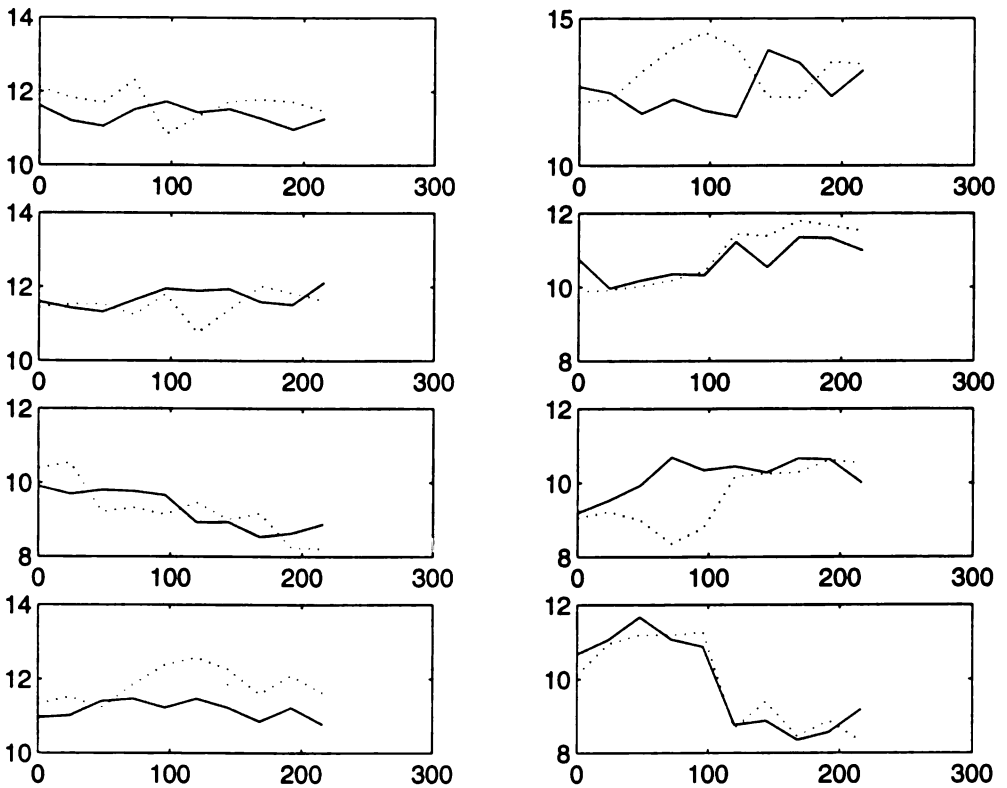
14
12
10
0
100
200
300
15
10
14
12
10
12
10
8
12
10
8
14
12
10
12
10
8

Figure 4.6. Position of centromeres and telomeres along spindle axis versus time, for each arm. (————) centromere position, (- - - - - - - -) telomere position. Position plotted on vertical axis, and time plotted on horizontal axis, given in mm and seconds.

spindle axis. However, it is known that during metaphase in Drosophila, the centromeres become roughly collinear, along a line perpendicular to the spindle axis (Hiraoka et al., 1990). Furthermore, due to the organization of mitotic spindles in Drosophila embryos, the metaphase plate and the spindle axis are roughly coplanar in the X-Y plane. Thus, we least-squares fit a straight line to the set of (x,y) positions of the centromeres (as determined by the chromosome arm models, in which, due to the polarized configuration of metaphase chromosomes in Drosophila (Hiraoka et al., 1990), the centromeres are at the highest vertical position). We form a unit vector $\langle v_x, v_y \rangle$ parallel to this line, and then use the perpendicular unit vector $\langle v_y, v_x \rangle$ as an estimate of the spindle axis. Positions of all points are then projected onto this axis to obtain a position along the spindle axis for each point. Because the datasets have been rotationally aligned as described above, it is reasonable to use the final spindle axis as an estimate of the spindle axis during congression. A plot of centromere and telomeres position along the spindle axis is given in figure 4.6. While both centromeres and telomeres are moving back and forth, the telomeres do not simple follow the centromeres passively. In some instances, telomeres and centromeres are moving in opposite directions. One goal of this analysis is to detect oscillations of the centromeres such as have been demonstrated in newt lung epithelial cells (Skibbens et al., 1993). Figure 4.6 does not reveal any obvious periodicity. However, in newt cells the period of oscillation is approximately 100 seconds. Given our temporal resolution of one dataset every 24 seconds, such oscillations would be difficult to detect because we would only be sampling position four times per cycle. One approach to improve temporal resolution is to acquire smaller datasets which include the centromere-proximal regions of the chromosome arms but not the telomeric regions. Faster CCD cameras and optimized staining procedures may also help reduce exposure time and increase data rate.

Discussion

We have presented a set of computational tools for the analysis of motion in three dimensions from time-lapse three-dimensional microscopy datasets. These algorithms were developed with an analysis of chromosomes in mind, but they represent a fairly general approach of model-based motion analysis. Now that these computational methods are available, there are several areas of application to which they will applied in the future in the Sedat lab. First, the Drosophila embryo provides an excellent system to study the mechanics of chromosome segregation and in particular we are in the process of analyzing the forces exerted on these chromosomes by the polar ejection force. A second promising area of investigation will be in meiosis, where chromosome flexibility is thought to be an important parameter determining the effectiveness of discrete interstitial pairing interactions in aligning the entire chromosome (Kleckner and Weiner, 1993). Adult C. elegans have transparent body walls and the meiotic chromosomes can be stained with DNA dyes and visualized inside the living adult worm (W. Marshall, unpublished observations). Application of the computational methods demonstrated here to such a system will allow analysis of the mechanics of meiotic chromosomes in vivo.

While we have made a tentative first step towards analysis of 4D structure, a number of technical advances are on the horizon which would further improve the analysis of cell structure and mechanics in four dimensions. Most important are automated segmentation techniques in which a computer program can construct 3D structural models from image data without user intervention. This is extremely important because interactive modelling by a human operator is both tedious and error-prone. A second key improvement is to use the motion estimate to detect errors in the model construction process. In particular, in many cases the limited resolution of the light microscope makes it difficult to tell the connectivity between chromosome arms. 4D data can be used to resolve this ambiguity, since regions that are truly connected will remain connected over time, while regions of adventitious overlap will eventually become separated due to random movements of the

chromosomes. Thus, it should be possible to automatically construct the optimal connectivity pattern that is most consistent with the long term motion data.

These methodologies are not limited to chromosomes, either. There are many instances where curve-like structures undergo interesting structural dynamics. For example, mitochondria in living cells form a highly dynamic reticulum which constantly undergoes breakage and fusion (Nunnari et al., 1997). Automated motion estimation methods could allow detailed determination of breakage and fusion rates, as well as allow measurements of translocation speeds of these organelles during, for example, cell division. In conclusion, we feel confident that analysis of four dimensional behavior of cellular structures is going to become an increasingly important aspect of cell biological research in the near future.

REFERENCES

Afshar, K., Barton, N.R., Hawley, R.S., and Goldstein, L.S. (1995). DNA binding and meiotic chromosomal localization of the Drosophila nod kinesin-like protein. Cell *81*, 129-38.

Awasthi, V., Doolittle, K.W., Parulkar, G., and McNally, J.G. (1994). Cell tracking using a distributed algorithm for 3-D image segmentation. Bioimaging *2*,98-112.

Castro, C.A. (1994). Measurements of the elasticity of single chromatinn fibers: the effect of histone H1. PhD. Dissertation, Univ. of Oregon.

De Boni, U., Mintz, A.H. (1986). Curvilinear, three-dimensional motion of chromatin domains and nucleoi in neuronal interphase nuclei. Science *234*, 863-6.

Doolittle, K.W., Reddy, I., and McNally, J.G. (1995). 3D analysis of cell movement during normal and myosin-II-null cell morphogenesis in dictyostelium. Dev. Biol. *167*,118-129.

Dubois, E. and Konrad, J. (1993). Estimation of 2-D motion fields from image sequences with application tomotion-compensated processing. in *Motion analysis and image sequence processing*, M.I. Sezan and R.L. Lagendijk, eds., Kluwer Academic Publishers, Boston.

Fuh, C.S. and Maragos, P. (1991). Motion displacement estimation using an affine model for image matching. Optical Eng. *30*,881-887.

Gittes, F., Mickey, B., Nettleton, J., and Howard, J. (1993). Flexural rigidity of microtubules and actin filaments measured from thermal fluctuations in shape. J. Cell Biol. *120*, 923-34.

Haralick, R.M. and Shapiro, L. (1993). Computer and robot vision vol II. Addison-Wesley Pub Co., Reading, Mass.

Hiraoka, Y., Agard, D.A., and Sedat, J.W. (1990). Temporal and spatial coordination of chromosome movement, spindle formation, and nuclear envelope breakdown during prometaphase in Drosophila melanogaster embryos. J. Cell Biol. *111*,2815-28.

Kleckner, N., and Weiner, B.M. (1993). Potential advantages of unstable interactions for pairing of chromosomes in meiotic, somatic, and premeiotic cells. Cold Spring Harbor Symp. Quant. Biol. *58*,553-565.

Kanatani, K. (1993). Geometric computation for machine vision. Oxford University Press, Oxford, pp 107-109.

Luby-Phelps, K., Lanni, F., and Taylor, D.L. (1988). The submicroscopic properties of cytoplasm as a determinant of cellular function. Ann. Rev. Biophys. Biophys. Chem. *17*, 369-96.

Mathog, D. (1985). Light microscope based analysis of three-dimensional structure: applications to the study of Drosophila salivary gland nuclei: II. Algorithms for model analysis. *J.* Microscopy *3*,253-73.

Nunnari, J., Marshall, W.F., Straight, A., Murray, A.W., Sedat, J.W., and Walter, P. (1997). Mitochondrial transmission in Saccharomyces cerevisiae. *Molecular Biology of the Cell*, in press.

Paddock, S.W. and Albrecht-Buehler, G. (1988). Rigidity of the nucleus during nuclear rotation in 3T3 cells. Exp. Cell Res. *175*,409-413.

Press, W.H., Flannery, B.P, Teukolsky, S.A., and Vetterling, W.T. (1989). Numerical Recipes in Pascal. Cambridge University Press, Cambridge, pp 366-374.

Rieder, C.L., and Salmon, E.D. (1994). Motile kinetochores and polar ejection forces dictate chromosome position on the vertebrate mitotic spindle. J. Cell Biol. *124*,223-233.

Skibbens, R.V., Skeen, V.P., and Salmon, E.D. (1993). Directional instability of kinetochore mobility during chromosome congression and segregation in mitotic newt lung cells: a push-pull mechanism. J. Cell Biol. *122*,859-875.

Thomas, C., Devries, P., Hardin, J., and White, J. (1996). Four-dimensional imaging: computer visualization of 3D movements in living specimens. Science *273*, 603-7.

Wakimoto, B.T., and Hearn, M.G. (1990). The effects of chromosome rearrangements on the expression of heterochromatic genes in chromosome 2L of Drosophila melanogaster. Genetics *125*,141-154.

Chapter 5. Conclusion

The nucleus, once viewed by many molecular biologists as a simple bag of DNA, is turning out to be a highly ordered structure. Cytological studies using a variety of techniques have suggested that chromosomes in the nucleus may be positioned in very specific arrangements, based largely on the localization of centromeres and/or telomeres. On the other hand, it is clear that many essential biological processes, such as recombination and meiosis, require movements of chromosomes, which would seem incompatible with the idea that the nucleus is highly organized. The purpose of the experiments in this dissertation was to answer two long-standing questions: to what extent is the position of a given locus fixed within the nucleus, and to what extent can a given locus move around within the nucleus. Clearly, these two questions are actually the same question viewed from two different viewpoints. The major findings of this work are that

-- Every chromosome locus in Drosophila embryos is consistently and reproducibly located in a particular region of the nucleus that differs from locus to locus.

-- There is a set of discrete sites on Drosophila chromosomes that are nonrandomly associated with the nuclear envelope. These sites are spaced roughly a megabase apart along the lengths of the chromosomes and do not correspond to scaffold attachment regions (SARs).

-- Interphase chromatin can undergo diffusional motion with a diffusion constant in the range 10^{-12} to 10^{-13} cm^2/s, a sufficiently fast rate to allow motion-requiring processes such as homology search to take place on the necessary time scale by diffusion. The diffusion of chromatin is, however, constrained, implying attachment to some internal nuclear structure. This confinement may be the physical basis of the specific positioning reported in chapter 2.

The most surprising finding was the extremely high degree of specific positioning within the nucleus demonstrated by the FISH experiments in chapter 2. Not only were

specific sites localized to the NE, other sites were nonrandomly localized to the nuclear interior, while others reproducibly occupied more intermediate regions. A very strong polarity of the nucleus was also observed. The fact that every locus occupies a defined position has strong implications for reactions that require interactions between two different loci. Unless the sub-nuclear positions of two loci partially overlap, they will never interact. Conversely, if the two positions do overlap an interaction is favored. Thus, a major biological effect of this positioning is regulation of chromosome interactions. This positional determination was also observed in the chromatin motion experiments of chapter 3, which revealed that a given locus is able to diffuse freely only within a limited sub-region of the nucleus. This again implies that if the confinement regions of two loci do not overlap, and interaction is strongly disfavored, while if the confinement regions do overlap, the collision probability is greatly enhanced.

These findings open up two major routes of inquiry. On one hand, it is important to being dissecting the molecular basis of this positioning. I have taken a step in this direction by narrowing down a NE association site using a double-label strategy. At this point the question becomes addressable by more traditional molecular approaches. The other important direction in which the work may be extended is to explore the biological ramifications of positioning and diffusional confinement. In particular, it will be of great interest to examine their roles in meiosis. To what extent does a defined nuclear architecture facilitate homology search, by placing homologous loci in similar locations? Is diffusional search sufficiently fast to explain the observed rates of homologous pairing? Answers to these questions will be essential for understanding the mechanism of meiotic pairing as well as other motion-requiring processes.

These studies illustrate the power of quantitative analysis of motion and structure using three-dimensional and four-dimensional microscopy. The approach of inferring interactions and mechanistic behavior from analysis of structure and motion should be applicable to a broad range of problems in cell biology.